Retrodialysis of Pharmacological Agents Mitigates Tissue Damage during Brain Microdialysis and Preserves Dopamine Activity in Surrounding Tissue

by

Kathryn M. Nesbitt

B.S. Chemistry, St. John Fisher College, 2010

Submitted to the Graduate Faculty of the

Kenneth P. Dietrich School of Arts and Sciences in partial fulfillment

Of the requirements for the degree of

Doctor of Philosophy

University of Pittsburgh

2015

UNIVERSITY OF PITTSBURGH

DIETRICH SCHOOL OF ARTS AND SCIENCES

This dissertation was presented

by

Kathryn M. Nesbitt

It was defended on

April 14, 2015

and approved by

Shigeru Amemiya, Professor, Department of Chemistry

Renã Robinson, Professor, Department of Chemistry

Xinyan Tracy Cui, Professor, Department of Bioengineering

Dissertation Advisor: Adrian C. Michael, Professor, Department of Chemistry

Retrodialysis of Pharmacological Agents Mitigates Tissue Damage during Brain Microdialysis and Preserves Dopamine Activity in Surrounding Tissue

Kathryn M. Nesbitt, PhD

University of Pittsburgh, 2015

Microdialysis is a powerful technique used to recover analytes from the brain. Microdialysis is compatible with multiple detectors allowing simultaneous analysis of neurotransmitters, metabolites, neuropeptides, and amino acids. The use of microdialysis has made advances in understanding brain function and diseases and is currently used to monitor traumatic brain injured patients. However, microdialysis probe implantation causes a penetration injury eliciting a foreign body response in the surrounding brain tissue. Tissue around the probe becomes unhealthy which brings into question, how the state of the tissue around the probe effects analytes that are recovered by microdialysis.

Dopamine, a neurotransmitter involved in a variety of physiological functionality and neurological disorders, is often recovered using microdialysis. Dopamine is electroactive, and can also be measured using carbon fiber microelectrodes coupled with voltammetry. The small size of these electrodes allows for high spatial resolution without damaging the tissue. Using microelectrodes our lab has previously found that probe implantation creates a gradient of reductions in evoked dopamine responses the closer the electrode is to the probe. This dissertation builds off of this finding, with the goal of mitigating the penetration injury to preserve dopamine neurotransmission. First, it was discovered that probe implantation completely abolished evoked dopamine responses near probes. Administration of a dopamine transporter inhibitor showed that terminals survive probe implantation justifying our efforts to

mitigate probe induced tissue damage. Retrodialysis of an anti-inflammatory drug dexamethasone and a reactive oxygen species scavenger XJB-5-131 prevented dopamine terminal loss and preserved evoked dopamine responses for four hours. Further work proved that dexamethasone preserves evoked dopamine release for up to 24 hours. As dexamethasone is a steroid that could potentially affect neurotransmission, other pharmacological agents were investigated, all proving to improve evoked DA responses in tissue surrounding probes. Pharmacological mitigation of tissue damage provides new insight into acute extenuation of probe induced damage which has the potential to successfully mitigate chronic implantation for long-term in vivo monitoring of neurochemicals.

In a separate study, microelectrodes were used to spatially map dopamine responses in the rat brain. Distinct dopamine kinetics exist in sub-regions of the striatum that correlate to patch-matrix compartments.

TABLE OF CONTENTS

LIST OF FIGURES

PREFACE

First, I would like to thank my research advisor, Dr. Adrian Michael. He taught me how to be a great scientist in and out of the lab. He showed me how to not only collect respectable data, but how to scientifically communicate through my writing and presentations. I also have to thank Adrian for all of the opportunities he has given me to attend conferences. Learning and networking with other scientists in the field has helped me grow significantly.

Next, I would like to thank Dr. Shigeru Amemiya, Dr. Renã Robinson, and Dr. Xinyan Tracy Cui for serving as committee members throughout my years at the University of Pittsburgh. I would also like to thank Dr. Steve Weber for all of his guidance on my research and my original proposal. I am also appreciative of the University of Pittsburgh Department of Chemistry staff, and the electronic and machine shops.

Thank you to the current members of the Michael lab, Erika Varner, Seth Walters, Elaine Robbins, Kendra Bobby and Michael Rerick for all of your help and support. Thank you to the past Michael lab members Mitch Taylor and Zhan Shu for inspiring me with your passion for science. Most importantly, thank you Andrea Jaquins-Gerstl. Andrea has been there for me from my first day in lab making microdialysis probes until the very end. Not only has she been a mentor to me but she has become a close friend and together we've accomplished some incredible work.

Last but not least, I must thank my family and friends. Their support and confidence in me have never faltered. Thank you to my parents and my brother, for always letting me pursue my dreams and giving me the support I need to make them realities. Thank you Louis. You believed in me more than anyone. You have and continue to make me the best person I can be. I couldn’t have done this without you. Finally, thank you Liz Williams. You were the reason I started this journey, and my inspiration to continue to grow in science. This is for you.

1.0 INTRODUCTION

1.1.1 Microdialysis

Microdialysis is a widely used technique in the field of neurochemistry. In general, microdialysis is used to recover analytes in the extracellular space of the brain. A solution similar to that of the area being sampled is perfused through a semi-permeable membrane. As the fluid diffuses out of the membrane small molecules diffuse into the membrane and are collected through outlet tubing. Microdialysis can be coupled with detection methods such as high-performance liquid chromatography, capillary electrophoresis, and mass spectrometry for analysis. This technique allows for simultaneous detection of multiple small molecules. One drawback is that microdialysis is slower than most dynamic central nervous system processes however, microdialysis sampling and analysis is becoming faster, with reported sample times of less than a minute.[1] Consequently it has been applied in numerous studies involving the brain.

Microdialysis explores brain function often times by recovery of neurotransmitters such as dopamine.[2-4] Experiments involving the collection of neurotransmitters have allowed for the study of drug addiction and systemic effects of drugs of the neurochemistry of the brain.[5] Retrodialysis or the use of the probe to delivery agents to the brain allows for local delivery and analysis of drugs to a particular brain region simultaneously.[6] Neurological diseases, such as Parkinson's disease, have also been studied using microdialysis.[7] Recently, microdialysis has

been used to examine traumatic brain injuries (TBI) in human patients. The diversity of microdialysis membranes allows for the recovery and analysis of a variety of analytes pertinent to understanding TBI, including amino acids, glucose and lactate and extracellular metabolites.[8-10]

1.1.2 Device Implantation

Unfortunately, implantation of any type of neuronal device for analysis causes a cellular response that can be damaging to the ultrastructure of the brain directly surrounding the implant. Astrocytes and microglia make up the majority of the cellular response to the foreign body. An initial reaction to implantation is observed followed by an unrelenting response weeks after implantation.[11] Devices have a limited functional lifetime in the brain defined by the glial barrier that encapsulates the device and prevents it from accessing the brain. Alterations in device material, shape and size have led to improvements to the cellular response and longevity of the device,[12-13] however development of a more permanent solution is still of importance.

This disadvantage is specifically a concern for microdialysis because of the larger size of microdialysis probes. Probes cause penetration injuries when implanted into the brain.[14-15] Analysis of tissue surrounding microdialysis probes implanted in the striatum by light microscopy unveiled tissue damage 1.4 mm and neuronal loss 400 μm from the probe track.[16] Not only does the large size of the microdialysis probe cause damage, but the tissue response to a foreign object also contributes to the severity of the injury. Probe implantation restricts blood flow (ischemia) and triggers gliosis.[17-18] Therefore, the tissue sampled by microdialysis is not in its normal state. Even though the injury associated with microdialysis probe implantation is

significant, it is important to note that overall brain function and animal behavior does not change, making it safe for clinical use.[19]

Efforts to reduce the tissue response associated with neural device implantation have been made. Anti-inflammatories for example reduce nitric oxide production from microglia.[20] Dexamethasone, an anti-inflammatory and immunosuppessant glucocorticoid, decreased gliosis and ischemia caused by neuronal device implantation. Both systemic treatment with dexamethasone and device coating with dexamethasone have been effective.[21-23] Dexamethasone was neuroprotective for dopamine terminals in the striatum during inflammatory reactions in rodent models for Parkinson's disease.[7, 24] Retrodialysis of dexamethasone extended microdialysis probe function by two days in a subcutaneous study.[25] In terms of probe implantation in the brain, dexamethasone by retrodialysis significantly inhibited gliosis and ischemia.[26]

1.1.3 Dopamine

Dopamine is a well-studied neurotransmitter in the brain that is often recovered from the brain by microdialysis. In the striatum, dopamine is synthesized and packaged into vesicles in dopamine terminals. Dopamine is released in the striatum upon arrival of an action potential. During an action potential, vesicles containing dopamine fuse to presynaptic membranes and release their contents into the synapse. The extracellular concentration of dopamine is regulated by dopamine receptors and transporters. Dopamine autoreceptors (D2 receptors) inhibit dopamine release once a sufficient concentration is reached. Dopamine transporters (DAT) are responsible for the reuptake of dopamine from the extracellular space back into the cell. During

stimulation to induce an action potential, evoked release, autoinhibition and uptake regulate the extracellular concentration of dopamine.[27]

1.1.4 Dopamine Detection

Fast scan cyclic voltammetry (FSCV) offers another method for measurement of brain analytes, specifically electro-active species in the brain such as dopamine. Carbon fiber microelectrodes (7 μm in diameter) are most commonly used for detection. Compared to microdialysis, temporal resolution is superior with microelectrodes as it can detect real-time (ms) neurological events. Microelectrodes are much less invasive than microdialysis probes therefore providing better spatial resolution. Acute studies with microelectrodes in the rat striatum displayed minimum damage at the implantation site by light and electron microscopy.[28] Fluorescence microscopy revealed no blood vessel disruption and an absence of gliosis 24 hours after microelectrode implantation.[18]

FSCV achieves dopamine detection by applying a triangular waveform potential to a microelectrode at a fast scan rate (400 V/s) every 400 ms. A fast scan rate allows for excellent selectivity. The potential is ramped from 0 to 1 V, then from 1 to -0.5 V, then back to 0 V. Dopamine is oxidized to dopamine-o-quinone at 0.7 V and reduced back to dopamine at -0.2 V. Oxidization and reduction occurs at the surface of the electrode. The current generated can be converted into dopamine concentration via post-calibration of the electrode in a flow cell.

There is a discrepancy between resting dopamine concentrations measured by microdialysis and microelectrodes. Dopamine in dialysate is in the low nanomolar range.[29] Dopamine as measured by FSCV coupled with microelectrodes is 2 μM.[30] Furthermore, probe implantation significantly alters stimulated (evoked) dopamine release in tissue surrounding

microdialysis probes. Probes completely abolished evoked dopamine release at microelectrodes directly adjacent to probes. Evoked dopamine release decreased 10-fold at microelectrodes 220-250 μm away.[29] This implies that probe implantation alters the dopaminergic system at least 220-250 μm away from probes.

Nomifensine, a DAT uptake inhibiter, revived evoked dopamine release near probes in the striatum.[29, 31] After nomifensine, evoked dopamine release returned at microelectrodes adjacent to microelectrodes and increased evoked dopamine release 220-250 μm from probes.[29] A combination of raclopride (D2 dopamine receptor antagonist) and nomifensine increased evoked dopamine release 200 μm from probes by 50 % of its pre-probe response.[31] This suggests that at least 50 % of dopamine terminals survive probe implantation.

1.1.5 Present Work

We used carbon fiber microelectrodes coupled with FSCV to monitor evoked dopamine release in the rat striatum in two distinct projects. First, chapters 2, 3, 4, and 5 focus on mitigation of microdialysis probe induced damage and preservation of dopamine and potassium in surrounding brain tissue. We hypothesize that microdialysis probe implantation suppresses dopamine terminals and that reducing the cellular damage and ischemia triggered by probe implantation will allow dopamine terminals to function on a more normal level. In chapter 2, the effect of probe implantation on evoked dopamine release near (70-100 μm away) microdialysis probes is examined. Pharmacological agents dexamethasone and XJB-5-131, a reactive oxygen species scavenger, increased blood flow, neurons, and dopamine terminals causing increased evoked dopamine responses in tissue near the probe.[32] Chapter 3 illustrates dexamethasone's ability to preserve evoked dopamine responses near probes for 24 hours. Dexamethasone effects are

limited to the tissue directly surrounding the probe. Probe implantation with and without dexamethasone had no effect on dopamine terminals themselves at 24 hours.[33] This implies that dexamethasone's actions are anti-inflammatory in nature and do not act on dopamine terminals. Chapter 4 exemplifies other anti-inflammatory agents and reactive oxygen species scavengers that improve evoked dopamine responses in tissue near probes. In Chapter 5, potassium ion selective microelectrodes were used in a preliminary study investigating microdialysis probe implantation on the ability to measure potassium changes in surrounding tissue.

Second, Chapter 6 investigates the relationship between the heterogeneity of evoked dopamine release and patch-matrix striatal compartments. Patch-matrix compartments in the striatum receive different dopamine inputs. In this study, the medial and lateral sub-regions of the striatum were found to be distinct with respect to dopamine kinetic diversity. Fast releasing dopamine domains dominate the lateral striatum where as slow releasing dopamine domains were abundant in the medial striatum. We also report strong evidence that fast domains correspond to patch compartments and slow domains to matrix compartments.

2.0 PHARMACOLOGICAL MITIGATION OF TISSUE DAMAGE DURING BRAIN MICRODIALYSIS

The contents of this chapter were previously published in: Nesbitt, K.M., Jaquins-Gerstl, A., Skoda, E.M., Wipf, P., Michael, A.C. *Anal. Chem.* **2013**, *85*, 8173-8179.

I would like to acknowledge that the immunohistochemistry work in this chapter was performed by Andrea Jaquins-Gerstl.

2.1 INTRODUCTION

Microdialysis sampling is used extensively in the chemical analysis of brain tissues in animals and, in some cases, human patients.[8-10, 34] Microdialysis offers several advantages for in vivo studies because the dialysis membrane eliminates cellular debris, blood, and macromolecules from the sample stream, which might otherwise clog or damage analytical systems. This affords a high degree of flexibility in the coupling of analysis techniques to the sampling probes. Furthermore, the probes collect essentially all substances below the membrane's molecular weight cutoff, which varies depending on the type of membrane.[35] For these reasons, applications of brain microdialysis are very broad and continue to expand.[5, 35-38] Increasing the spatial resolution and temporal response of microdialysis sampling is a recent development, with temporal response approaching the timescale of a few seconds in some cases.[1, 39-40]

Despite its several advantages, brain microdialysis suffers from a persistent and challenging problem stemming from the wound that is caused when the probes are inserted into brain tissues.[14-18, 26] Typical probes have a diameter of 220 μm or more, whereas the typical spacing between blood vessels in brain tissue is around 60 μm.[28] Consequently, implanting a microdialysis probe damages blood vessels and causes ischemia in the surrounding tissue.[17-18] The penetration injury activates the brain's astrocytes, which engulf the probe and eventually form a glial scar around it: scar formation is clearly evident 5 days after implanting the probe.[26] Microglia, a second class of brain glial cell, respond to a penetration injury within a few minutes.[41]

The penetration injury results in a progressive disruption of the tissue adjacent to the probe. For example, Holson et al. described progressive declines in the response of dopamine (DA), a neurotransmitter, to several pharmacological challenges (methamphetamine, bupropion, haloperidol, and potassium ion) at 2, 4, and 6 h after implanting the probe.[42-43] The declines depended only on the time since probe implantation and not the type or sequence of the manipulations: the authors concluded that a progressive loss of DA activity occurs in the tissue surrounding the probe. We reached the same conclusion by 'voltammetry next to microdialysis probes'. We used a carbon fiber microelectrode to record DA release in the rat striatum during electrical stimulation of the afferent DA pathway. Implanting a microdialysis probe next to the microelectrode either attenuated or abolished the DA response, providing a direct observation of a progressive decline in DA activity adjacent to the probe.[29, 31]

Penetration injury is not unique to microdialysis probes and is a matter of concern also in the case of neuron recording electrodes, such as those used for brain-machine interfaces.[11-13] A number of laboratories have examined the effects of protective drugs, including dexamethasone,

on the tissue response to neuron recording electrodes.[20-23, 44] Likewise, in a subcutaneous microdialysis study, dexamethasone suppressed the immune response to probes.[25] Motivated by these positive findings, we investigated the retrodialysis of dexamethasone, a potent anti-inflammatory and immunosuppressant glucocorticoid, into the rat striatum. Dexamethasone exhibited a profound ability to restore blood flow and suppress gliosis but only negligibly affected DA microdialysis results.[26] It is possible that the DA results are mainly dependent on the state of the brain tissue immediately adjacent to the probe, where the penetration injury is likely at its most severe.[26] The goal of the present study was to investigate the consequences of the retrodialysis of protective compounds while using voltammetry to measure DA a short distance away from the probe (70-100 μm, see Methods), i.e. at a location where the penetration injury is possibly less severe and thus more amenable to mitigation but also sufficiently close to the probe for effective drug delivery via retrodialysis.

We used voltammetry next to microdialysis probes to record electrically evoked DA release in the rat striatum during the retrodialysis of dexamethasone (DEX) or XJB-5-131 (XJB). Whereas DEX is an anti-inflammatory drug, XJB is a reactive oxygen species (ROS) scavenger targeted with high selectivity to mitochondria.[45-47] Recent studies show that XJB decreases lipid oxidation and improves neurocognitive function in rats after traumatic brain injury.[48] Based on these observations, we hypothesized that XJB might also mitigate penetration injury. We further hypothesized that XJB might be particularly effective at protecting DA axons and terminals, which are highly sensitive to oxidative stress and mitochondrial dysfunction.[49-50] Following voltammetry next to the microdialysis probe, brain tissue containing the probe track was examined by fluorescence microscopy using markers for ischemia (fluorescent nanobeads),

neuronal nuclei (Neu-N), blood born macrophages (ED-1), and DA axons and terminals (tyrosine hydroxylase, TH).

2.2 EXPERIMENTAL SECTION

The procedures used herein have been employed in several prior studies.[17-18, 26, 29, 31] Therefore, only key aspects are described here and additional details are provided as Supplementary Information.

2.2.1 Reagents and Solutions

Artificial cerebrospinal fluid (aCSF: 142 mM NaCl, 1.2 mM $CaCl_2$, 2.7 mM KCl, 1.0 mM $MgCl_2$, 2.0 mM NaH_2PO_4, pH 7.40) was used for voltammetric DA calibration and as the perfusion fluid for microdialysis. Dexamethasone sodium phosphate (APP Pharmaceuticals LLC, Schaumburg, IL) and nomifensine maleate (Sigma Aldrich, St. Louis, MO) were used as received from their respective suppliers. XJB-5-131 was prepared as described by Wipf and coworkers.[45] For retrodialysis, DEX (7.6 μM) and XJB (10 μM) were dissolved in aCSF and aCSF containing 1% DMSO, respectively (we lowered the concentration of DEX slightly compared to our previous study during which an adverse reaction to DEX was observed;[26] the XJB concentration used here is near the solubility limit in 1% DMSO). Nomifensine was dissolved in phosphate-buffered saline (PBS: 155 mM NaCl, 100 mM NaH_2PO_4, pH 7.40) and administered at 20 mg/kg (i.p.). All solutions were prepared with ultrapure water (Nanopure; Barnstead, Dubuque, IA).

2.2.2 Voltammetry and Microdialysis

DA was measured in vivo by fast scan cyclic voltammetry (FSCV) with carbon fiber microelectrodes (7 μm in diameter, 400 μm in length). Concentric-style microdialysis probes (300 μm in diameter, 4 mm in length) were built in-house using membranes with a 13 kDa MWCO (Spectra/Por hollow fiber, Spectrum Laboratories Inc., Rancho, Dominquez, CA). The probe inlet tubing (PE-20) was connected to a syringe pump (Harvard Apparatus, Holliston, MA) running at 0.610 μL/min. The probe outlet tubing (fused silica) was led to waste: the dialysate fluid was not analyzed during this work.

2.2.3 Voltammetry Next to a Microdialysis Probe

All procedures involving animals were approved by the University of Pittsburgh's Animal Care and Use Committee. Voltammetry next to a microdialysis probe was performed in three groups of rats (n=6 rats per group). Each group underwent microdialysis with a different perfusion fluid: aCSF, aCSF with DEX (7.6 μM), or aCSF with XJB (10 μM and 1% DMSO: a fourth group was perfused with aCSF with 1% DMSO but the results are omitted because they were identical to those obtained with aCSF alone).

A carbon fiber voltammetric electrode was inserted into the striatum of an anesthetized rat and a stimulating electrode was lowered into the DA afferent pathway in the medial forebrain bundle (MFB). Electrically evoked release was recorded by FSCV during electrical stimulation of the MFB (stimulus waveform: biphasic, square, constant current pulses at 45 Hz, 300 μA pulse height, 2 ms pulse width, for 25 s). At least three stimulus responses were recorded to

establish a stable, pre-probe response: at least 20 min intervals were inserted between stimulus procedures.

Next, a microdialysis probe was implanted in the same coronal plane as the microelectrode. The final position of the probe was such that the distance between the tip of the microelectrode and the surface of the probe was 70 μm and the distance between the top of the electrode and the probe was 100 μm (Figure 2.1). The relative position of the devices described here is nominal: it is based on adjustments made to the stereotaxic micropositioners (10 μm resolution). We relied on the nominal position because it is not possible to visualize the location of a carbon fiber track without making a lesion:[18] the lesion destroys the tissue and would have prevented the immunohistochemical analysis described in the following section.

Next, 2 h after implanting the probe, three more stimulus responses were recorded: this is now 'voltammetry next to the microdialysis probe'. Each rat then received a single dose of nomifensine (20 mg/kg i.p.), and a final stimulus response was recorded 25 min later.

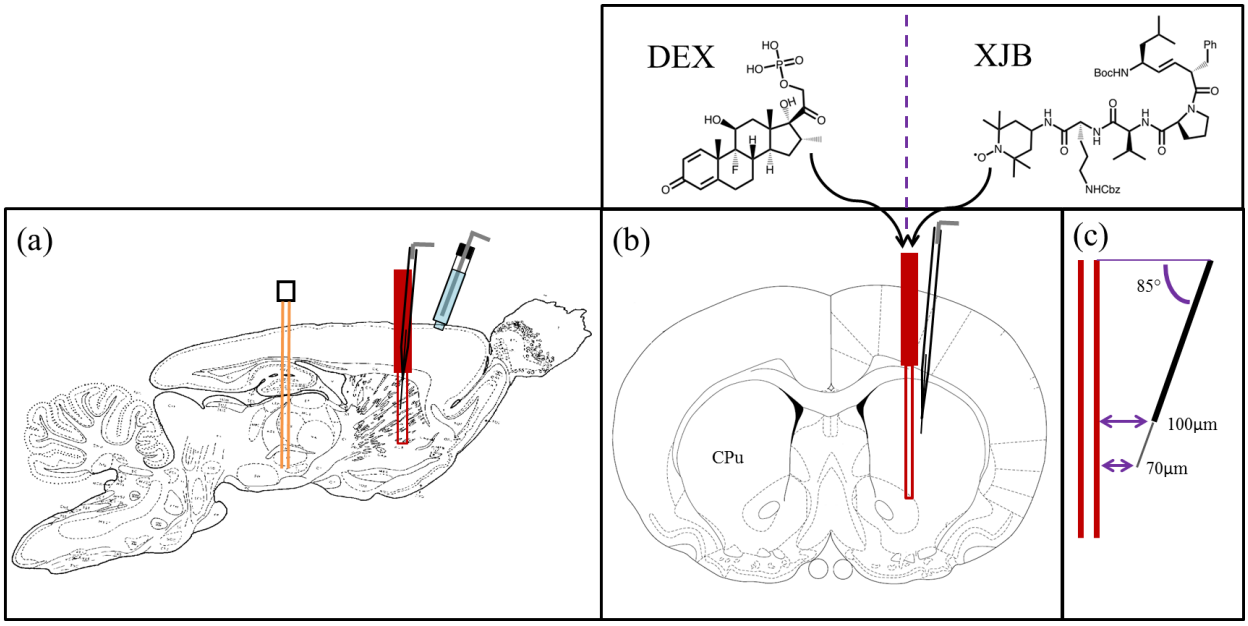

Figure 2.1. **A** schematic of the placement of the devices in the rat brain. (a) A sagittal view of the stimulating electrode (orange) in the MFB, the microelectrode (black) and the microdialysis probe (red) in the striatum (CPu), and the Ag/AgCl reference electrode (blue) in contact with the brain surface. (b) A coronal view showing the microelectrode at a 5° angle from the probe. (c) The tip of the carbon fiber is 70 µm from the probe and the top of the fiber is 100 µm from the probe.

2.2.4 Tissue Fixation and Immunohistochemistry

After recording the stimulus responses, the probe was left in place for a total of 4 h. Then, the rats were systemically perfused through the heart with fixative followed by a suspension of fluorescent nanobeads (Invitrogen, Eugene, OR), after which the tissue was post-fixed.[17-18] The brain tissue containing the microdialysis probe track was sliced in a cryostat and the sections were immunolabeled with antibodies for NeuN (Chemicon, Temecula, CA), ED-1 (AbD Serotec, Raleigh, NC), or TH (Millipore, Temecula, CA).[51] The secondary antibody was goat anti-rabbit IgG-CY3 (Invitrogen, Eugene, OR).

2.2.5 Fluorescence Microscopy and Image Processing

Fluorescence microscopy was performed with a 20X objective (Olympus BX61, Olympus; Melville, NY) and filter sets as appropriate for the nanobeads and IgG-CY3 (Chroma Technology; Rockingham, VT). Quantitative image processing was performed with Metamorph/Fluor 7.1 software (Universal Imaging Corporation; Molecular Devices) and OriginPro. A threshold value was established to eliminate background light from each image and a freehand tool was used to exclude the track and adjacent edge effects from the region of interest (see Supplementary Information for additional details). In the case of tissues labeled with nanobeads and anti-TH, the number of fluorescent pixels was expressed as a percentage of the total number of pixels in the region of interest (% fluorescent pixels). In the case of tissues labeled with anti-NeuN and anti-ED-1, the number of labeled cells was counted and normalized with respect to the area of the region of interest (cells/mm^2). Please note: the procedure used here to quantify the images does not account for differences in the intensity (i.e. brightness) of the fluorescence: this is because the fluorescence intensity is influenced by several factors that are difficult to control, such as the scattering properties of the tissue section, the tissue penetration by the antibody and blocking reagent, the extent of photobleaching, the power of the laser, etc. Statistical analyses of the fluorescent counts from the images obtained with aCSF, DEX, or XJB were based on ANOVA. For comparison, images of non-implanted tissue obtained from the brain hemisphere opposite to the microdialysis probes were processed and counted in the same fashion: results from the opposite hemisphere were omitted from the statistical analyses, which were intended to assess the impact of perfusion conditions on the tissue at the probe tracks.

2.3 RESULTS AND DISCUSSION

2.3.1 Electrically Evoked DA Release

Before implanting the probe, electrical stimulation of the DA afferent pathway evoked robust DA release in the rat striatum (Figure 2.2, blue lines). The solid lines in Figure 2.2 are the average DA concentration measured in each group of animals and the dashed lines are confidence intervals based on the SEM of each data point.

2.3.2 Microdialysis Probes Disrupt Evoked DA Release

In the case of microdialysis probes perfused with aCSF (i.e. no DEX, no XJB), implanting the probe next to the voltammetric electrode abolished all the electrically evoked DA responses. DA was not detected during any of the electrical stimuli applied after implanting the probe. Next, we gave the rats nomifensine (20 mg/kg i.p.), a DA reuptake inhibitor that increases the concentration of DA observed during electrical stimulation procedures.[52-53] Stimulated DA release was observed after the dose of nomifensine (Figure 2.2a, green).

The experiment in Figure 2.2a is similar, but not identical, to those reported previously by Borland et al. and by Wang and Michael.[29, 31] In the current work, we placed the microelectrode 150 μm closer to the probe, so the responses in Figure 2.2 are smaller than those we reported before. We decreased the spacing during this work in order to increase the likelihood that the microelectrode would be in the diffusion zones of DEX and XJB in the following experiments.

The response obtained after nomifensine administration (Figure 2.2a, green) has an interesting feature. That is, the DA signal is detected right away when the stimulus begins, i.e. during the first FSCV scan performed 250 ms after the stimulator is activated. Using the reported diffusion coefficient of DA in the rat striatum, 2.4x10-6 cm^2/s,[54] the average diffusion distance in 250 ms is ~11 μm. Thus, the DA detected when the stimulus begins was released from DA terminals in close proximity to the microelectrode. This supports a previous suggestion from our laboratory that some surviving DA terminals are present near the microelectrode, although they may be in a suppressed state.[31] This motivates our on-going efforts to protect and preserve the activity of those surviving DA terminals.

2.3.3 DEX and XJB Preserve Evoked DA Activity Next to Microdialysis Probes

In the case of microdialysis probes perfused with DEX, implanting the probe next to the microelectrode diminished, but did not abolish, electrically evoked DA release (Figure 2.2b, red). Thus, retrodialysis of DEX diminished the loss evoked DA activity, possibly indicating improved survival of DA terminals in the tissue near the probe. To facilitate comparison with the results obtained using probes perfused with unmodified aCSF, we again recorded a stimulus response after treating the animals with nomifensine (Figure 2.2b, green): DEX substantially enhanced the amplitude of the post-nomifensine response. Implanting probes perfused with XJB also had beneficial effects on evoked DA release: similarly to DEX, XJB diminished but did not abolish evoked DA release next to the microdialysis probe (Figure 2.2c, red), although XJB was less effective than DEX in this regard (and see Figure 2.3, below, for statistical evaluation). However, similarly to DEX, XJB substantially enhanced the amplitude of the post-nomifensine response (Figure 2.2c, green). As was the case during aCSF perfusion, DA was rapidly detected

at the start of the stimulus after nomifensine administration, indicating the presence of surviving DA terminals in close proximity to the voltammetric microelectrode. Overall, these results confirm that both DEX and XJB preserved DA activity in the tissue next to the microdialysis probes.

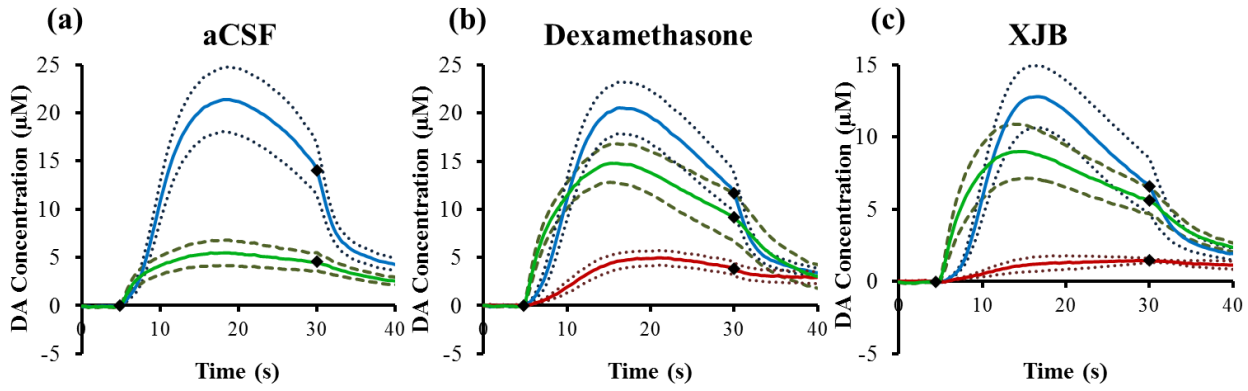

Figure 2.2. The effect of aCSF (a), DEX (b), or XJB (c) on electrically evoked DA responses measured before implanting the probe (blue lines), 2 h and 40 min after implanting the probe (red lines, the response was non-detectable in a), and 25 min after nomifensine (green lines). The solid lines are the average of the responses in each group of rats (n=6 per group) and the broken lines are confidence intervals based on the standard error of the mean of each data point. The black diamonds show when the stimulus begins and ends.

2.3.4 Statistics

To facilitate statistical analysis of these results, we prepared a histogram of the maximum DA response amplitudes normalized with respect to the maximum amplitude of the responses recorded before each probe was implanted (Figure 2.3). In the case of perfusion with aCSF, no DA was detected before nomifensine administration. Therefore, we used one-sample, one-tailed t-tests to compare the DEX and XJB (Figure 2.3, red bars) results to zero: both DEX and XJB significantly increased the evoked response amplitude. The normalized nomifensine results

(Figure 2.3, green bars) were subjected to a one-way ANOVA and posthoc Tukey test. Both DEX and XJB significantly increased the post-nomifensine response amplitude. These findings demonstrate that perfusion with DEX or XJB preserves robust DA uptake activity in the tissue nearby the microdialysis probes. This robust DA uptake activity likely contributed to keeping the pre-nomifensine amplitudes small. The responses observed after uptake inhibition by nomifensine, therefore, more directly reflect the protection of DA release afforded by DEX and XJB. Based on Figure 2,3, we conclude that both DEX and XJB significantly attenuate the loss of DA activity in the tissue near the microdialysis probes.

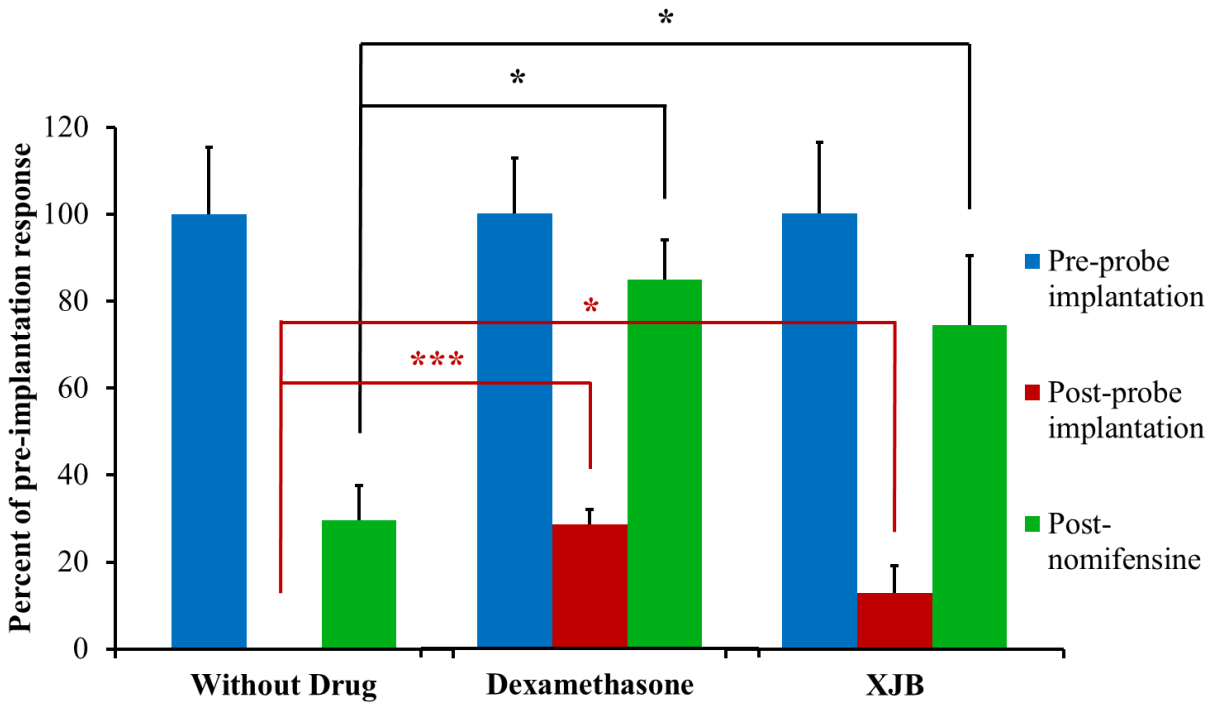

Figure 2.3. The amplitude of evoked DA responses in the rat striatum in the presence of probes perfused with aCSF, DEX, or XJB. The response amplitudes observed after implanting the probes (red) and after nomifensine (green) are normalized with respect to the amplitude observed before implanting the probes (blue = 100%). The bars show the mean ± SEM (n=6 rats per group) of the normalized results. DEX significantly increased evoked DA after implanting the probe (one-sample t-test: $t(5)=8.208$, $p<0.0005$). XJB significantly increased evoked DA after implanting the probe (one-sample t-test: $t(5)=2.015$, $p<0.05$). Both DEX and XJB significantly increased evoked DA after nomifensine administration (one-way ANOVA: $F(2,15)=7.43$, $p=0.006$; and Tukey posthoc test: $p<0.05$. and $p<0.05$ respectively). *$p<0.05$, ***$p<0.0005$.

2.3.5 DEX and XJB Mitigate the Histochemical Effects of Microdialysis Probes

We used fluorescence microscopy to examine thin horizontal sections of brain tissue containing the tracks of the microdialysis probes perfused with aCSF, DEX, or XJB (Figure 2.4). For comparison, Figure 2.4 includes images of non-implanted control tissue (taken from the brain hemisphere opposite to the microdialysis probe) immunolabeled in the same fashion as the probe

tracks. As we have reported before, probes perfused with unmodified aCSF caused profound ischemia (diminished blood flow), as indicated by a near-total absence of fluorescent nanobeads in the tissues surrounding the probe tracks.[17-18] Both DEX and XJB increased the presence of nanobeads near the probe tracks (see Figure 2.5, below, for statistical evaluation), indicating in both cases a decrease in ischemia. However, DEX was more effective in this regard, which is consistent with DEX's classification as an anti-inflammatory drug.

Probes perfused with unmodified aCSF decreased NeuN labeling, indicating a loss of striatal neurons near the probes, and increased ED-1 labeling, indicating the infiltration and activation of macrophages near the probes. The ED-1 marker specifically labels blood-derived macrophages and so indicates an opening of the blood-brain barrier.[55] Both DEX and XJB increased NeuN labeling and decreased ED-1 labeling, indicating that both compounds protected the brain tissue near the probes.

In non-implanted striatal tissue, TH labeling is punctate, corresponding to the size and distribution of DA axons and terminals. Probes perfused with unmodified aCSF eliminated the punctate labeling in the surrounding tissue. Intense labeling was observed at the edges of the probe track but this was not punctate and likely reflects non-specific binding.[56] The loss of punctate TH labeling does not necessarily mean a loss of DA axons and terminals, but rather that the axons and terminals have lost their TH. Despite this caveat, the images confirm that probes perfused with aCSF profoundly disrupt DA axons and terminals. Both DEX and XJB diminished the non-specific edge effect and preserved punctate TH labeling.

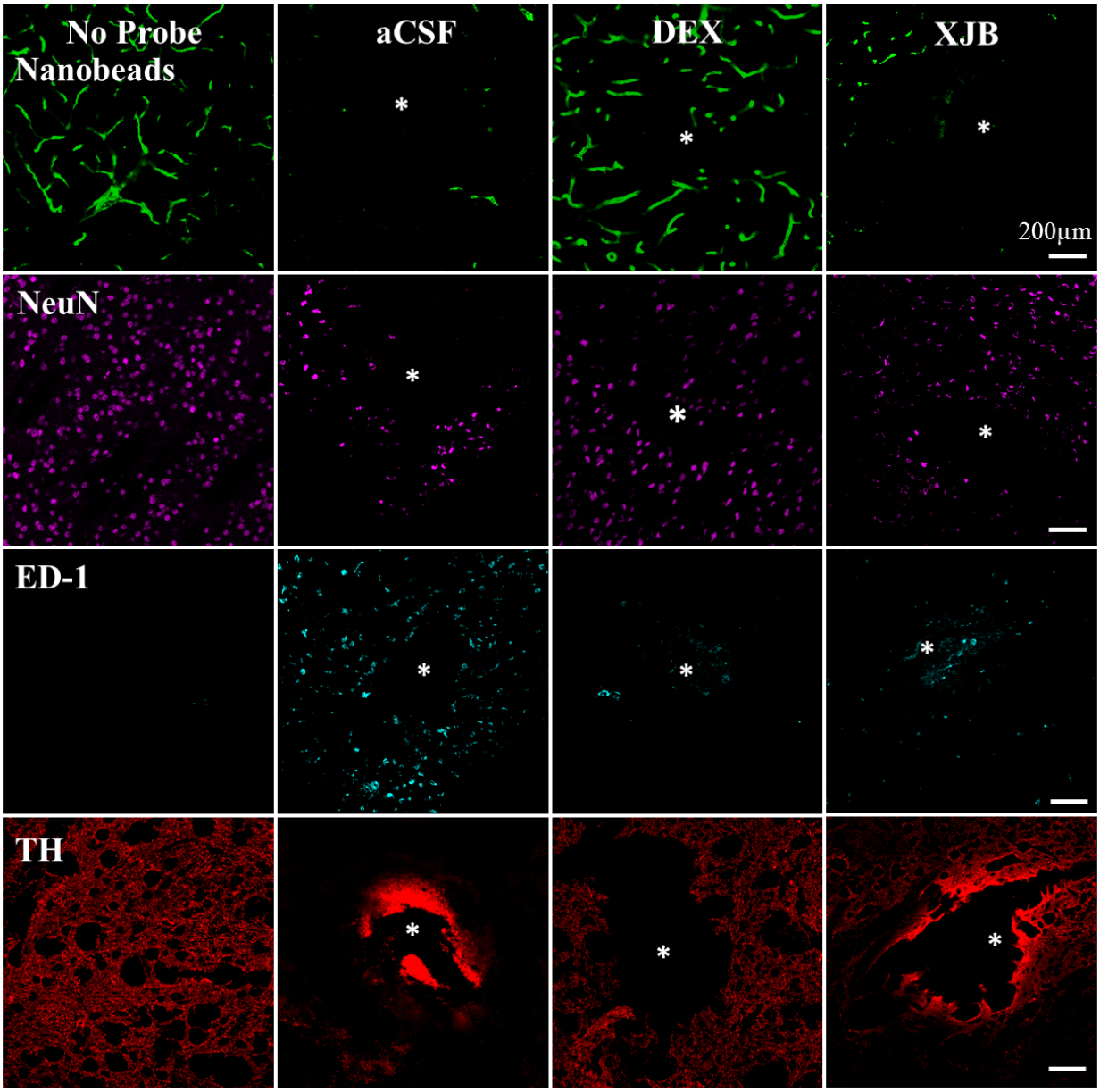

Figure 2.4. DEX and XJB mitigate the histochemical impact of penetration injury. Separate columns provide representative images of tissue after retrodialysis of aCSF, DEX, and XJB for 4 h. The left-most column shows images of non-implanted control striatal tissue. Separate rows provide representative images of tissue labeled with markers for blood flow (nanobeads), neuronal nuclei (NeuN), macrophages (ED-1), and dopamine axons and terminals (TH). The probe track is in the center of the images and marked with an asterisk. Scale bars are 200 µm.

2.3.6 Statistics

We quantified these images using Metamorph's built-in tools. After setting a threshold fluorescence intensity for each image, the software quantified the percentage of pixels exhibiting nanobead and TH fluorescence, and counted the number of NeuN-positive and ED-1-positive cells in the region of interest: the quantitative results are reported as histograms in figure 2.5. The numerical results for each marker were subjected to one-way ANOVA (details in the figure legend). Compared to probes perfused with unmodified aCSF, retrodialysis of DEX significantly increased nanobead, NeuN, and TH labeling, and significantly decreased ED-1 labeling. Retrodialysis of XJB significantly increased NeuN labeling and decreased ED-1 labeling. Retrodialysis of XJB also increased nanobead and TH labeling, but these effects were not statistically significant.

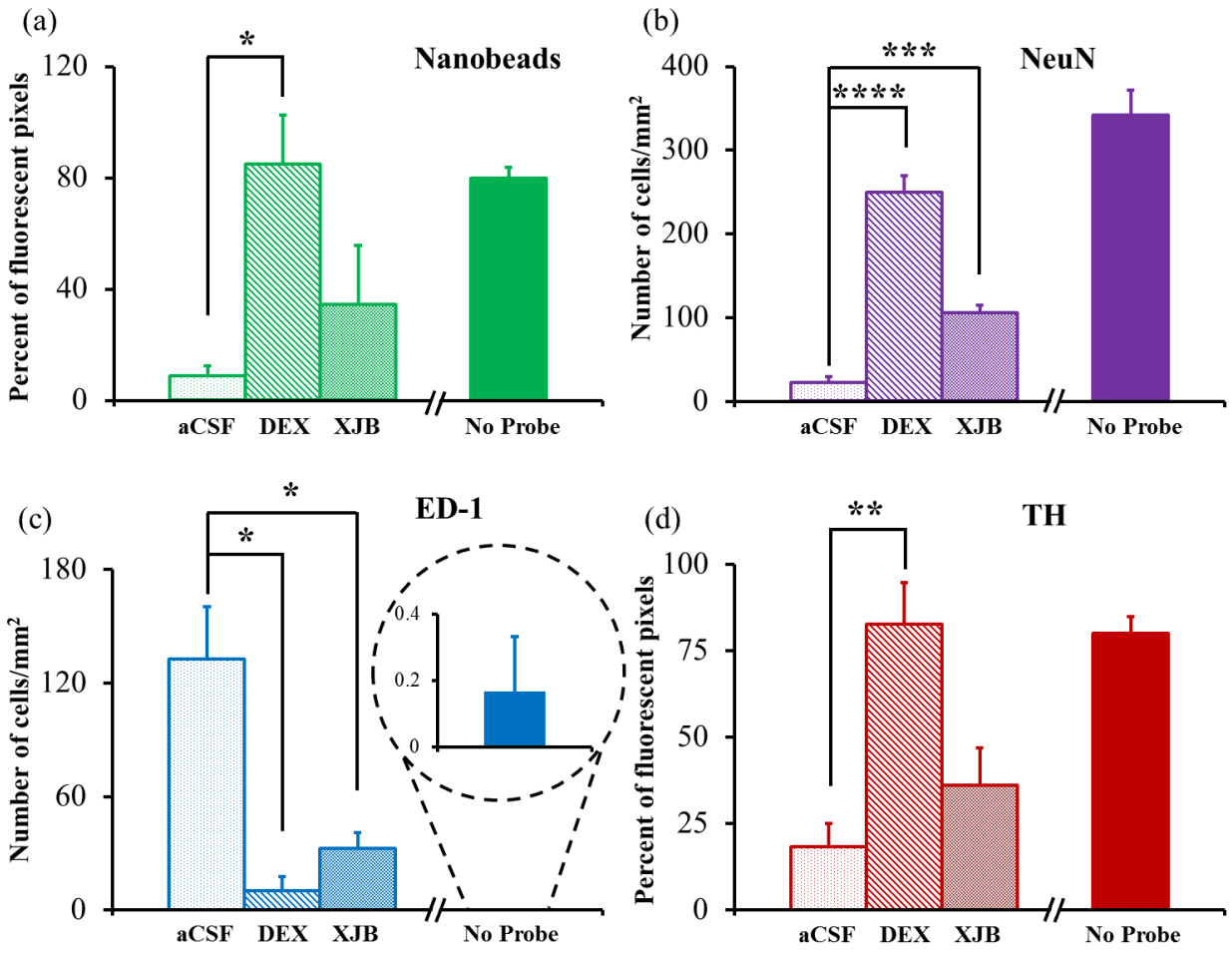

Figure 2.5. Normalized counts of the individual histochemical markers were performed in the region of interest in horizontal tissue sections containing the track of the microdialysis probes. Nanobead (a) and TH (d) results are reported as the percentage of fluorescent pixels (mean± SEM). NeuN (b) and ED-1 (c) results are reported as the number of cells/mm2 (mean± SEM). Statistical analyses were performed by one-way ANOVA and Tukey or Tamhane T2 post hoc tests: *p<0.05, **p<0.005, ***p<0.00005, ****p<0.00000005. Images of non-implanted tissue from the brain hemisphere opposite the microdialysis probes were quantified by the same procedures (no-probe) but omitted from the ANOVAs.

2.3.7 Correlation of Voltammetry and Immunohistochemistry

Our findings reveal, for the first time, a general correlation between the ability of DEX and XJB to preserve DA activity as assessed by voltammetry next to microdialysis probes and their ability to protect the tissue near the probes as assessed by immunohistochemical labeling. The most direct correlation can be expected between DA activity and punctate TH labeling, since DA activity derives from DA axons and terminals. Figure 2.6 compares TH images with the DA responses taken from the same tissue: the white box in each image identifies the nominal location of the microelectrode. Even from this small sampling, it is clear that the intensity of the punctate TH labeling near the probe correlates with the amplitude of the stimulus response. Note that in the case of the probe perfused with unmodified aCSF, the bright TH labeling is non-punctate: it is the non-specific edge effect explained above.

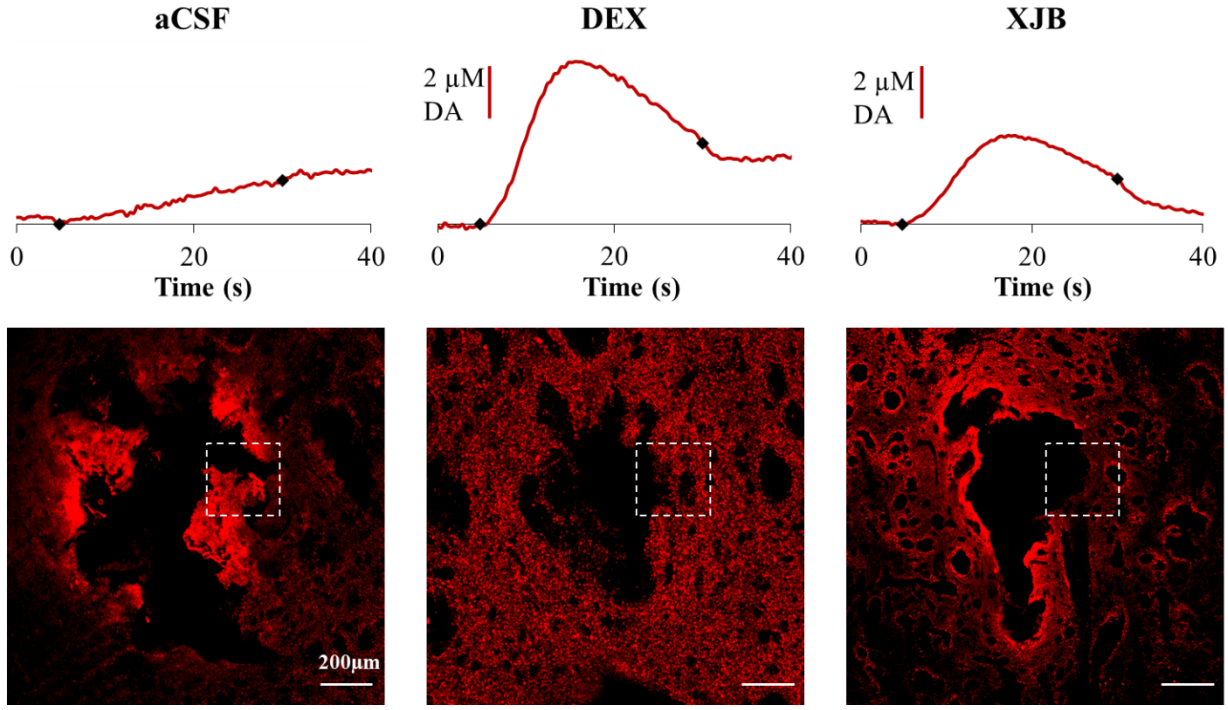

Figure 2.6. Correlation of voltammetry next to a microdialysis probe with TH immunohistochemistry. Individual DA responses recorded after implanting the probe (without nomifensine) are compared with the TH immunohistochemistry from the same rat. The white box indicates the nominal position of the microelectrode. Columns represent retrodialysis of aCSF, DEX, and XJB for 4 h. Scale bars are 200 µm.

2.4 CONCLUSION

The present study confirms that retrodialysis of dexamethasone or XJB-5-131 mitigates penetration injury during brain microdialysis. Both compounds protected striatal DA activity as assessed by voltammetry next to microdialysis probes and both also mitigated the histochemical effects of the penetration injury. The general correlation between the effects of DEX and XJB on DA activity and observed histochemical changes is potentially significant, because reports on

the impact of neuroprotection strategies on the tissue responses to implanted devices are expanding rapidly.[57-60]

The protective effects observed during this study were partial, as neither the evoked DA activity nor the histochemical attributes of the tissue near the probe were preserved in their normal, completely uninjured state. Nevertheless, the mitigation observed during this study is substantially larger than during our previous observations of DA no-net-flux, which were negligibly affected by DEX.[26] Thus, as we anticipated, the tissue even a small distance from the probe (70-100 μm) appears to be more amenable to protection by DEX and XJB. However, it is important to appreciate that measuring DA via microdialysis is an especially challenging task due to DA reuptake, which rapidly removes DA from the extracellular space and limits how far it can diffuse. This challenge is illustrated by the large impact of the DA reuptake inhibitor, nomifensine, on the evoked DA responses. Accordingly, we conclude that even though DEX and XJB protected the tissue 70-100 μm from the probe, DA's ability to diffuse across the gap to the microdialysis probe was constrained, as usual, by reuptake. It is important to appreciate this point because microdialysis has applications to numerous other substances of interest that are not subject to such avid reuptake. It will be of great interest in the future to examine the effect of DEX, XJB, and other candidates on the microdialysis of substances other than DA.

Finally, this investigation focused on acute implants only 4 h in duration. Tremendous interest in chronic implants exists as well, and in particular, XJB has demonstrated significant efficacy in long-term neuroprotective studies.[61] We reason that any protective strategy must be effective during the acute phase of the implant in order to preserve the tissue into the chronic phases, i.e. cell death in the acute phase is unlikely to be reversible. Accordingly, we envision

that successful acute mitigation is needed as a precursor to successful chronic mitigation of penetration injury effects.

2.5 SUPPLEMENTARY INFORMATION

2.5.1 Fast Scan Cyclic Voltammetry

Carbon fiber microelectrodes were constructed by pulling borosilicate capillaries (0.58 mm I.D., 1.0 mm O.D., Sutter Instruments, Novato, CA) to fine tips around a single carbon fiber (7 µm diameter, T650, Cytec Carbon Fibers LLC., Piedmont, SC) with a vertical puller (Narishing Tokyo, Japan). The tips were sealed with a low viscosity epoxy (Spurr Epoxy, Polysciences Inc., Warrington, PA) and cured overnight at 70 ºC. The exposed fibers were cut to a length of 400 µm. The capillaries were filled with mercury and a nichrome wire (Goodfellow, Oakdale, PA) was inserted to complete electrical contact. Microelectrodes were pre-treated by soaking the tip in isopropyl alcohol (Sigma Aldrich, St. Louis, MO) containing carbon decolorizing (Fisher Scientific, Pittsburgh, PA) for one hour.

Fast scan cyclic voltammetry was performed using a computer controlled potentiostat (EI-400, Ensman Instruments, Bloomington, IN) and CV Tarheels version 4.3 software (Michael Heien, University of Arizona, Tucson AZ). The potential was applied between a Ag/AgCl reference electrode and a carbon fiber working electrode. The potential was ramped at a scan rate of 400 V/s from 0 V to 1 V, then to -0.5 V, and then back to 0 V. Scans were performed at 2.5 Hz. Dopamine (DA) oxidation peaks were monitored between 0.6 V and 0.8 V on the initial potential sweep. DA voltammograms were created by background subtraction. DA current was

converted to DA concentration by post-calibration of electrodes in a flow cell with at least three different concentrations of DA (Sigma Aldrich, St. Louis, MO) dissolved in nitrogen purged artificial cerebrospinal fluid (aCSF).

2.5.2 Animal and Surgical Procedures

All procedures involving animals were approved by the Institutional Animal Care and Use of Committee of the University of Pittsburgh. Male Sprague-Dawley rats (250-350 g) were intubated, anesthetized with isofurane (0.5 % by volume, Baxter Healthcare, Deerfield, IL), placed in a stereotaxic frame and wrapped in a heating blanket. The scalp was shaved and the skull was exposed. Three holes were drilled through the skull and the dura was carefully cut away to expose the brain. The incisor bar was adjusted so that the dorsal ventral measurements at lamda and bregma were no more than 0.01 mm apart (flat skull).

Evoked DA release was measured with microelectrodes 70-100 µm away from probes. Electrical connection between the brain and a Ag/AgCl reference electrode was achieved by creating a salt bridge with a Kimwipe soaked in aCSF and placed in a plastic pipette tip. A microelectrode was implanted into the striatum at a 5° angle from the vertical (0.7 mm anterior from bregma and 5.0 mm below dura). A bipolar stimulating electrode (MS303-1-untwisted, Plastics One, Roanoke, VA) was lowered into the ipsilateral medial forebrain bundle (MFB, 4.3 mm posterior from bregma, 1.2 mm lateral from midline, and 7.2 mm below dura) until evoked DA release was detected in the striatum.

Evoked release was measured three times at 20 min intervals. A microdialysis probe perfused with aCSF, aCSF with dexamethasone (DEX) or aCSF with XJB-5-131(XJB) was lowered into the striatum over the course of 30 min in the same coronal plane as the

microelectrode (0.7 mm anterior to bregma, 2.5 mm lateral from midline, and 7 mm below dura). Two hours after implantation, stimulation of the MFB resumed at 20 min intervals. Nomifensine (20 mg/kg) was administered by intraperitoneal (i.p.) injection after the third stimulus and evoked release was measured 25 min later.

2.5.3 Statistics

Statistical analysis was performed with SPSS software. The statistical tests used for each analysis are explained in the results and discussion section.

2.5.4 Tissue Processing and Immunohistochemistry

The tissue was fixed by transcardial perfusion with 200 mL of 0.2 g/mL phosphate buffer saline (1x PBS: 155 mM NaCl, 100 mM phosphate, pH 7.40) followed by 250 mL of 4 % paraformaldehyde (PFA) and 50 mL of 0.1 % fluorescent nanobeads (Invitrogen, Eugene, OR). After the brains were removed, the tissue was postfixed for 2 h in 4 % PFA, soaked overnight in 30 % sucrose at 4 °C for cryoprotection, and stored at -80 °C until sliced. For TH staining, brains were postfixed for 24 h in cold 4 % PFA and then sectioned.

Horizontal tissue sections (perpendicular to the probes) were cut at 30 or 40 µm using a cryostat. For NeuN and ED-1 labeling, the slides were stored at -20 °C, washed three times in 1x PBS, incubated with Triton X-100 in PBS for 15 min, washed in 0.5 % bovine serum albumin (BSA), and soaked in 2 % BSA for 45 min. Then, the sections were incubated with antibody (NeuN or ED-1) for 1 h at room temperature, rinsed repeatedly in 0.5 % BSA, and incubated with the secondary antibody in 0.5 % BSA for 1 h at room temperature. Sections were rinsed in

0.5 % BSA and 1x PBS. For TH labeling, the sections were rinsed multiple times in 1x PBS at room temperature for 1 h, incubated in a blocking solution containing 2 % BSA, 0.3 % Triton X-100 in 1x PBS for 1 h at room temperature. Free floating sections were incubation with the TH antibody in the blocking solution at room temperature for 2 h followed by incubation at 4 ^{0}C for 48 h. Sections were rinsed three times for 10 min each in 1x PBS and incubated with the secondary antibody in blocking solution for 1 h at room temperature. Sections were then covered with gelvatol mounting medium (polyvinyl alchohol, gycerol, Tris buffer pH 8.5, and sodium azide in water) and coverslipped.

2.5.5 Image Processing and Quantification

As explained in the main text (see Fluorescence Microscopy and Image Processing), normalized counts of the four histochemical markers were obtained from images after the images were treated with a threshold to eliminated scattered light and after the use of a freehand graphics cursor to eliminate the probe track and its edges (in the case of tissues labeled for TH) from the region of interest. Figure S2.1 illustrates these procedures by means of an example. Figure S2.1a is a raw image (not yet processed) of tissue surrounding a microdialysis probe track labeled with a primary antibody for tyrosine hydroxylase and a secondary antibody tagged with CY3. Note that the entire image is at least slightly red, including the center of the probe track that contains no tissues. This pale red background is due to light scattering. The first step in image processing is to set a threshold value to eliminate the background (Figure S2.1b): setting the threshold is a built-in function in Metamorph. Once the user has set the threshold intensity, the software turns off any pixel with a subthreshold intensity value. This removes the pale background (note in Figure S2.1b that the center of the probe track now appears black) but does not affect other

features of the image. Figure S2.1c shows a line drawn by means of a freehand graphics cursor tool in the software package. This line is placed around the probe track and its brightly labeled edges. In TH-labeled images such as this, the edges of the probe track exhibited bright fluorescence but this is most likely nonspecific binding. Inspection of the edge feature at high magnification did not reveal the expect pattern of labeling of axons or terminals. The software is then instructed to define the region of interest as that portion of the image outside the freehand line. Prior to counting, the software turns each pixel with an intensity above the threshold to white and leaves pixels with sub-threshold intensity black (Figure S2.1d). The software then counts and reports the number of black and white pixels in the defined region of interest. Note, this procedure reports just a count of the number of above-threshold pixels and does not attempt to account for variations in fluorescence intensity. This is a typical approach to quantifying images such as these, because the fluorescence intensity can be affected by several factors, such has how well the antibody penetrates the tissue slice, etc., that are difficult to control from one image to the next.

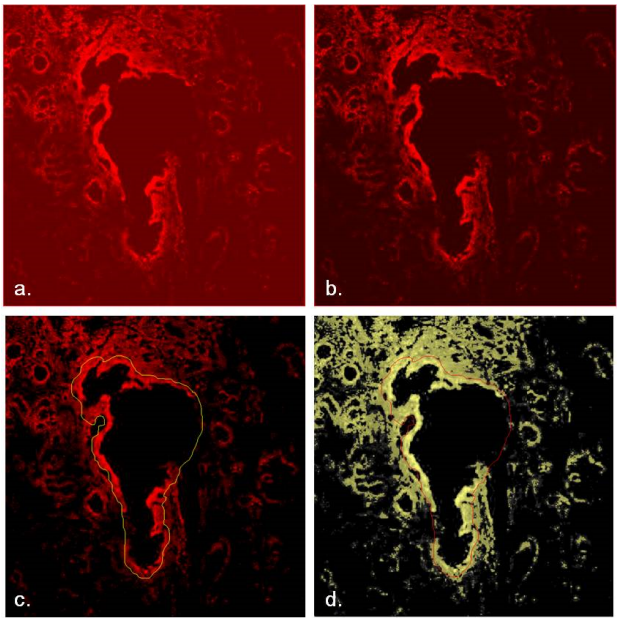

Figure S2.1. Representative images of labeled brain tissue surrounding a microdialysis probe track. The tissue has been labeled with primary antibody for tyrosine hydroxylase and secondary antibody tagged with CY3. Images were processed using Metamorph software. The probe track is in the center of the each image. a) The raw image as imported into Metamorph. b) The same image after setting the threshold. c) The thin line was placed with a freehand graphics cursor. The region of interest is the portion of the image outside the freehand line. d) Prior to counting, pixels above the threshold are set to white and pixels below the threshold are left black. The software reports the number of white and black pixels in the region of interest.

3.0 MICRODIALYSIS IN THE RAT STRIATUM: EFFECTS OF 24-HR DEXAMETHASONE RETRODIALYSIS ON EVOKED DOPAMINE RELEASE AND PENETRATION INJURY

The contents of this chapter were previously published in: Nesbitt, K.M., Varner, E.L., Jaquins-Gerstl, A., Michael, A.C. *ACS Chem. Neurosci*. **2015**, *6*, 163-173.

I would like to acknowledge that the immunohistochemistry work in this chapter was performed by Andrea Jaquins-Gerstl.

3.1 INTRODUCTION

Intracranial microdialysis has made multiple seminal contributions to our knowledge of the neurochemistry of the living brain.[5, 8, 34, 62-72] The benefits and power of microdialysis for intracranial chemical monitoring, which are well known and have been reviewed often,[35, 37, 73-79] stem from the efforts of many laboratories to refine both the microdialysis probes and the instrumental methods used to analyze dialysate samples.[4, 39, 80-83] There has been tremendous progress, for example, in lowering the detection limits for key substances, including neurotransmitters, which has in turn reduced sampling times and increased temporal resolution.[36, 38, 84-86] Here, we wish to contribute to this on-going refinement effort by focusing attention on what happens when the probes are implanted into brain tissue.

Typical microdialysis probes, those in widespread use, have diameters of at least 250 μm.[37, 43, 87-88] Implanting these into the brain causes tissue damage, which in turn triggers a wound response.[14-18, 26, 32, 89-94] The wound response involves a cascade of events, some of which begin right away and some of which develop over the course of several days. Microglial cells respond within minutes to focal brain injury whereas astrocytes respond later.[41, 95] Astrocytes form a scar around microdialysis probe tracks by 5 days post implantation.[26] Probe implantation also causes ischemia, disruption of the blood brain barrier, and neuron loss.[17-18, 26, 32] Neurochemical instability over the post-implantation intervals has been reported as well.[29, 31, 42-43, 87, 96-98] Even so, the dialysate content of neurotransmitters exhibits sensitivity to tetrodotoxin,[71] responds predictably to various drugs,[80, 99-101] and correlates with behaviors.[5, 35, 67, 78, 102] These observations show that microdialysis provides valid and useful indices of neurochemical activity. Nevertheless, evidence of neurochemical instability over the post-implantation time window has been a long-standing issue in the field.

We hypothesize that mitigating disruption of the tissue near the probes would continue the refinement of intracranial microdialysis. To date, we have obtained encouraging results from the retrodialysis of dexamethasone (DEX), an anti-inflammatory drug, and XJB-5-131 (XJB), a novel scavenger of reactive oxygen species.[32] During acute experiments conducted 2-4 hr after implanting microdialysis probes, both DEX and XJB diminished the loss in amplitude of evoked dopamine (DA) responses measured by fast-scan cyclic voltammetry (FSCV). Histochemical studies provide clear indications that DEX and XJB offer anti-inflammatory protection of the tissues surrounding the probes. Without DEX or XJB, the probes cause ischemia, disrupt endothelial cells, activate both astrocytes and microglia, and cause a loss in both neurons and

axons near the probe tracks.[32] DEX was slightly more effective than XJB.[32] DEX retrodialysis for 5 days prevented the formation of a glial scar.[26]

We implanted microdialysis probes in the rat striatum for 4 and 24 hr, both with and without DEX in the perfusion fluid, and then measured evoked DA release next to probes with FSCV. We report here for the first time that DEX significantly diminishes the loss in amplitude of evoked responses measured in the tissue next to the probe both at 4 and 24 hr after implanting the probes. Surprisingly, DEX had no significant effect on two key tissue markers for dopamine terminals, tyrosine hydroxylase (TH) and the dopamine transporter (DAT): 24 hr after probe implantation, these markers were not significantly different than in control, non-implanted tissues. We therefore attribute DEX's effects on evoked dopamine responses next to microdialysis probes to its anti-inflammatory actions, as opposed to any direct actions on dopamine terminals. Finally, we report for the first time that the penetration of DEX into the tissue near the probe is extremely limited. Fluorescein-labeled DEX was found no further than 80 μm from its delivery probe. Moreover, DEX failed to abolish gliosis near a second probe placed 2 mm from the probe with DEX. We therefore conclude that DEX's anti-inflammatory actions are tightly confined to the immediate, local vicinity of the probe.

3.2 EXPERIMENTAL SECTION

The methods used during this study have been described previously.[17-18, 26, 29, 31-32] We provide key details here and full descriptions in the Supporting Information document.

3.2.1 Reagents and Solutions

All solutions were prepared with ultrapure water (Nanopure, Barnstead, Dubuque, IA). All reagents were used as received from their suppliers. Artificial cerebrospinal fluid (aCSF: 142 mM NaCl, 1.2 mM $CaCl_2$, 2.7 mM KCl, 1.0 mM $MgCl_2$, 2.0 mM NaH_2PO_4, pH 7.4) was the perfusion fluid for microdialysis. DEX sodium phosphate (DEX, APP Pharmaceuticals LLC Schaumburg, Il) was diluted to 10 μM in aCSF. This dose was used as we have previously observed a dramatic reduction in tissue disruption at 10 μM DEX for 24 hr.[26] DEX fluorescein (DEX-FL, Life Technologies Grand Island, NY) was diluted to 10 μM in aCSF. Nomifensine maleate and S(-)-raclopride (+)-tartrate salts (Sigma Aldrich, St. Louis, MO) were dissolved in phosphate-buffered saline (PBS: 155 mM NaCl, 100 mM NaH_2PO_4, pH 7.40) and administered at 20 mg/kg (i.p.) and 2 mg/kg (i.p.) respectively. Isopropyl alcohol (Sigma Aldrich, St. Louis, MO) and decolorizing carbon (Fisher, Pittsburgh, PA) were used to pre-treat carbon fiber electrodes for DA voltammetry. DA (Sigma Aldrich, St. Louis, MO) standards were prepared in nitrogen-purged aCSF.

3.2.2 Microdialysis Probes

Concentric microdialysis probes (300 μm diameter, 4 mm length) were constructed with hollow fiber membranes (13 kDa MWCO, Specta/Por RC, Spectrum Laboratories Inc., Ranco Dominguez, CA). The inlet tubing (PE, Becton Dickinson, Franklin Lakes, NJ) was connected to a 1-mL gas tight syringe driven by a microliter syringe pump (Harvard Apparatus, Holliston, MA) at a rate of 0.610 μL/min. The outlet was a fused silica capillary (75 μM I.D., 150 μM O.D.,

10 cm long; Polymicro Technologies, Phoenix, AZ). Probes were perfused with either aCSF or aCSF containing 10 μM DEX.

3.2.3 Microdialysis Probe Implantation

All procedures involving animals were approved by the University of Pittsburgh's Animal Care and Use Committee. Male Sprague-Dawley rats (250-350g; Hilltop, Scottsdale, PA) underwent sterile stereotaxic surgery under isoflurane anesthesia. The probes were lowered into the brain at 5 μm/sec with an automated micropositioner (Model 2660, David Kopf Instruments, Tujunga, CA) and secured to the skull with screws and acrylic cement. Following surgery, the rats were placed in a Raturn Microdialysis Bowl (MD-1404, BASI, West Lafayette, IN) and the probes were perfused with aCSF or DEX for 24 hr.

3.2.4 Voltammetry next to Microdialysis Probes

Voltammetry next to microdialysis probes was performed in two groups of rats (n=6 rats per group). An additional control group (n=5) underwent an initial surgical procedure without probe implantation (a sham control). Four-hour maximum dopamine amplitudes previously collected43 were used for probe temporal comparisons (Figure. 3.4 - 4 hr results).

After spending 24 hr in the Raturn bowl the rats were anesthetized a second time and returned to the stereotaxic frame. A carbon fiber electrode (400 μm in length) was implanted in the same coronal plane as the probe. As before,[32] the electrode was implanted an angle of 5° from vertical so that it could be placed very close to the probe. At its final location, the tip of the carbon fiber was 70 μm and the base of the fiber (where it meets the tip of the glass capillary)

was 100 μm from the probe: we call this the E1 location (Figure S3.1). A second carbon fiber was implanted vertically 1 mm posterior to and in the same sagittal plane as the probe: we call this the E2 location (Figure. S3.1). The relative position of the two carbon fibers to the probe is nominal: it is based on the adjustments made using stereotaxic micropostioners (10 μm) resolution.[32]

A stimulating electrode was lowered towards the MFB until evoked DA was detected at E2 (stimulus waveform: biphasic, square, constant current). The parameters for subsequent stimuli are listed in the Results and Discussion section.

3.2.5 Tissue Immunohistochemistry

After the in vivo measurements, the rats were deeply anesthetized and the brain tissues were collected for immunohistochemical analysis.[18] Thin horizontal sections (35 μm) were cut in a cryostat at -21 to -22°C and labeled together with antibody for tyrosine hydroxylase (TH; 1:1000, Millipore, Temecula, CA) and the DA transporter (DAT; 1:400, Synaptic Systems, Göttingen, Germany). The secondary antibody was goat anti-rabbit IgG-Cy3 or IgG-Cy5 (Invitrogen, Eugene, OR). In another group of rats, probes perfused with DEX-FL were implanted for 4 hr. Tissue processing details can be found the Supporting Information. In an additional group of rats, two probes were implanted 2 mm apart, one perfused with aCSF and the other perfused with DEX for 24 hr. Tissue sections (30 μm) were then stained with antibodies for GFAP (BD Biosciences Pharmingen, San Diego, CA). Fluorescence and optical differential interference contrast (DIC) images were acquired with an Olympus BX61 (Olympus; Melville, NY) equipped with a 20x objective. Non-implanted tissue (from the hemisphere opposite the microdialysis probe) was used as control tissue. Quantitative image analysis was performed with

NIS-Elements Advanced Research-version 4.00 software (Nikon Instruments Inc., Melville, NY). See Figure. S3.5 for further details.

3.2.6 Statistics

IBM Statistical Package for the Social Sciences (SPSS) 22 software was used for all statistical analysis.

3.3 RESULTS AND DISCUSSION

3.3.1 Characteristics of Evoked DA Release in the Rat Striatum

Electrical stimulation of DA axons in the medial forebrain bundle (MFB) evokes DA release in the ipsilateral striatum, which is easily measurable by FSCV (Figure. 3.1a).[103-106] We measured evoked dopamine responses both in the absence of microdialysis probes and with microelectrodes positioned 70-100 μm (E1) and 1 mm (E2) from the probes (Figure. S3.1). In the absence of a microdialysis probe, there is no significant difference in the amplitude of evoked responses (45 Hz, 300 μA, 25 s) measured at the E1 and E2 locations (Figure. 3.1a and 3.2). The 24-hr sham control surgery (see Methods) had no significant effect on the response amplitudes measured at E1 (Figure. S3.2).

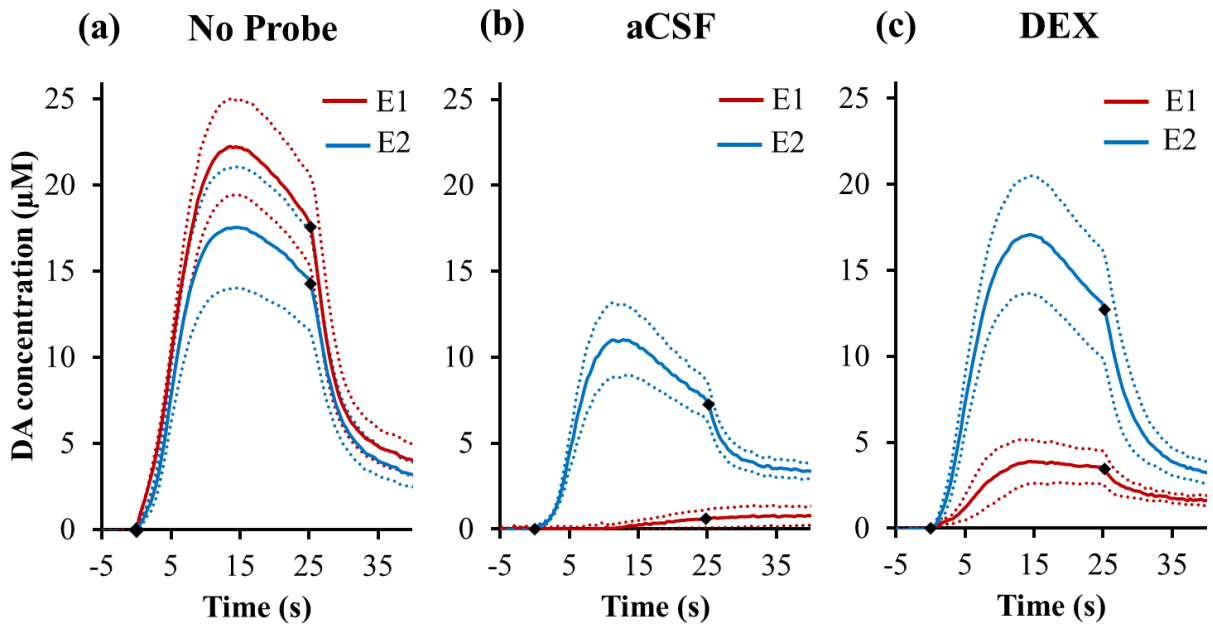

Figure 3.1. Evoked responses observed at the E1 (red) and E2 (blue) locations (a) with no microdialysis probe (n=5), (b) after 24 hr perfusion with aCSF (n=6), and (c) after 24 hr perfusion with DEX (n=6). The solid lines are the averages of the responses and the dotted lines are the SEMs. The black diamonds show when the stimulus begins and ends (see Figure. 4.2 for statistics).

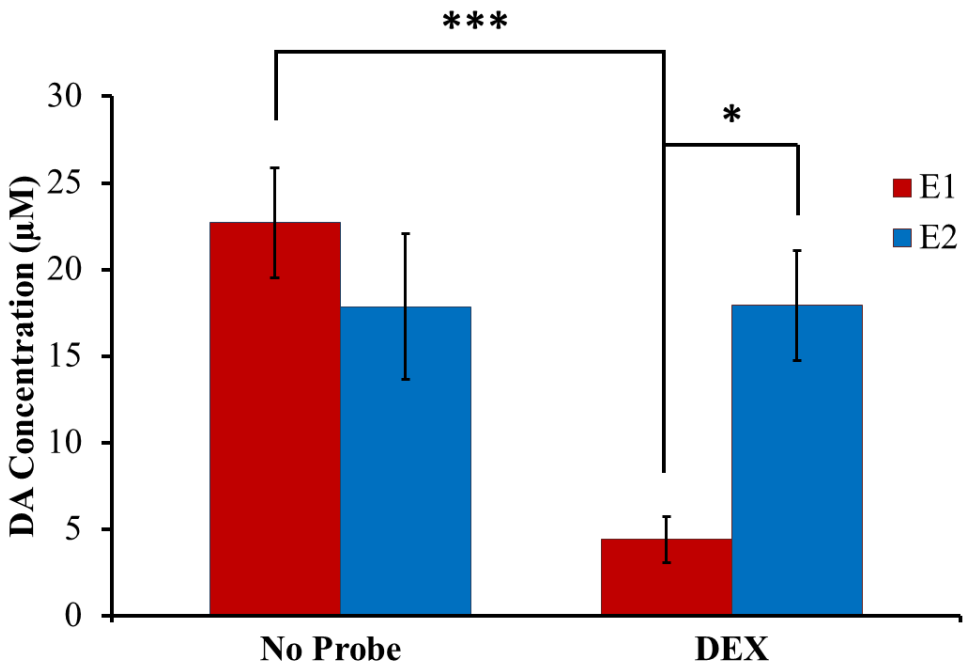

Figure 3.2. Summary of the amplitude of evoked responses (average ± SEM) at the E1 (red) and E2 (blue) locations without microdialysis probes (n=5) and 24 hr after probes were implanted and perfused with DEX (n=6). The evoked response at the E1 location after perfusion with aCSF was non-detectable, so the aCSF results were excluded from the statistical analysis. Statistical analysis was performed by two-way ANOVA with location (E1, E2, repeated measure) and probe (no probe, probe with DEX) as the factors. Location is not a significant factor ($F(1,9)=1.99$, $p > 0.05$). Probe is a significant factor ($F(1,9)=9.08$, $p < 0.05$). Interaction between factors is significant ($F=(1,9)=8.91$, $p < 0.05$). Post-hoc pairwise comparisons with Bonferroni corrections showed that in the presence of DEX the response amplitude at the E1 location is significantly smaller compared to the amplitude at E1 with no probe (*** $p < 0.0005$) and compared to the amplitude at E2 (*$p < 0.05$). A separate one-sample t-test shows that the response amplitude at E1 after 24 hr of perfusion with DEX was significantly elevated above zero $t(5)= 3.33$, $p < 0.05$ (aCSF group).

3.3.2 Voltammetry Next to the Probes

We report here for the first time that evoked responses at the E1 location are abolished 24 hr after implantation of microdialysis probes perfused with aCSF (Figure. 3.1b-red line). This extends our prior acute study,[32] which showed that evoked responses were abolished 4 hr after probe implantation. Together, these findings support previous evidence of neurochemical disruption of the tissue near probes over the 4-24 hr post-implant interval,[29, 31] when most microdialysis studies are performed.[4, 37-38, 71]

We report here for the first time that retrodialysis of DEX for 24 hr diminishes, but does not eliminate, the loss in amplitude of evoked responses at the E1 location (Figure 3.1c-red line). Evoked responses at the E1 location were significantly elevated compared to zero response, although they were significantly smaller than the responses at the E2 location (Figure 3.2, statistics reported in the figure legend). In the presence of DEX, there was no significant difference in the response amplitude at the E2 location compared to that observed in the absence of a probe (Figure 3.2). Thus, DEX offers partial protection of evoked responses at the E1 location without affecting the responses at the E2 location. The lack of significant effects at the E2 location suggests that the tissue disruption is confined to the tissue in close proximity to the probe.

DA reuptake affects the in vivo microdialysis recovery of DA[90, 107-108] Therefore, it is of interest to know how inhibition of the DA transporter (DAT) affects evoked DA responses next to the probes. Consistent with numerous reports in the absence of microdialysis probes,[52-53, 109-111] nomifensine (20 mg/kg i.p.) increased the amplitude of evoked DA responses at the E1 location 24 hr after implanting the probes (Figure 3.3-green lines). In the case of probes

perfused with aCSF, nomifensine elevated the evoked response from below to above the detection limit of FSCV (Figure 3.3).

When probes were perfused for 4 or 24 hr without DEX, evoked DA responses at the E1 location were non-detectable (Figure 3.4a). Therefore, we must rely on responses measured in nomifensine-treated animals to compare the effects of DEX at 4 and 24 hr post-implantation (Figure 3.4b). Statistical analysis was by 2-way ANOVA (details in the figure legend) with time (4 hr, 24 hr) and perfusion condition (aCSF, DEX) as factors with post-hoc tests. The perfusion condition, but not time, was a significant factor (interaction was not significant). Thus, DEX significantly affected the response amplitudes and those amplitudes were stable between 4 and 24 hr post implantation.

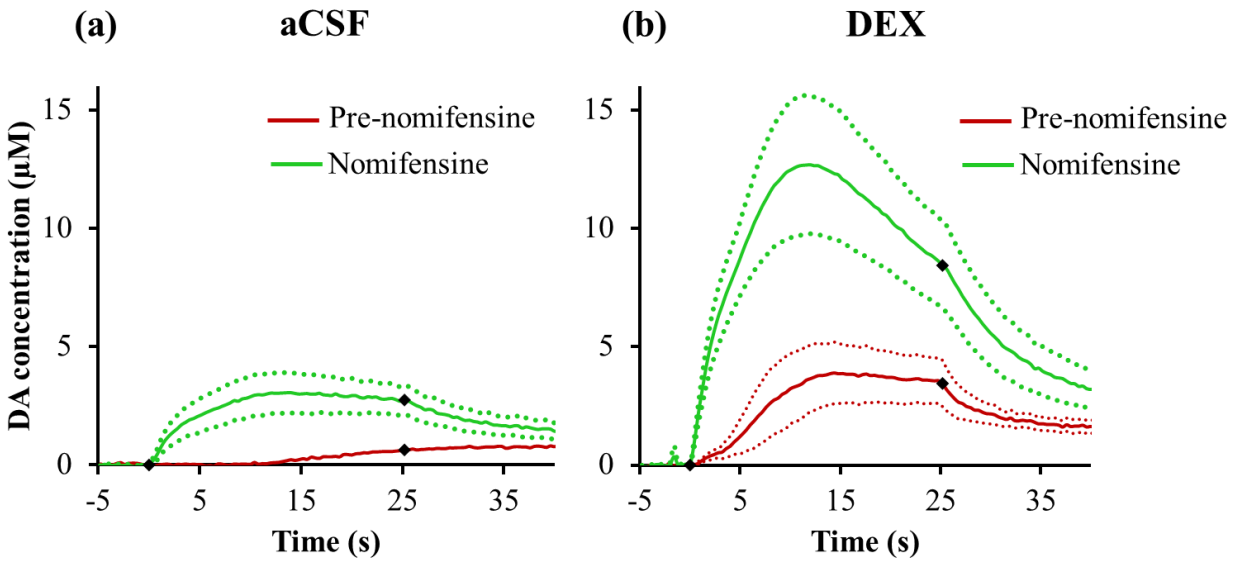

Figure 3.3. Nomifensine increases the amplitude of evoked responses at the E1 location (green = post-nomifensine, red = pre-nomifensine, responses in red are from Figure. 3.2; solid lines = response averages, dotted lines = SEMs, n=6 per group; black diamonds indicate where the stimulus begins and ends).

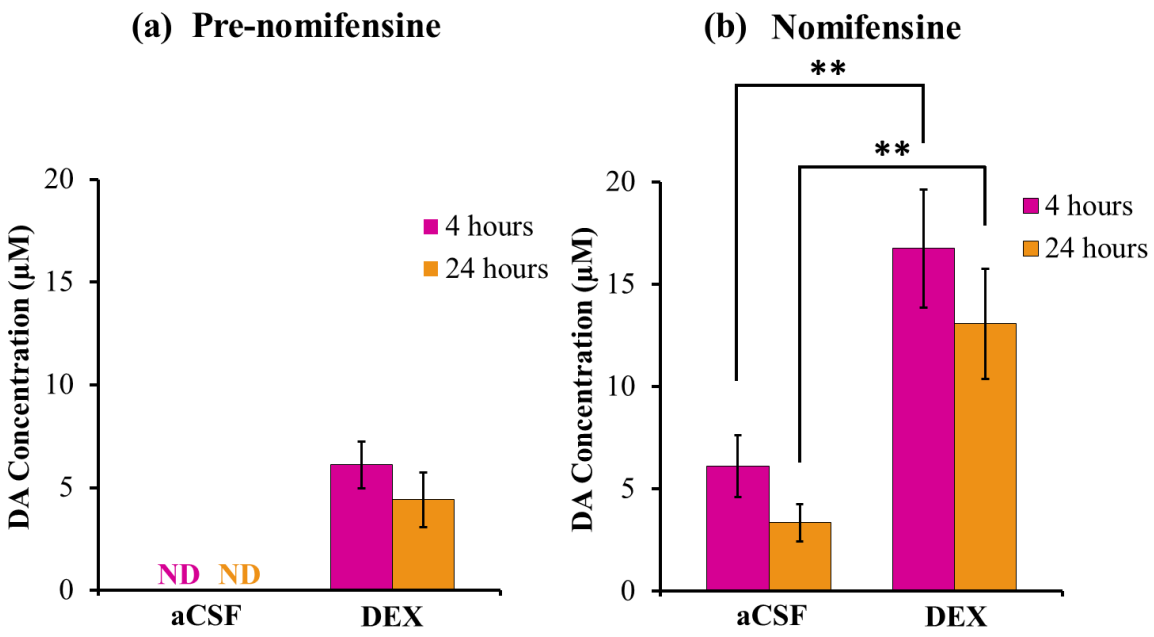

Figure 3.4. A summary of the amplitudes of evoked DA responses at the E1 location (average ± SEM) observed 4 hr (pink)[32] and 24 hr (orange) after probe implantation (a) before and (b) after administration of nomifensine. In the absence of nomifensine, DA was non-detectable (ND) near probes perfused with aCSF: so, statistical analysis was confined to the results obtained after nomifensine administration (panel b). Statistical analysis was by two-way ANOVA with time (4 hr, 24 hr), and perfusion condition (aCSF, DEX) as factors. Time is not a significant factor ($F(1,20)=2.22$, $p > 0.05$). The perfusion condition was a significant factor ($F(1,20)=22.1$, $p < 0.0005$). The interaction between factors was not significant ($F(1,20)=0.046$, $p > 0.05$). Post-hoc pairwise comparisons with Bonferroni correction show that DEX significantly increased the post-nomifensine responses at 4 and 24 hr compared to those observed with aCSF (** $p < 0.005$).

3.3.3 Immunohistochemistry of the Probe Track

We performed histochemical analysis of striatal tissues using antibodies for two widely accepted markers of DA terminals, tyrosine hydroxylase (TH) and the DAT.[112-114] Non-implanted, control tissue (contralateral to microdialysis probes) exhibits punctate TH labeling (Figure 3.5 left). Punctate labeling is diminished in images of tissue near the tracks of probes perfused with aCSF,

which also exhibit diffuse TH labeling (Figure 3.5 middle): control experiments did not reveal non-specific binding, which indicates that the diffuse labeling is specific binding. The exact cause of the diffuse labeling is unknown at this time but represents disruption of the tissue adjacent to the probe. Punctate, but not diffuse, labeling is clearly visible in the image of tissue near the track of a probe perfused with DEX (Figure 3.5 right). These images support the conclusion that DEX protects DA terminals near microdialysis probes.

At lower magnification (Figure 3.6) control tissue labeled for TH and DAT exhibit non-labeled areas corresponding to myelinated axon bundles, which are also visible under differential interference contrast (DIC). The probe tracks are clearly visible (Figure 3.6, middle and bottom rows). Some diffuse labeling around probes perfused with aCSF is evident in the TH image (Figure 3.6, middle row): we have observed such binding before and consider it an edge-effect.[32, 115] Overall, TH and DAT labeling was clearly evident near the tracks of probes perfused both with and without DEX (quantification is discussed, below).

The intense TH labeling near probe tracks perfused with aCSF for 24 hr stands in clear contrast to the absence of TH labeling that we observed 4 hr after implantation.[32] The exact mechanism whereby this interesting rebound of TH labeling occurs is not yet known: possibilities, to be explored further in future studies, might include the synthesis of new TH protein by surviving DA terminals and/or the sprouting of new DA terminals.[116-117] The TH and DAT images were converted to 2D intensity scatter plots (Figure 3.7a), from which we determined Pearson's Correlation Coefficient (PCC) and Manders' Overlay Coefficient (MOC) (see the Supporting Information document for explanations of these coefficients).[118] The correlation coefficients in images with and without probe tracks are indistinguishable for probes perfused with DEX (Figure 3.7b). The correlation coefficients are only slightly reduced with

aCSF compared to DEX, most likely due to the non-specific edge effect.[119] Overall, the probes with DEX had no significant effect on the correlation of TH and DAT labeling in the nearby tissue (see Figure 3.7 legend). Regions of interest in the TH and DAT labeled images were defined to eliminate the probe track (for details, see Supplementary Information document Figure S3.3). There were no significant differences in the quantitative TH and DAT labeling in non-implanted control tissue and the regions of interest around the tracks of probes perfused for 24 hr with either aCSF or DEX (Figure 3.7c).

Overall, probe implantation had no significant effect on TH and DAT, two key markers for DA terminals. This supports our conclusion that DEX's effects on evoked responses are attributable to its previously documented anti-inflammatory actions,[26, 32] as opposed to direct actions on DA terminals. Our prior studies show that DEX profoundly decreases ischemia, glial activation, and neuron loss in the tissues near microdialysis probes.[26, 32] It appears that these actions are responsible for the effects of DEX on evoked DA responses next to microdialysis probes over the 4-24 hr post-implantation interval.

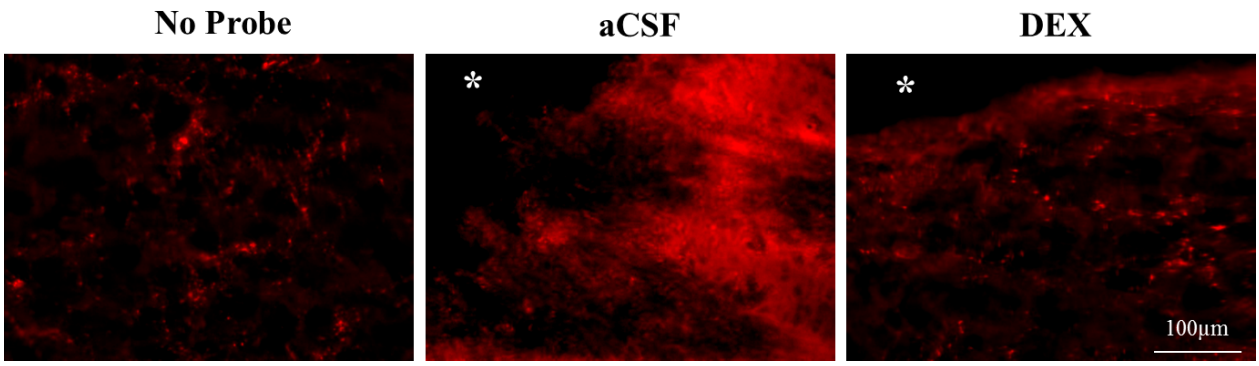

Figure 3.5. High magnification images (60X) of punctate TH labeling in control tissue (left), tissue near the tracks of probes perfused for 24 hr with aCSF (middle) and DEX (right). Punctate TH labeling is diminished near probes perfused with aCSF and diffuse TH labeling is increased. Control experiments did not indicate non-specific binding, so the diffuse labeling is presumed to derive from specific binding. Punctate labeling is evident in the DEX image, which does not exhibit diffuse TH labeling. The asterisk near the top of the middle and right hand images mark a portion of the probe track.

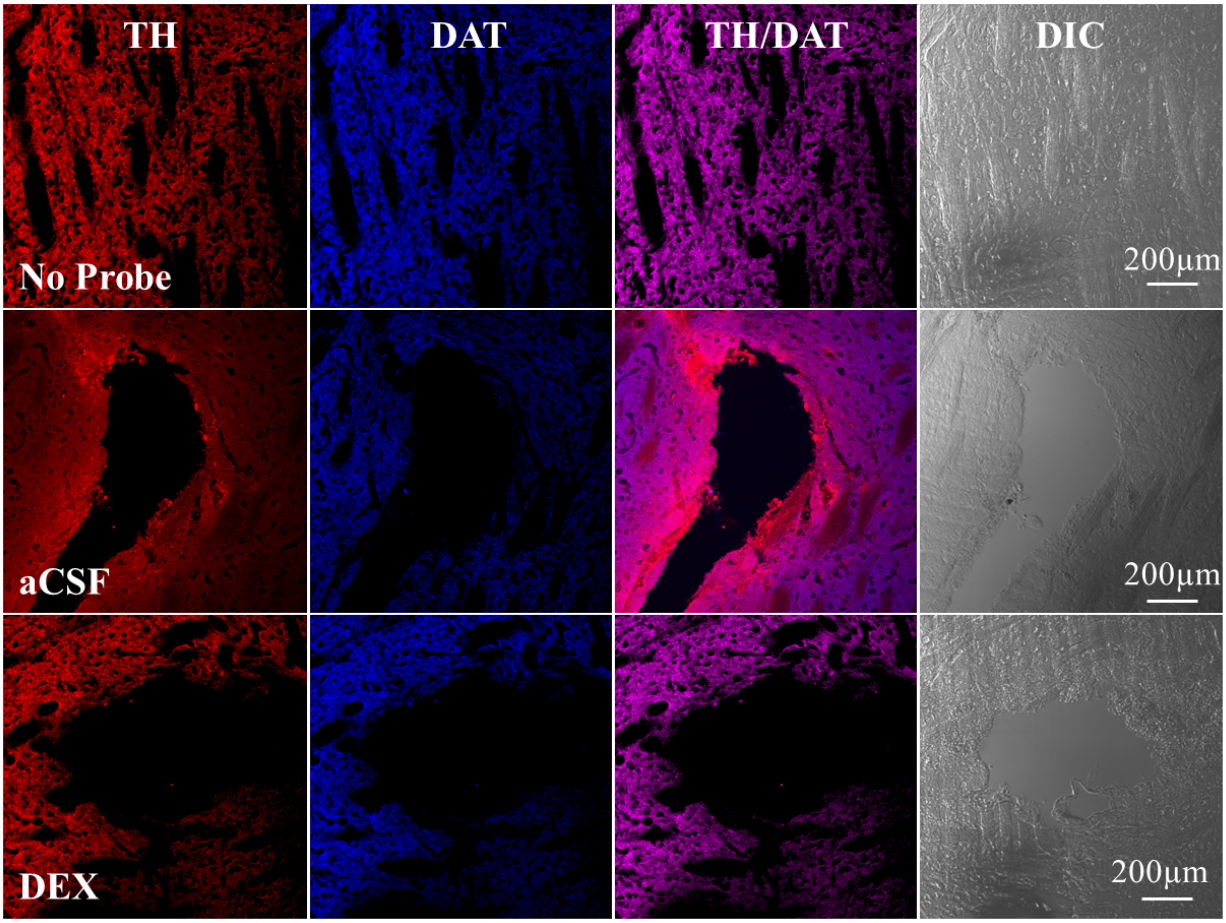

Figure 3.6. Separate rows illustrate representative fluorescent images of striatal tissue with no probe, or after retrodialysis of aCSF, or DEX for 24 hr. Separate columns provide tissue (from left to right) labeled with TH, DAT, their respective overlaid images and corresponding DIC images. Scale bars are 200 µm.

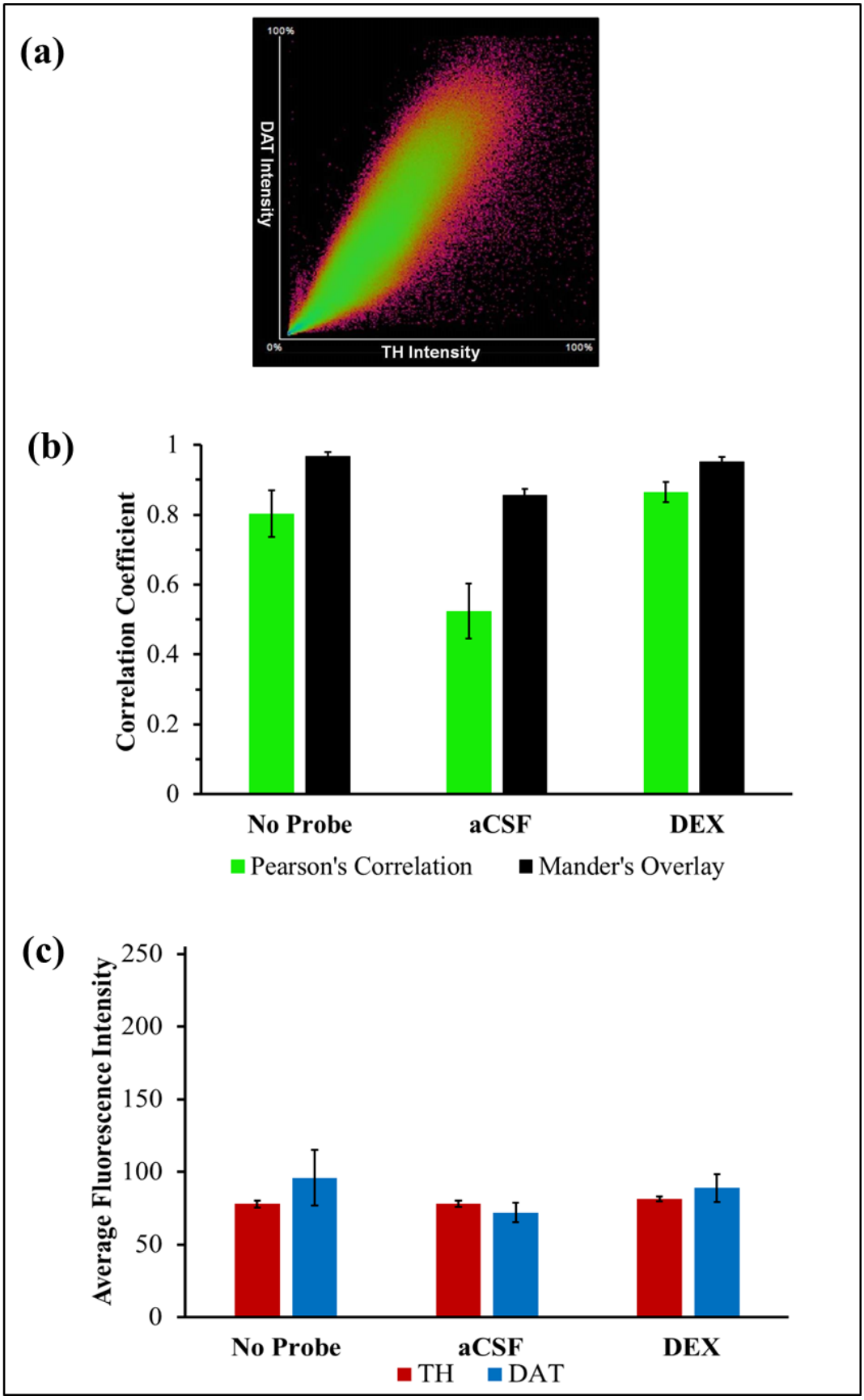
(a)
100%
DAT Intensity
0%
TH Intensity
100%
(b)
Correlation Coefficient
1
0.8
0.6
0.4
0.2
0
No Probe
aCSF
DEX
Pearson's Correlation
Mander's Overlay
(c)
Average Fluorescence Intensity
250
200
150
100
50
0
No Probe
aCSF
DEX
TH
DAT

Figure 3.7. (a) Represents a scatterplot of TH and DAT intensities. (b) The correlation coefficients between TH and DAT pixels among the three groups (no probe, aCSF and DEX, n=3 rats (total of 6 images per group)) for both Mander's Overlay (black) and Pearson's Correlation (green). A two-way ANOVA comparing the treatment (no probe, aCSF, and DEX) and analysis (Pearson's Correlation and Mander's Overlay) showed that there were significant differences in treatment $F(2,28)=14.2$, $p < 0.0001$, analysis $F(1,28)=29.7$, $p < 0.00001$, and the interaction treatment*analysis $F(2,28)=3.87$, $p < 0.05$. A post-hoc Tukey test further showed aCSF correlation coefficients were significantly reduced compared to no probe ($p < 0.0005$) and DEX ($p < 0.0001$). A post hoc pairwise comparisons with Bonferroni corrections showed that Mander's Overlay and Pearson's Correlation differ from each other with no probes ($p < 0.05$) and aCSF ($p < 0.00005$). (c) The average fluorescent intensity for TH (red) and DAT (blue) for no probe, aCSF and DEX (n=3 rats (total of 6 images per group)). Fluorescent intensity ranges from 0-255 with 255 being the highest value. In a two-way ANOVA comparing treatment (no probe, aCSF, and DEX) $F(2,30)=0.97$, $p > 0.05$ and stain (TH and DAT) $F(2,30)=0.74$, $p > 0.05$ there were no significant differences in average fluorescent intensity.

3.3.4 Evaluating the Tissue Penetration and the Physical Extent of DEX's Anti-inflammatory Actions

First, we used fluorescein-labeled DEX (DEX-FL) to assess how far DEX penetrates into the tissue near microdialysis probes. After 4 hr of retrodialysis, DEX-FL penetrated only to 78.6 ± 46.1 µm from the probe track (Figure 3.8). This result, however, might be affected by the detection limit of the fluorescence measurement and possibly by loss of soluble DEX-FL during tissue processing. So, second, we performed dual-probe microdialysis experiments (n=3) with the probes implanted 2 mm apart. One probe was perfused with DEX for 24 hr, the other with aCSF. DEX abolished gliosis, as measured with GFAP, near the probe with DEX but not near the probe 2 mm away (Figure 3.9). We therefore conclude that DEX does not penetrate deeply into brain tissue and that its actions are confined to within close proximity to the delivery probe.

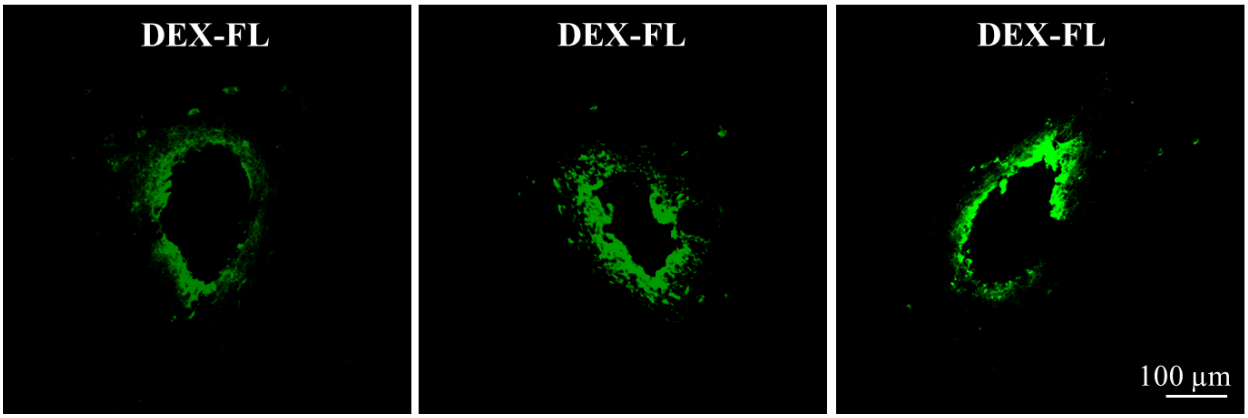

Figure 3.8. Images of the microdialysis probe track, from three different rats, after 4 hr perfusion of DEX-FL. DEX-FL is delivered locally only to the tissue directly surrounding the probe.

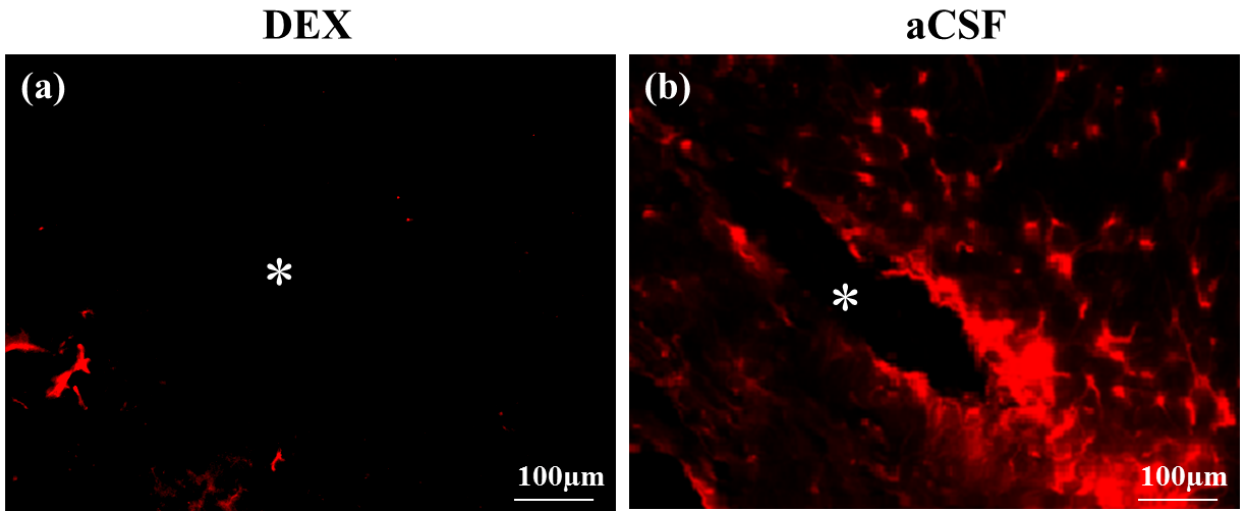

Figure 3.9. Fluorescently labeled GFAP images (a) with and (b) without DEX (b). Retrodialysis was performed for 24 hr in striatal tissue. The asterisks indicate the center of the probe tracks.

3.4 CONCLUSION

Our findings reiterate that tissue damage occurs when a microdialysis probe is implanted into brain tissue.[14-18, 26, 32] The extent of damage is documented to be sufficient to cause time-dependent neurochemical and histological disruptions in the tissue next to the probes over the 4-

24 hr post-implant interval, a typical time frame for microdialysis studies.[4, 37-38, 71] Here, based on the properties of evoked DA responses measured next to microdialysis probes and on histological findings, we have documented for the first time that DEX offers protective mitigation against such disruptions over the 4-24 hr time interval following probe implantation. The actions of DEX reported here appear to derive from its previously-documented anti-inflammatory actions,[26, 32] rather than any direct neurochemical action on DA terminals per se. We have also documented here a surprising rebound of TH labeling in the tissue surrounding probe tracks by 24 hr post-implantation: this might indicate the presence of surviving DA terminals, which justifies our efforts to protect and preserve their neurochemical activity. Finally, we document here for the first time that the actions of DEX are tightly confined to the immediate, local vicinity of the microdialysis probe used for delivery.

3.5 SUPPLEMENTARY INFORMATION

3.5.1 Fast Scan Cyclic Voltammetry

Carbon fiber electrodes were constructed by threading a single carbon fiber (7 µm diameter, T650, Cytec Carbon Fibers LLC., Piedmont, SC) through borosilicate capillaries (0.58 mm I.D., 1.0 mm O.D., Sutter Instruments, Novato, CA). The capillaries were pulled to fine tips around the carbon fiber with a vertical puller (Narishing Tokyo, Japan). Carbon fibers were glued in place with a low viscosity epoxy (Spurr Epoxy, Polysciences Inc., Warrington, PA) and cured overnight at 70 ºC. The exposed carbon fiber was cut to a length of 400 µm for in vivo studies or 800 µm for detection at the outlet of microdialysis probes. Capillaries were backfilled with

mercury and a nichrome wire (Goodfellow, Oakdale, PA) was placed into the mercury to make an electrical connection.

Fast scan cyclic voltammetry (FSCV) was executed using a computer controlled EI-400 potentiostat (Ensman Instruments, Bloomington, IN) with CV Tarheels version 4.3 software (Michael Heien, University of Arizona, Tucson AZ). A triangular waveform was applied as a linear sweep (vs Ag/AgCl) from 0 V to 1 V, then to -0.5 V, and then back to the resting potential of 0 V at a scan rate of 400 V/s. Scans were performed at a frequency of 2.5 Hz unless otherwise noted. Background subtracted voltammograms were used to quantify dopamine (DA) on the initial potential sweep between 0.6 V and 0.8 V. The DA current was converted to concentrations by post-calibrations with freshly prepared standard solutions of DA (Sigma Aldrich, St. Louis, MO) dissolved in nitrogen purged aCSF.

3.5.2 Surgical and Stimulation Procedures

All procedures involving animals were approved by the Institutional Animal Care and Use of Committee of the University of Pittsburgh. Male Sprague-Dawley rats (250-350 g, Hilltop, Scottsdale, PA) were anesthetized with isoflurane (0.5 % by volume, Henry Schein Animal Health, Elizabethtown, PA). Rats were wrapped in a heating blanket (37°C) and placed in a stereotaxic frame. The incisor bar was adjusted so the dorsal ventral measurements at lambda and bregma were no more than 0.01 mm apart (flat skull). For all voltammetry experiments, the reference and stimulating electrodes were placed in the same positions in the brain. Reference electrodes were connected to the brain via a salt bridge. Bipolar stimulating electrodes were lowered into the medial forebrain bundle (MFB) until maximum DA release was observed (4.3 mm posterior and 1.2 mm lateral from bregma). Electrically evoked DA release was recorded by

FSCV during stimulation of the MFB (stimulus waveform: biphasic, square, constant current pulses 300 μA pulse height, 4 ms pulse width).

3.5.3 24 hr Microdialysis Probe Implantation Procedure

A small craniotomy was made over the striatum. Microdialysis probes were perfused with aCSF or DEX using a syringe pump. Probes were lowered slowly (5 μm/sec) into the striatum (1.6 mm anterior and 2.5 mm lateral from bregma) over the course of approximately 23 min using a micropositioner (Model 2660, David Kopf Instruments, Tujunga, CA) to final position of 7 mm below dura. Probes were secured with bone screws and acrylic cement. Anesthesia was removed and animals were placed in a Raturn Microdialysis Bowl Stand-Alone System (MD-1404, BASI, West Lafayette, IN) for one day.

3.5.4 Electrode Placement for Voltammetry Next to Microdialysis Probes after 24 hr

After 24 hr animals were re-anesthetized and placed back in the stereotaxic frame. Without disturbing the probe, holes were drilled for the reference electrode, stimulating electrode and both carbon fiber electrodes. One electrode (E1) was implanted lateral to the probe so that the tip of the carbon fiber was 70 μm and the base 100 μm from the probe. The second electrode (E2) was implanted 1 mm posterior to the probe (0.45 mm anterior from bregma, 2.5 mm lateral from midline, and 5 mm below dura). A stimulating electrode was placed into the MFB and evoked DA was recorded (Figure S3.1).

3.5.5 Fluorescent Dexamethasone Procedure

Microdialysis probes were implanted for 4 hr during which dexamethasone fluorescein (10 µM) was perfused through the probe (n=3 rats). Horizontal sections (30 µm) were taken along the probe tract (130 slices per rat). Three random sections from each rat were imaged, thresholded and masked. Using NIS Element Advanced Research software random line measurements were perform in the area defined as a positive fluorescent signal. Nine different line measurements were made from each image for a total of 81 measurements.

3.5.6 Defining TH and DAT Colocalization

Fluorescence microscopy was used to examine the colocalization of tissue labeled for tyrosine hydroxylase (TH) and dopamine transporters (DAT). For each probe track, images of both TH and DAT were collect using sequential mode, allowing for images to be merged and a composite image created. Since it is difficult to visualize the degree of colocalization from a pair of images, an important alternative is to display the intensities of the pairs of homologous pixels in a 2D scatterplot. The two antibodies were analyzed for the degree of colocalization by measuring the equivalent pixel position in each of the acquired images by generating a 2D-scatterplot (Figure 3.7a). Each axis covers the range of intensities of the fluorophores, in our case Cy3 and CY5 (respectively, TH and DAT). The scatterplot shows the frequency of occurrence between the pair of intensities which reveals any correlation between the fluorophores. The relationship between the intensities in the two images is calculated by linear regression. The slope of this linear approximation provides the rate of association of the two fluorophores.[120] Following the generation of the scatterplot it is possible to quantitatively evaluate colocalization between the

fluorophores (TH and DAT). Values calculated for the scatterplot using NIS Element Advanced Research software include Pearson's Correlation Coefficient (PCC), and Manders' Overlap Coefficient (MOC). Pearson's Correlation and Manders' Overlap are mathematically similar differing in the use of either absolute intensities (Manders') or the deviation from the mean (Pearson's).[120-121] Pearson's Correlation is well defined and is an accepted means for describing overlap between image pairs. It's computed values are between -1 to 1 with -1 being no overlap, 1 being perfect overlap and 0 representing random distributions between images. Only the similarities of shapes between images are account for not their intensities. PCC is defined as:[122-123]

$$PCC = \frac{\sum_i (R_i - \bar{R}) * (G_i - \bar{G})}{\sqrt{\sum_i (R_i - \bar{R})^2 * \sum_i (G_i - \bar{G})^2}}$$

where R_i= intensity in red channel, $\bar{R}$= average intensity in red channel, G_i= intensity in green channel and $\bar{G}$= average intensity in green channel.

MOC is also used to describe overlap however this method does not perform any pixel averaging functions like that of PCC therefore values range from 0 to 1. This method is also not sensitive to intensity variations between images. MOC is defined as:[122]

$$MOC = \frac{\sum_1 (R_i * G_i)}{\sqrt{\sum_1 R_i^2 * \sum_i G_i^2}}$$

3.5.7 Thresholding Images

Specifying correct threshold limits is a crucial procedure for image analysis. The point is to determine which pixels will and will not be included in the analysis, therefore distinguishing pixels to be analyzed from background. Figure S3.3 illustrates this procedure by means of an example. In the center of each image is the probe track, each channel corresponds to a specific antibody (red=TH and blue=DAT), and the far right column is the overlay of both channels. The top row (a) is unprocessed raw data, certain pixels in this row appear very bright (especially toward the center around the probe track) and other pixels are very dim. The build in “smart threshold function” of the NIS Element Advanced Research software automatically disregards these pixels and applies a mask to only the pixels to be used in the analysis. In our case, the mask is colored in white (bottom row (b)). Since all the images are imported into the software at the same time they are batch processed thereby allowing for all images to be analyzed in the same manner avoiding user bias.

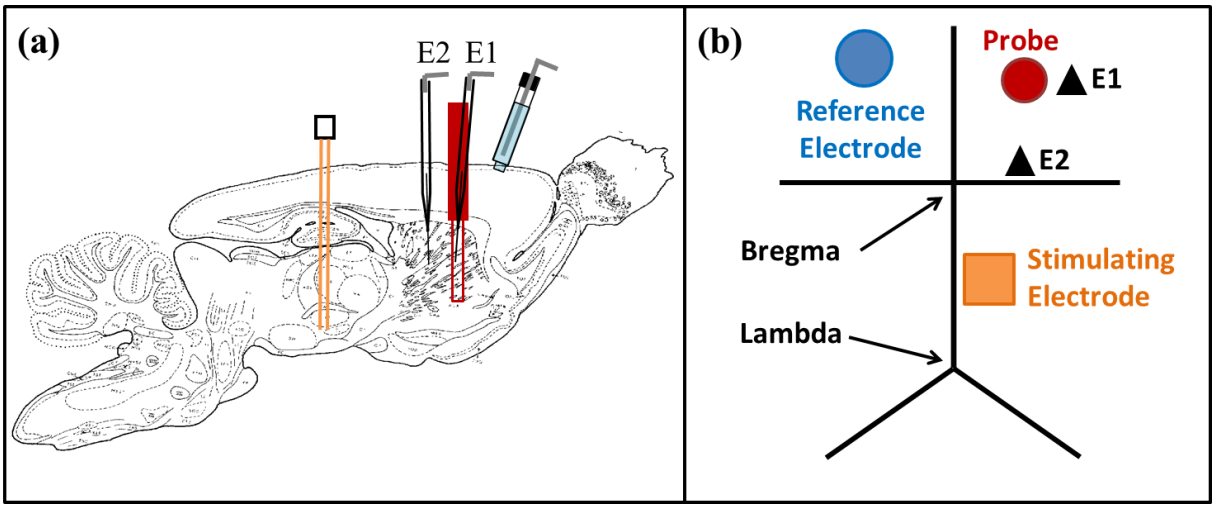

Figure S 3.1. Device placement in the brain after 24 hr probe implantation for evoked DA detection next to probes. (a) Represents a sagittal brain slice illustrating the microdialysis probe (red) expanding the length of the dorsal striatum. The reference electrode (blue) was in contact with the surface of the brain, a stimulating electrode (orange) was positioned in the medial forebrain bundle. E2 was implanted 1 mm posterior to the probe and E1 was implanted at a 5° angle 70-100 µm lateral to the probe. (b) Top-down view of device placement.

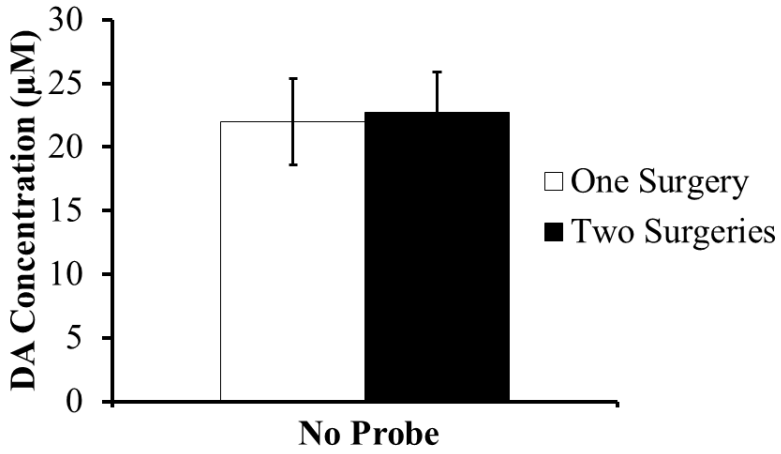

Figure S 3.2. Maximum average (±SEM) evoked DA measured in two separate groups of rats during only one surgery (white) and after a second surgery (black). There was no significant difference in maximum evoked DA release after the second surgery t-test: $t(9)=0.15$, $p>0.05$.

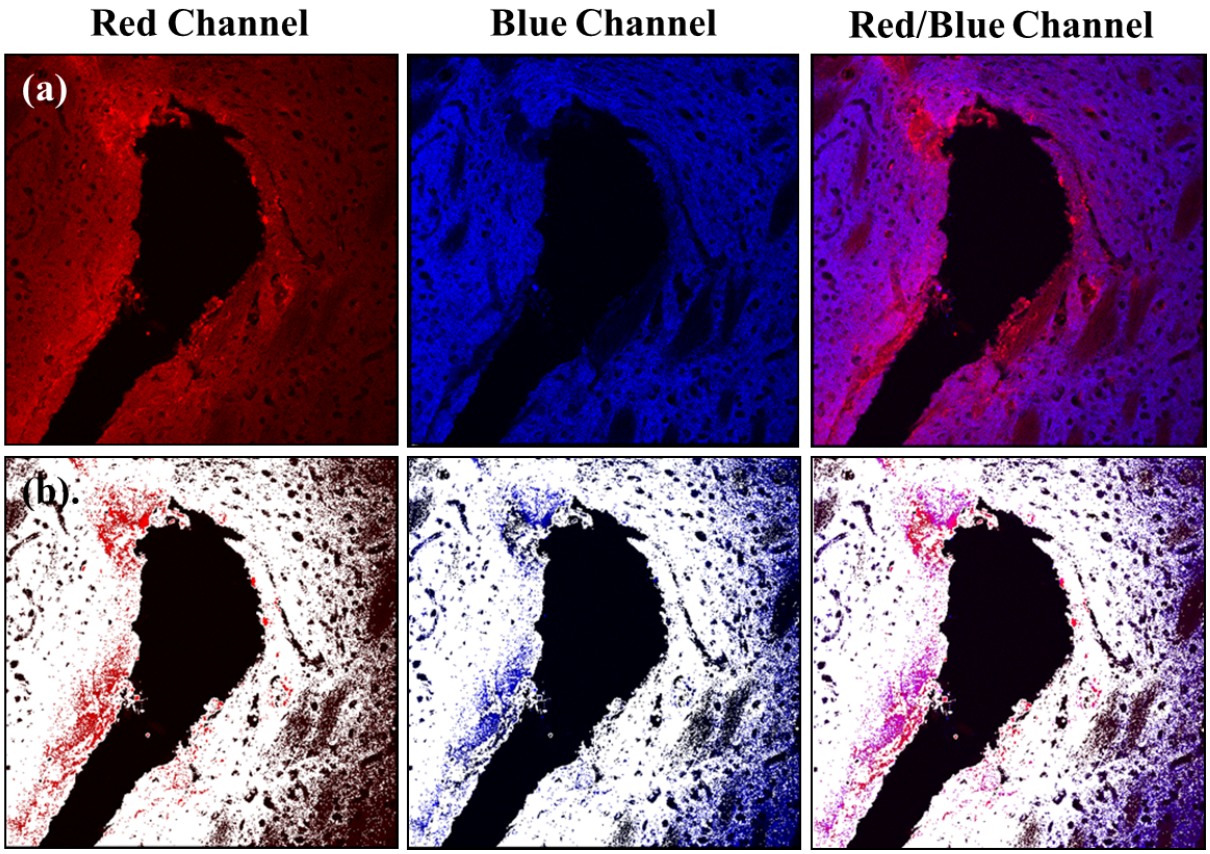

Figure S 3.3. Example of the thresholding process by NIS Element Advanced Research software. The brain tissue contains a probe track in the center of each image. Columns represent individual channels. The last column is overlaid channels of the red and blue. Row (a) represents raw images and row (b) is the images after thresholding. Only the area in white is used in analysis. Pixels outside this region are not considered as they are either over or under the threshold limit.

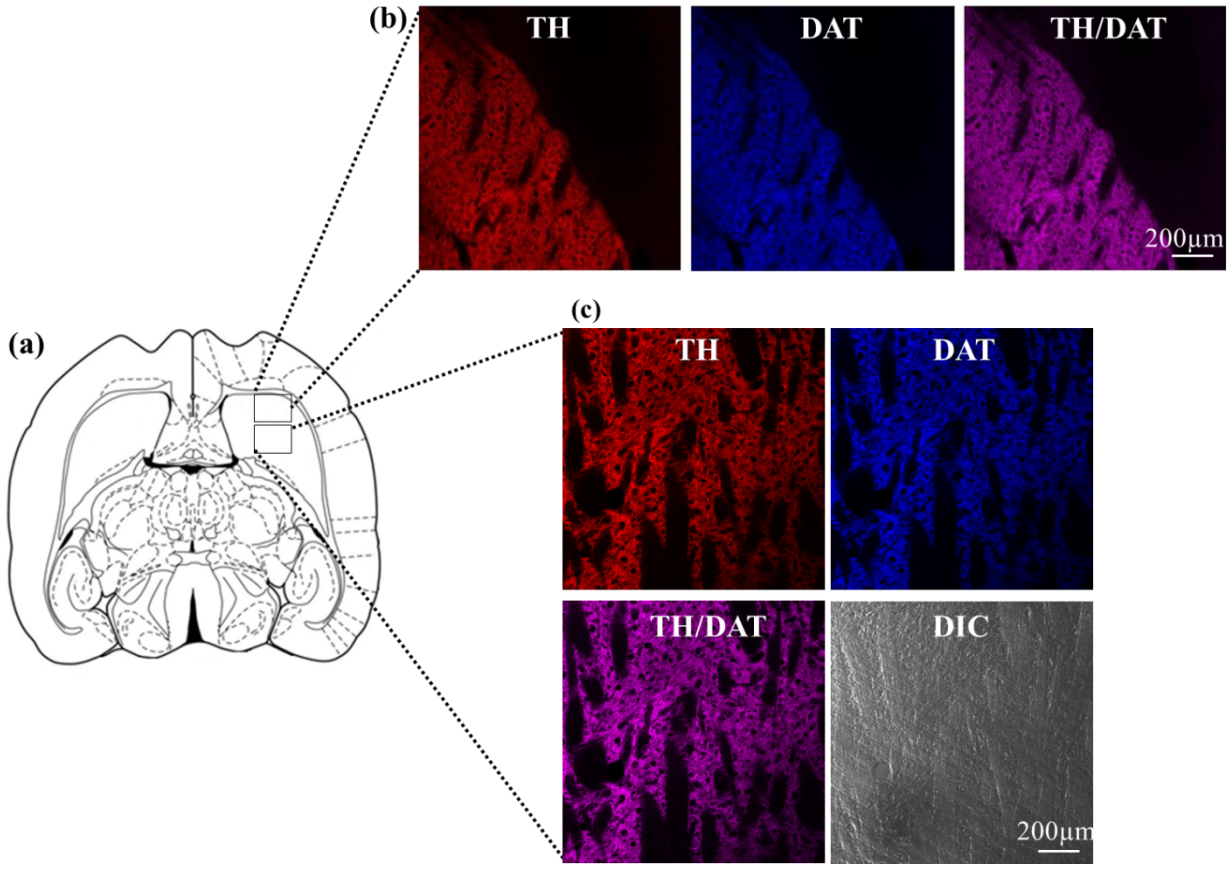

Figure S 3.4. Labeling scheme of striatal tissue. (a) Horizontal slices cut 30 µm thick. (b) and (c) are representative images of tissue stained with TH and DAT antibodies and the corresponding overlay. (b) Indicates the edge of the striatum showing that only the striatum is stained with these antibodies. (c) Also includes the differential interference contrast image (DIC). Scale bars are 200 µm.

4.0 EFFECTS OF ANTI-INFLAMMATORY AND REACTIVE OXYGEN SPECIES SCAVENGERS ON MICRODIALYSIS PROBE PENETRATION INJURY IN THE BRAIN

4.1 INTRODUCTION

Microdialysis is a powerful analytical technique used to recover analytes from the extracellular space of the brain (neurotransmitters, metabolites, amino acids, neuropeptides).[8, 34-35, 66, 69, 71, 84, 124] Microdialysis probes consist of inlet tubing that leads to a semi-permeable membrane at which analytes diffuse across the membrane and are collected through outlet tubing. This simple technique can be coupled to various analytical methods (high-performance liquid chromatography, mass spectrometry, capillary electrophoresis) for simultaneous detection of small molecules. Commonly used probes are 200-300 μm in diameter. Implantation of probes into the brain damages the surrounding tissue decreasing blood flow, neurons and increasing microglia and astrocytes.[14, 17-18, 26, 32-33] This penetration injury causes a progressive decline in dopamine (DA) an important neurotransmitter often studied using microdialysis.[29, 33, 42-43, 97] Specifically, probe implantation significantly decreases evoked DA release in the surrounding tissue.[32-33] Although, DA terminals survive probe implantation, they do not seem to function on a normal level in tissue surrounding the probe.[32-33] This often leads to in accurate sampling of the neurotransmitter, DA by microdialysis.

Retrodialysis of dexamethasone (DEX), an anti-inflammatory steroid increases blood flow to the area surrounding the probe and reduces gliosis for at least 5 days.[26, 32-33] By improving the health of the tissue DEX preserves neurons, DA terminals, and subsequently evoked DA release near probes at 4 and 24 hours.[32-33] Pharmacological mitigation of probe induced tissue damage through the use of an anti-inflammatory provides a platform for improving long-term microdialysis. However, a concern with the steroid DEX is that it can cause negative side effects such as aggression and weight gain in animals and humans monitored by microdialysis. Steroids are also known to effect neurotransmission, some steroids acting specifically on the central dopaminergic systems.[125-127] Therefore it is of important to investigate other non-steroidal anti-inflammatory agents and their ability to prevent tissue damage and loss of evoked DA release near probes.

XJB-5-131, a reactive oxygen species (ROS) scavenger also partially prevented evoked DA loss near probes for 4 hours by improving overall tissue health.[32] This particular ROS scavenger is unique in that it targets the inner mitochondrial membrane and contains a potent nitroxide group responsible for electron and radical scavenging.[45] Although its effect on preserving evoked DA release was not as stunning as DEX's, ROS's neuroprotective qualities still make them good candidates for 'pharmacologically enhanced microdialysis.'

The current study investigates the effects of two non-steroidal anti-inflammatories, ibuprofen (IBU) and pyridoxalphosphate-6-azophenyl-2',4'-disulfonic acid tetrasodium salt (PPads) and two ROS scavengers, JP4-039 (JP4) and JRS527 (JRS) on the preservation of evoked DA responses near microdialysis probes. As the effects of both DEX and XJB were profound after only 4 hours, this timeframe was used for the present study. Carbon fiber microelectrodes were coupled with fast scan cyclic voltammetry (FSCV) for detection of evoked

DA release in tissue near probes perfused separately with each pharmacological agent. Results were compared to evoked DA responses without pharmacological agent.

4.2 EXPERIMENTAL SECTION

4.2.1 Reagents and Solutions

Dexamethasone sodium phosphate (DEX: AAP Pharmaceruticals LLC, Schaumburg, IL), ibuprofen (IBU: Sigma Aldrich, St. Louis, MO) pyridoxalphosphate-6-azophenyl-2',4'-disulfonic acid tetrasodium salt (PPads: Sigma Aldrich, St. Louis, MO), were used as received from their suppliers. XJB-5-131 (XJB), JP4-039 (JP4), JRS527 (JRS) were prepared as described by Wipf and co-workers. All solutions were prepared with ultrapure water (Nanopure, Barnstead, Dubuque, IA). Artificial cerebrospinal fluid (aCSF: 142 mM NaCl, 1.2 mM $CaCl_2$, 2.7 mM KCl, 1.0 mM $MgCl_2$, 2.0 mM NaH_2PO_4, pH 7.4) was used as the perfusion fluid for microdialysis. DEX, and PPads were diluted to 10 µM in aCSF, IBU, XJB, JP4, JRS were dissolved in aCSF containing 1% DMSO (Sigma Aldrich, St. Louis, MO). Nomifensine (20 mg/kg, i.p., Sigma Aldrich, St. Louis, MO) was used as received. Nomifensine was dissolved in phosphate-buffered saline (PBS: 155 mM NaCl, 100 mM NaH_2PO_4, pH 7.40) for i.p. injections and diluted to 1 µM in aCSF for microdialysis perfusion. Electrodes were pre-treated in isopropyl alcohol (Sigma Aldrich, St. Louis, MO) and decolorizing carbon (Fisher, Pittsburgh, PA) Post-calibration of electrodes was performed with DA (Sigma Aldrich, St. Louis, MO) standards prepared in N_2-purged aCSF.

4.2.2 Voltammetry and Microdialysis

Carbon fiber microelectrodes (7 µm in diameter, and 400 µm in length) were coupled with fast scan cyclic voltammetry for in vivo measurement of evoked DA.[29, 32-33] Concentric microdialysis probes (300 µm diameter, 4 mm length) were constructed in house as previously described with hollow fiber 13 kDa MWCO membranes (Specta/Por RC, Spectrum Laboratories Inc., Ranco Dominguez, CA).[32] The probe inlet tubing (PE-20, Becton Dickinson, Franklin Lakes, NJ) was connected to a syringe pump (Harvard Apparatus, Holliston, MA) at a rate of 0.610 µL/min. The outlet made of fused silica capillary was led to waste as the dialysate fluid was not analyzed in this experiment.

4.2.3 Voltammetry Next to Microdialysis Probes

All procedures involving animals were approved by the University of Pittsburgh's Animal Care and Use Committee. Male Sprague-Dawley rats (250-350g; Charles Rivers, Raleigh, NC) were anesthetized with isoflurane (2.5 % by volume) and placed in a stereotaxic frame. Voltammetry next to microdialysis probes was performed in six groups of rats (6 rats per perfusion fluid unless otherwise noted).

A carbon fiber electrode was implanted at a 5 degree angle into the striatum of each rat. A stimulating electrode was lowered towards the medial forebrain bundle (MFB) until maximum evoked DA was observed at the carbon fiber electrode (4.3 mm below bregma, 1.2 mm lateral to bregma, and 7.2-8.5 mm below dura). Electrical stimulation of the MFB was performed for 25 s at 45 Hz (waveform: biphasic, square, constant current, 300 µA) and evoked DA release was measured in the striatum in twenty minute intervals.

Once consistent evoked responses were observed, a microdialysis probe was slowly (over 30 minutes) implanted next to the electrode (0.7 mm above bregma, 2.5 mm lateral from bregma, and 7 mm below dura). In its final position, the microdialysis probe was 70 µm from the tip of the carbon fiber, and 100 µm from the base of the electrode (Figure 4.1a). The probe was left to perfuse in the brain for 2 hours. Following this, three more stimulus responses were recorded. Finally, nomifensine was administered (20 mg/kg i.p.) and one more stimulus response was collected.

4.2.4 Data Analysis

For comparison, evoked DA responses near probes perfused with only aCSF (no pharmacological agent) were used as the control. These results have previously been reported in Nesbitt et al 2013 and are presented in Figure 4.1b.[32] For statistical analysis, all results were normalized with respect to the maximum amplitude of the responses recorded before probe implantation. Statistical analysis was performed using IBM Statistical Package for the Social Sciences (SPSS) 22 software.

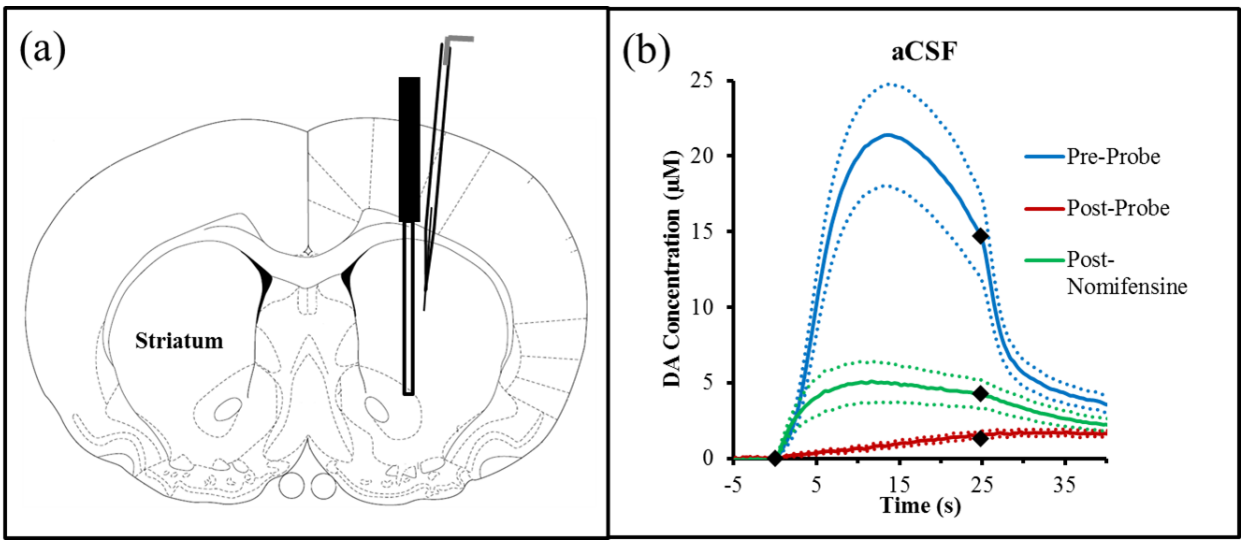

Figure 4.1. (a) Schematic of microdialysis probe (left) and microelectrode (right) positions in striatum. (b) Average (±SEM) DA responses to a 25 s stimulation of the MFB recorded in the striatum pre-microdialysis probe implantation (blue), post-probe implantation (red), and post-probe, post-nomifensine (green). Microdialysis probes were perfused with aCSF (n=6 rats per agent). Solid lines represent the mean response and dotted lines the SEM. Black diamond indicate the beginning and end of stimulation. Data previously published.[32]

4.3 RESULTS AND DISCUSSION

4.3.1 Control Experiments

In all of the following experiments evoked DA release was measured in the striatum during a 25 s stimulation of the MFB. Responses measured pre-probe implantation showed robust maximum evoked DA release ranging from 12-20 µM (blue responses in Figure 4.1b, 4.3, and 4.5). As previously reported, microdialysis probes perfused with aCSF (no pharmacological agent) eliminated evoked DA release nearby (70-100 µm away). To determine if any DA terminals survived probe implantation, a competitive DA transporter inhibitor, nomifensine was

administered by i.p. injection. Nomifensine revived evoked DA release near probes. The immediate response to stimulation proves that DA terminals survive directly next to the electrode, no further than 70 μm from the probe.[32] These results even though previously published are represented in Figure 4.1b for ease of reference.[32]

4.3.2 Anti-Inflammatory and ROS Scavenger Agents

This study compares the effects of three anti-inflammatory agents and three ROS scavengers' on preserving evoked DA release in tissue surrounding microdialysis probes. DEX and XJB have previously been reported on,[32] and are represented here for comparison purposes. The chemical structures of all pharmacological agents are represented in figure 4.2. The top panel illustrates the inflammatory agents and the bottom panel the ROS scavengers.

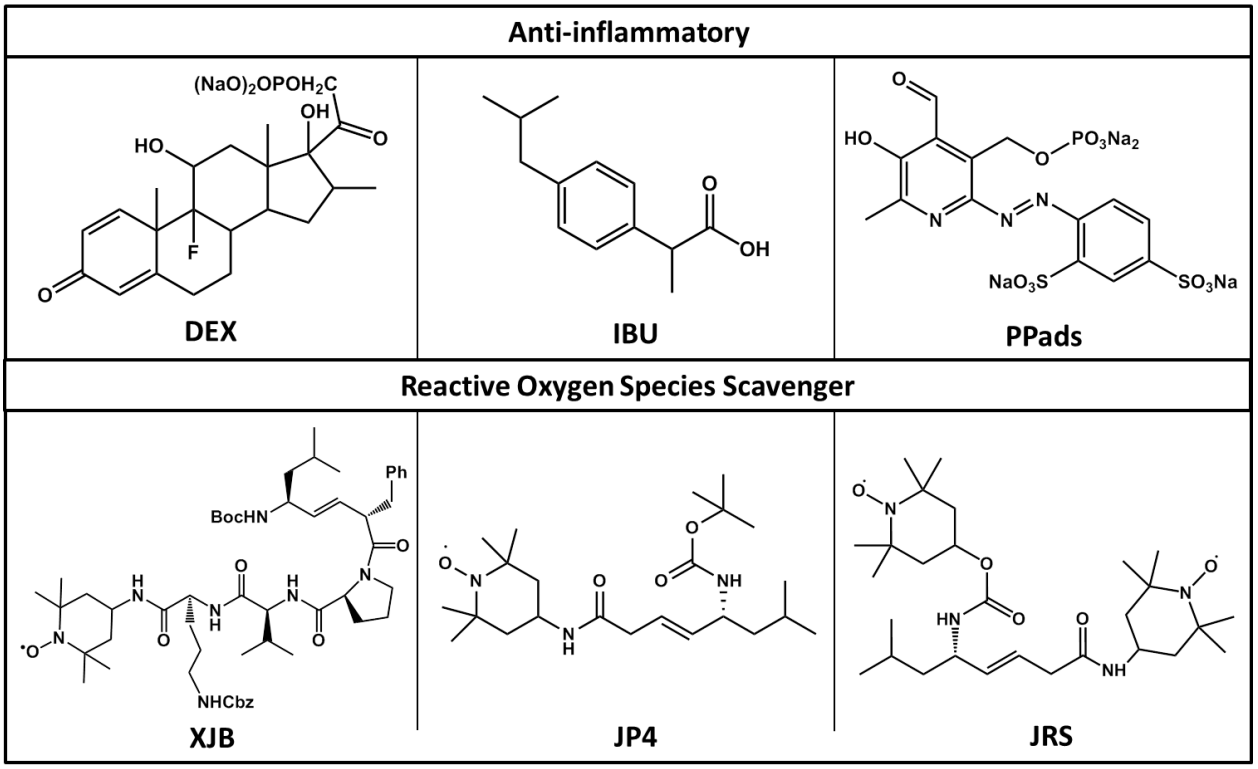

Figure 4.2. Top panel: Chemical structures of anti-inflammatory agents. Bottom panel: Chemical structures of reactive oxygen species scavenger provided by Wipf and co-workers.[45]

4.3.3 IBU and Ppads Preserve Evoked DA Release Near Probes

During an inflammatory event such as microdialysis probe implantation,[14, 18, 26] cells up-regulate production of pro-inflammatory proteins causing activation of phospholipase A2. Through cyclooxygenase (COX) modification a cascade of inflammatory mediators are produced.[128] Both DEX and IBU work to intervene at different stages of the inflammatory cellular mechanism. DEX acts by down-regulating pro-inflammatory proteins in cells and up-regulating anti-inflammatory proteins produced by the cell.[129] IBU is considered a COX-1 and COX-2 inhibitor thereby inhibiting COX modification and preventing inflammatory mediator signaling.[130]

The non-steroidal anti-inflammatory IBU, when perfused through microdialysis probes prevented complete loss of evoked DA release near probes (Figure 4.3-middle panel, red). Administration of nomifensine greatly impacted maximum evoked DA release near probes, increasing it to nearly pre-probe implantation amplitude (Figure 4.3-middle panel, green). IBU had similar effects as DEX suggesting that DEX's effects on evoked DA release are due to both its anti-inflammatory actions, not steroidal actions on DA terminals.

PPads is a non-selective P2 purinergic antagonist that blocks P2Y receptors. PPads reduces inflammation in the brain by blocking purine receptors on microglia limiting their response.[41] Microglia are immune cells that are the first to respond to injury in the central nervous system. In a study investigating the migration of microglia, PPads significantly decreased the number and motility of the microglia responding to the site of an injury.[41] PPads perfused through microdialysis also preserved evoked DA release near probes (Figure 4.3-right panel, red). Nomifensine further increased evoked DA release but not as dramatically as DEX and IBU (Figure 4.3-right panel, green).

For statistical analysis, maximum DA release was normalized with respect to the maximum amplitude of the responses recorded before each probe was implanted and presented in histograms (Figure 4.4, 4.6). As in the case of probe perfusion with aCSF, DA was undetected after probe implantation but before nomifensine, a one-sample t-test was performed comparing DEX, IBU, and PPads to zero. DEX, IBU, and PPads all significantly increased evoked DA release near probes (Figure 4.4a). DEX's effect was more significant than IBU and PPads, and this is most likely due to DEX's duel action to both decrease pro-inflammatory proteins and increase anti-inflammatory proteins. Post-nomifensine maximum evoked DA responses were subject to a one-way ANOVA. DEX, IBU, and PPads all significantly increased maximum

evoked DA release, DEX and IBU to above 80% of the pre-probe response. These findings demonstrate the ability of anti-inflammatories to preserve DA release and uptake activity in tissue near microdialysis probes.

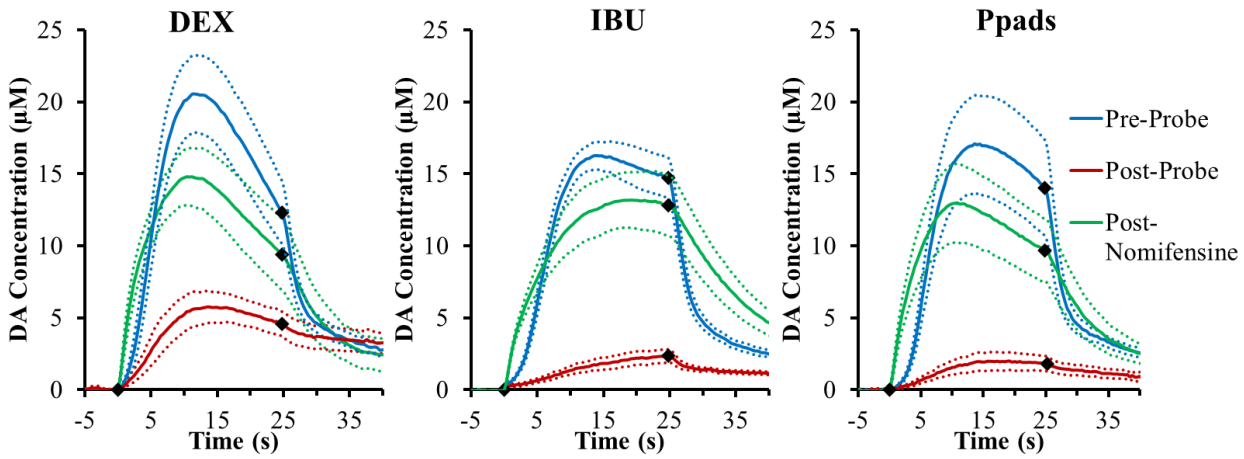

Figure 4.3. Average (±SEM) DA responses to a 25 s stimulation of the MFB recorded in the striatum pre-microdialysis probe implantation (blue), post-probe implantation (red), and post-probe, post-nomifensine (green). Microdialysis probes were perfused with either DEX, IBU, or PPads (n=6 rats per agent). Solid lines represent the mean response and dotted lines the SEM. Black diamond indicate the beginning and end of stimulation. DEX data previously published.[32]

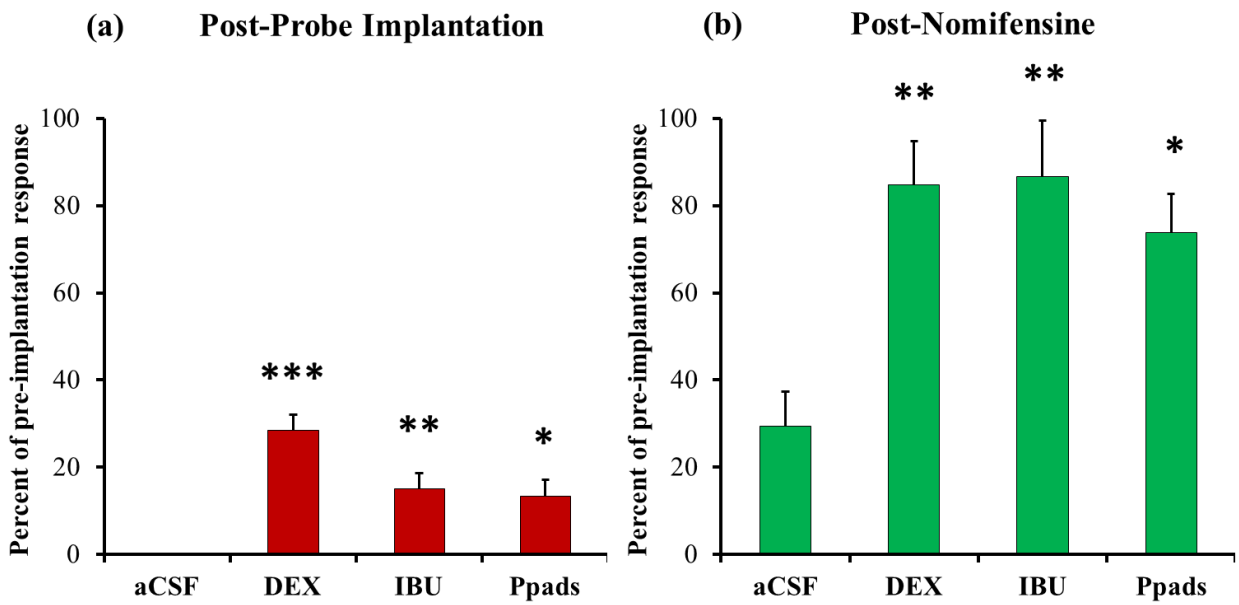

Figure 4.4. Effects of anti-inflammatory retrodialysis of agents on maximum evoked DA (a) post-probe implantation and (b) post-nomifensine. (a) As DA was non-detectable in the case of aCSF a one-sample t-tests was performed to compare each post-probe response to zero. DEX, IBU and PPads significantly increased maximum evoked DA compared to aCSF: One-sample, one-tailed t-test: DEX $t(5)=8.21$, ***$p<0.0005$, IBU $t(5)=4.11$,**$p<0.005$, PPads $t(5)=3.46$, *$p<0.05$. DEX is significantly different from IBU and PPads: one-way ANOVA $F(2,15)=5.20$, $p<0.05$, Post-hoc tukey DEX is significantly different from IBU $p<0.05$, PPads $p<0.05$. (b) Post-nomifensine, DEX, IBU, and Ppads increased evoked DA compared to aCSF: One-way ANOVA $F(3,20)=7.28$, $p<0.005$, Post-hoc tukey DEX: **$p<0.005$, IBU: **$p<0.005$, PPads: *$p<0.05$.

4.3.4 JRS Preserve Evoked DA Release Near Probes

Inflammation is known to induce mitochondrial dysfunction and dopaminergic neurodegeneration in the nigrostriatal system.[131] XJB infiltrates mitochondria, scavenging ROS thereby providing neuroprotection. XJB prevents neuronal loss and preserves evoked DA near probes.[32] Wipf and co-workers developed a smaller analog of the XJB, JP4, to increase accumulation in mitochondria making the analog more potent. JP4 specifically targets

mitochondria, similar to XJB catalyzing the dismutation of superoxide radical anions and other reactive oxygen species. JP4 protective qualities mitigate radiation damage in blood cells in vitro and vivo.[132-133] JRS is another analog of XJB however containing two nitroxide groups (Figure 4.2) As the nitroxide group is the portion of the molecule responsible for scavenging ROS is expected this will increase potency.

Similar to anti-inflammatory drugs, probes perfused with JP4 and JRS decreased but did not abolish evoked DA release near probes (Figure 4.5). JP4 and JRS all substantially increased the post-nomifensine response. For statistical analysis, maximum DA release was again normalized with respect to the maximum amplitude of the responses recorded pre- probe implanted. Histograms representing ROS effect on evoked DA release are represented in Figure 4.6. A one-sample t-test was performed comparing XJB, JP4, JRS to zero (aCSF response post-probe implantation). XJB and JRS significantly increased evoked DA release near probes (Figure 4.6a). All responses post-probe with JP4 gave a measurable DA signal however, this increase was not significantly greater than zero. JRS significantly increased evoked DA release compared to aCSF (Figure 4.6b: One-way AVONA comparing post-nomifensine responses with ROS scavengers and aCSF). Nomifensine increase all ROS DA responses, but it is clear that JRS had the greatest effect on protective evoked DA near probes, which was expected.

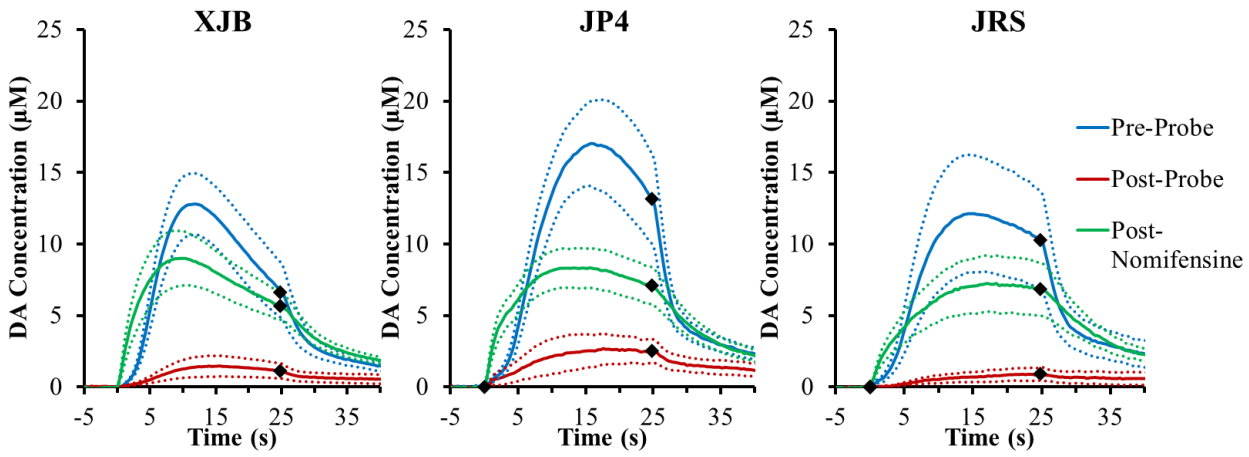

Figure 4.5. Average (±SEM) DA responses to a 25 s stimulation of recorded in the striatum pre-microdialysis probe implantation (blue), post-probe implantation (red), and post-probe, post-nomifensine (green). Microdialysis probes were perfused with either XJB, JP4, or JRS (n=6 rats per agent). Solid lines represent the mean response and dotted lines the SEM. Black diamond indicate the beginning and end of stimulation. XJB data previously published.[32]

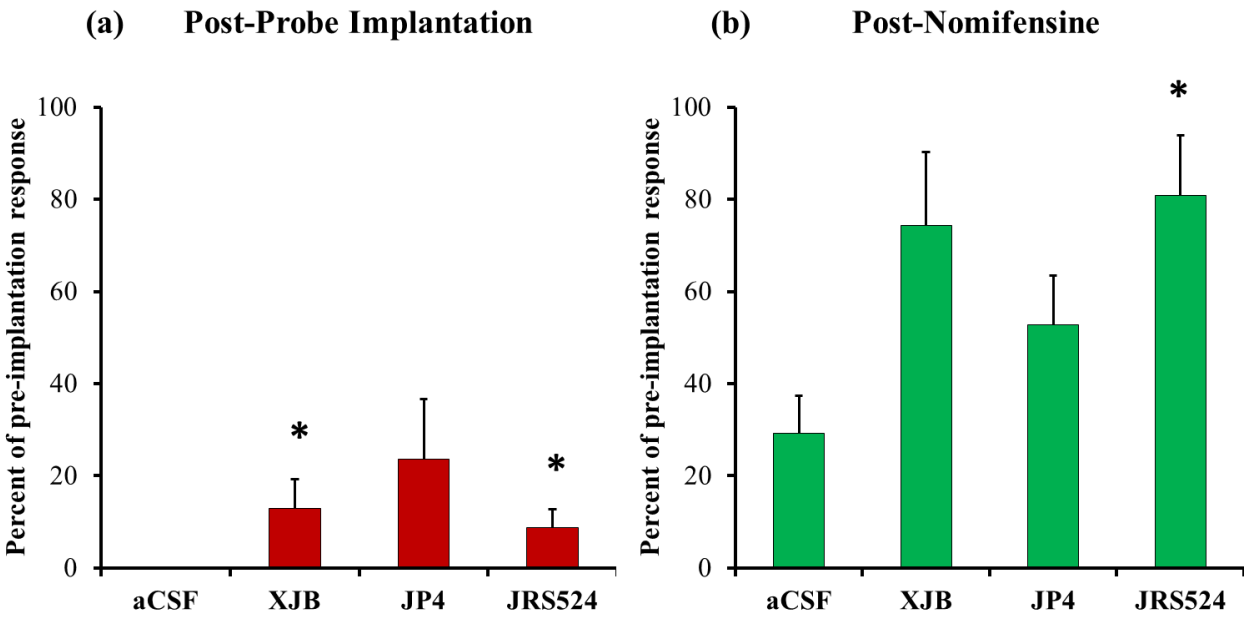

Figure 4.6. Effects ROS scavengers retrodialysis of maximum evoked DA (a) post-probe implantation and (b) post-nomifensine. (a) As DA was non-detectable in the case of aCSF a one-sample t-tests was performed to compare each post-probe response to zero. XJB, and JRS significantly increased maximum evoked DA compared to aCSF: One-sample, one-tailed t-test XJB $t(5)=2.02$, $^*p<0.05$, JRS $t(5)=2.24$, $^*p<0.05$. (b) Post-nomifensine, JRS increased evoked DA compared to aCSF: One-way ANOVA $F(3,20)=3.98$, $p<0.05$, post-hoc tukey test: JRS: $^*p<0.05$.

4.3.5 Nomifensine Perfusion does not Impact DA Terminals 70-100 µm Away

In a final study, nomifensine was administrated by perfusion through microdialysis probes instead of an i.p. injection. Voltammetry near probes perfused with nomifensine was performed in two groups of rats (n=3 rats/group), one group with perfusion of aCSF plus 1 µM nomifensine, and the other with perfusion of DEX plus 1 µM nomifensine.

Post-probe implantation responses were recorded before nomifensine was added to the perfusion fluid and gave similar results to experiments performed previously.[32] At probes perfused with only aCSF DA was not detected (Figure 4.7a) and at probes perfused with DEX,

evoked DA was measured (Figure 4.7b). Note that the aCSF results are reported as current (Figure 4.7a and 4.7c) as DA was undetected (aka. results did not produce a corresponding DA cyclic voltammograms). Nomifensine was added to each perfusion fluid and evoked DA responses were monitored near probes every 20 minutes for at least 2 hours. Nomifensine had no effect on evoked DA responses near probes whether DEX was present or not in the perfusion fluid.

Nomifensine, a competitive DA transporter inhibitor was unable to act on DA terminals 70-100 µm away from the probe. However nomifensine perfusion through microdialysis is known to increase extracellular levels of DA within 10 minutes of administration. When measured by microdialysis probes.[107] Nomifensine is a smaller molecule than DEX; therefore it would expect to diffuse through brain tissue more efficiently than DEX. We have previously shown that DEX's effects on evoked responses are attributable to its anti-inflammatory actions, not direct actions on DA terminals.[33] This evidence further supports our conclusion that DEX is acting on the tissue and blood vessels to improve tissue health during inflammation as opposed to DEX acting on DA terminals specifically the DA transporter.

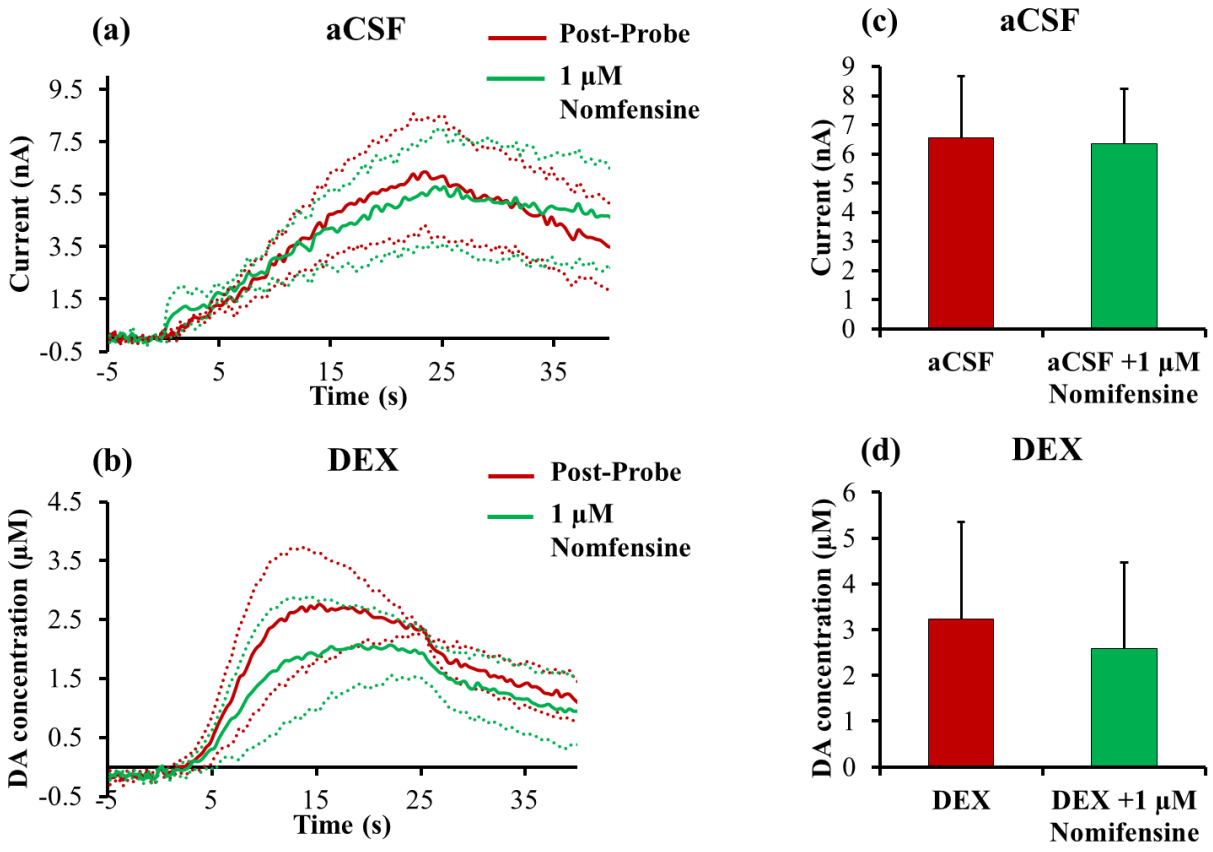

Figure 4.7. Effects of nomifensine added to perfusion fluid of microdialysis probes on evoked DA release near probes (n=3 rats/group). (a) Average (±SEM) current responses to a 25 s stimulation of the recorded in the striatum post-probe implantation with aCSF (red), and post-probe with aCSF plus nomifensine (green). (b) Average (±SEM) DA responses to a 25 s stimulation of the MFB recorded in the striatum post-probe implantation with DEX (red), and post-probe with DEX plus nomifensine (green). (c) There was no difference in maximum current post-probe implantation with aCSF (red), and post-probe with aCSF plus nomifensine (green), paired t-test ($p>0.05$). (d) There was no difference in maximum DA release post-probe implantation with DEX (red), and post-probe with DEX plus nomifensine (green), paired t-test ($p>0.05$).

4.4 CONCLUSIONS

Our lab has previously shown that microdialysis probe implantation decreased evoked DA release in tissue near probes.[29, 31-33] Through mitigation of the injury site with an anti-inflammatory steroid, DEX, and a novel ROS scavenger, XJB, DA activity is preserved.[32] Here we show other non-steroidal anti-inflammatory agents and ROS scavengers that protect DA release and uptake near microdialysis probes. IBU, PPads, XJB and JRS significantly attenuate the loss of DA activity in tissue near microdialysis probes. As we have previously shown long-term protection with DEX preserves evoked DA release measured in tissue near the probe and at the outlet of probes, these drugs present other options to improve chronic microdialysis.[33]

The protective effects were only partial, not completely restoring evoked DA release to its pre-probe response amplitude. Future dose response experiments are necessary to determine the optimal concentration of these agents and potential to completely restore DA activity near probes. Cocktails of these pharmacologically agents may also further promote evoked DA release in probe induced tissue damage. Overall, pharmacological enhanced microdialysis provides new insight into acute mitigation of microdialysis probe penetration injury and has the potential to successfully mitigate chronic implantation for long-term in vivo monitoring of neurochemicals.

5.0 THE EFFECT OF MICRODIALYSIS PROBE IMPLANTATION ON EXTRACELLULAR POTASSIUM IN SURROUNDING TISSUE

I would like to acknowledge undergraduate researchers Kendra J. Bobby and Michael Rerick for their contribution to the data set presented in this chapter.

5.1 INTRODUCTION

In the United States 1.7 million people per year sustain traumatic brain injury (TBI) which results in 53,000 deaths.[134] Days after a TBI event, forty percent of patients deteriorate due to the onset of a secondary injury.[135] These secondary injuries occur in the hours and days following the primary injury and play a large role in the brain damage and death that result from TBI. The incidence of secondary injury is not restricted to brain trauma, but also occurs in other acute brain injuries such as intracranial hemorrhage, ischemic stroke.[136-137]

Secondary injuries are suspected to be caused by spreading depolarizations (SDs). Recent studies confirmed that the incidence of SDs was a significant risk factor that predicted outcomes in patients with head trauma.[138] Based on the incidence of SD during days after initial treatments in the intensive care unit, it has now been suggested that SD is an important target to prevent progression of injury.[139-140] SDs are propagating waves of near complete depolarization of a volume of tissue, including both neurons and glial cells. SDs are generally initiated by a harsh

stimulation (e.g. potassium, ischemia) that severely depolarizes local brain tissue. This initiating depolarization results in a loss of transmembrane ionic gradients, significant cellular swelling, continuous potassium efflux and release of neurotransmitters including glutamate.[141] It is the accumulation and diffusion of these excitatory solutes which trigger severe depolarization of neurons and glia in the surrounding tissue, that slowly spreads across brain tissue at a rate of 2-5 mm/min.[141] The large ion fluxes associated with SD result in modulation of extracellular ionic concentrations and cause large shifts in extracellular field potential.[142] The wave-front of SD is thus electrically detected as a steep extracellular DC potential shift. This sharp potential shift coincides with a steep drop in the extracellular sodium concentration and increase in extracellular potassium concentration. It is widely assumed that SDs generated in metabolically compromised tissue sets up an additional metabolic burden that contributes to neuronal damage.

Currently, SDs and their metabolic products are studied in traumatic brain injured patients using online rapid sampling microdialysis.[9, 34, 36, 143] This method can detect metabolic signatures of SD with 1 minute temporal resolution. Temporal profiles of SDs can be achieved using rapid sampling microdialysis in combination with online potassium ion selective electrode (ISE) to detect potassium changes and hence the start of an SD event.

A serious limitation with this approach is that microdialysis probe implantation causes a penetration injury that triggers ischemia and gliosis at the sampling site due to the large size of the microdialysis probe (200-300μm).[14-16, 18, 26, 32, 93] The wounded tissue at the sampling site is different from the surrounding parenchyma:[18] ischemia impacts delivery of metabolic substrates to the probe and gliosis slowly develops, so the sampling site evolves over several days following insertion.[26] Microdialysis probes disrupt neurotransmission in the brain, specifically probe implantation decreases the release of the neurotransmitter dopamine.[29, 31-33, 108] It is

possible that probes also affect potassium concentrations in the brain which would in turn compromise the detection of SDs. In a study monitoring potassium concentration changes during an ischemia event, ISE (size: <50 μm) monitoring directly in the brain tissue measured much greater changes in potassium concentrations than microdialysis probes coupled online to an ISE.[144]

Potassium is a key marker for monitored SDs in TBI patents therefore it is important to understand if and how penetration injury affects potassium levels in the brain. Thus, it is the goal of this study to investigate whether probes significantly impact the monitoring of brain potassium levels during SDs to determine the reliability of clinical microdialysis.

Previously our lab has investigated the impact of microdialysis probes on evoked dopamine release in tissue near the probe. Decreasing the proximity from the probe creates a gradient decrease in evoked dopamine release.[29] Probes impact dopamine release in tissue adjacent to the probe,[29] 100 μm,[32] 200 μm from the probe, but have no effect 1 mm away.[29] Following this lead, we used potassium ion selective microelectrodes (ISME) to monitor potassium in the cortex of the rat brain. We implanted microdialysis probes in tissue 1 mm from ISME to determine the effect of probe implantation on potassium levels and its effect on the measurement of SDs.

5.2 EXPERIMENTAL SECTION

5.2.1 Reagents and Solutions

All solutions were prepared with ultrapure water (NANOPURE; Barnstead, Dubuque, IA). All reagents were used as received. Artificial cerebrospinal fluid (aCSF: 142 mM NaCl, 1.2 mM $CaCl_2$, 2.7 mM KCl, 1.0 mM $MgCl_2$, 2.0 mM NaH_2PO_4, pH 7.4) was used as the perfusion fluid for microdialysis. All potassium solutions were made by dissolving KCl (Sigma Aldrich, St. Louis, MO) in artificial cerebrospinal fluid without potassium (aCSF without K+: 142 mM NaCl, 1.2 mM $CaCl_2$, 1.0 mM $MgCl_2$, 2.0 mM NaH_2PO_4, pH 7.4). The silanizing agent used was hexamethyldisilazane (Sigma Aldrich, St. Louis, MO). Valinomycin was used as the potassium ionophore and purchased in a cocktail solution (Potassium Ionophore 1-cocktail, Sigma Aldrich, St. Louis, MO).

5.2.2 Potassium Ion Selective Microelectrodes (ISME) and Microdialysis Probes

Potassium ISME were constructed using borosilicate capillaries (0.58 mm I.D., 1.0 mm O.D., Sutter Instruments, Novato, CA). Capillaries were cleaned by soaking in acetone for 30 minutes and dried vertically at 70 °C for 2 hours. Capillaries were pulled to fine tips with a vertical puller (Narishing Tokyo, Japan) and gently broken to open the tip. The tip size of the electrodes were <50 µm. The electrodes were silanized by backfilling the capillary tips with hexamethyldisilazane. Silanization took place for 2 hours, then electrodes were placed tip down in the oven to dry for 2 hours at 200 °C (protocol provided by D. Feuerstein).

Electrodes were built by first dipping the tip of the electrode into potassium ionophore 1-cocktail.[145] The remainder of the electrodes were backfilled with 10 mM KCl. Ag/AgCl wire was inserted into the KCl solution completing the electrical contact (Figure 5.1). The end of the electrodes was sealed using 5-min epoxy (Devcon, Davers, MA).

Microdialysis probes were constructed in-house as previously described.[32]

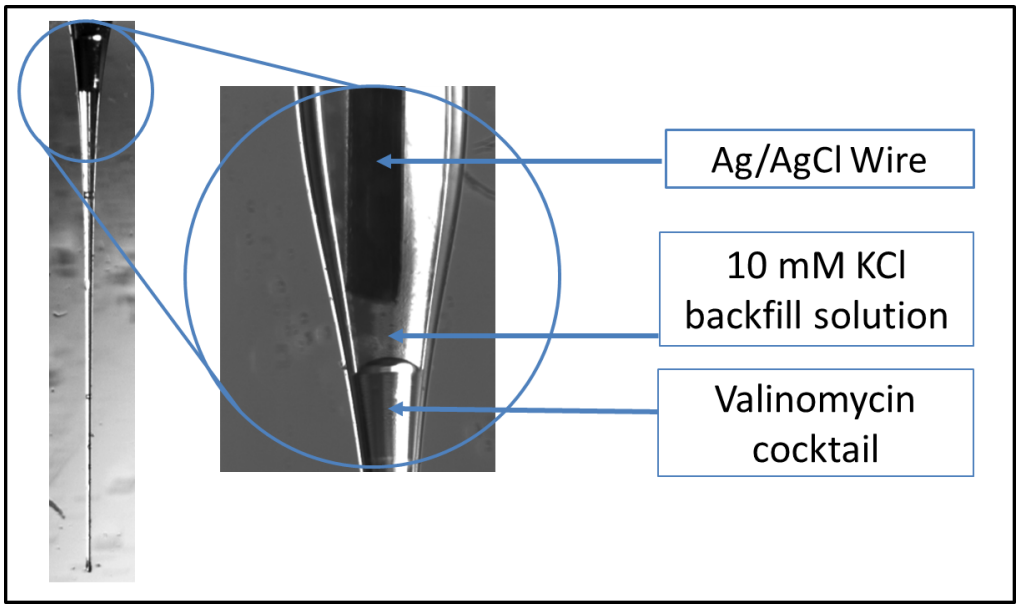

Figure 5.1. Potassium ISMEs consist of a capillary pulled to a fine tip. The tip contains a valinomycin cocktail. The electrode is backfilled with a 10 mM KCl. Electrical contact is made by a Ag/AgCl wire.

5.2.3 Potassium Detection

The potential verse a Ag/AgCl reference electrode was monitored by a differential amplifier (DP-301: Warner Instruments LLC, Hamden, CT) and recorded using a digital converter (NI-USB-6009 National Instruments, Austin, TX) linked to a Labview computer software program (Chuck Fleishaker, electronic shop, University of Pittsburgh).

Potassium concentrations were determined by pre-calibration of electrodes with at least five different concentrations of KCl dissolved in aCSF without K^+. Normal calibration curves had slopes of 50-58 mV for a 10 fold change in potassium.

5.2.4 Animals and Surgical Procedures

All procedures involving animals were performed under approval of the Institutional Animal Care and Use of Committee of the University of Pittsburgh. Adult male Sprague-Dawley rats (250-350 g; Charles Rivers, Raleigh, NC) were anesthetized with isofurane (2.5 % by volume, Baxter Healthcare, Deerfield, Il), intubated and placed in a stereotaxic frame. Anesthesia was maintained throughout the rest of the experiment. The skull was exposed and holes were drilled into the skull to access the brain.

Potassium ISME were implanted at a 5 degree angle in the cortex of the rat brain (1.0 mm anterior from bregma, 2.85 mm lateral from bregma, and 1.0 mm below dura). Electrical connection between the brain and a Ag/AgCl reference electrode was achieved by creating a salt bridge with a Kimwipe soaked in aCSF placed in a plastic pipette tip. Potassium was continuously measured throughout the whole experiment. Once a stable baseline was reached, an 18 gauge needle was used to prick the surface of the rat brain. After three needle pricks, a microdialysis probe was implanted into the cortex 1 mm from the ISME. With the probe in place, three more needle pricks were performed in the same location as pricks performed before the probe was implanted. Potassium levels were allowed to return to a stable baseline between needle pricks and after probe implantation.

5.3 RESULTS AND DISCUSSION

ISME were used to continuously monitor potassium levels during induced SD events. SD events were brought on by a needle prick to the surface of the brain. A typical experiment consisted of three needle pricks (NP), implantation of a microdialysis (MD) probe, then three more needle pricks (Figure 5.2). All experiments were performed in a Faraday cage, reducing outside interference with the ISME. Entering the cage to perform the needle pricks created a non-potassium related potential spike in the data; however we determined that this interference did not affect the monitoring of SDs as the wave did not reach the ISME for a least 1 minute after each needle prick. Extracellular basal potassium concentration was between 2-3 mM throughout the experiment which is consistent with the potassium concentration in rat cerebral spinal fluid (2.7 mM). Needle pricks caused a large increase in extracellular potassium as measured by ISMEs.

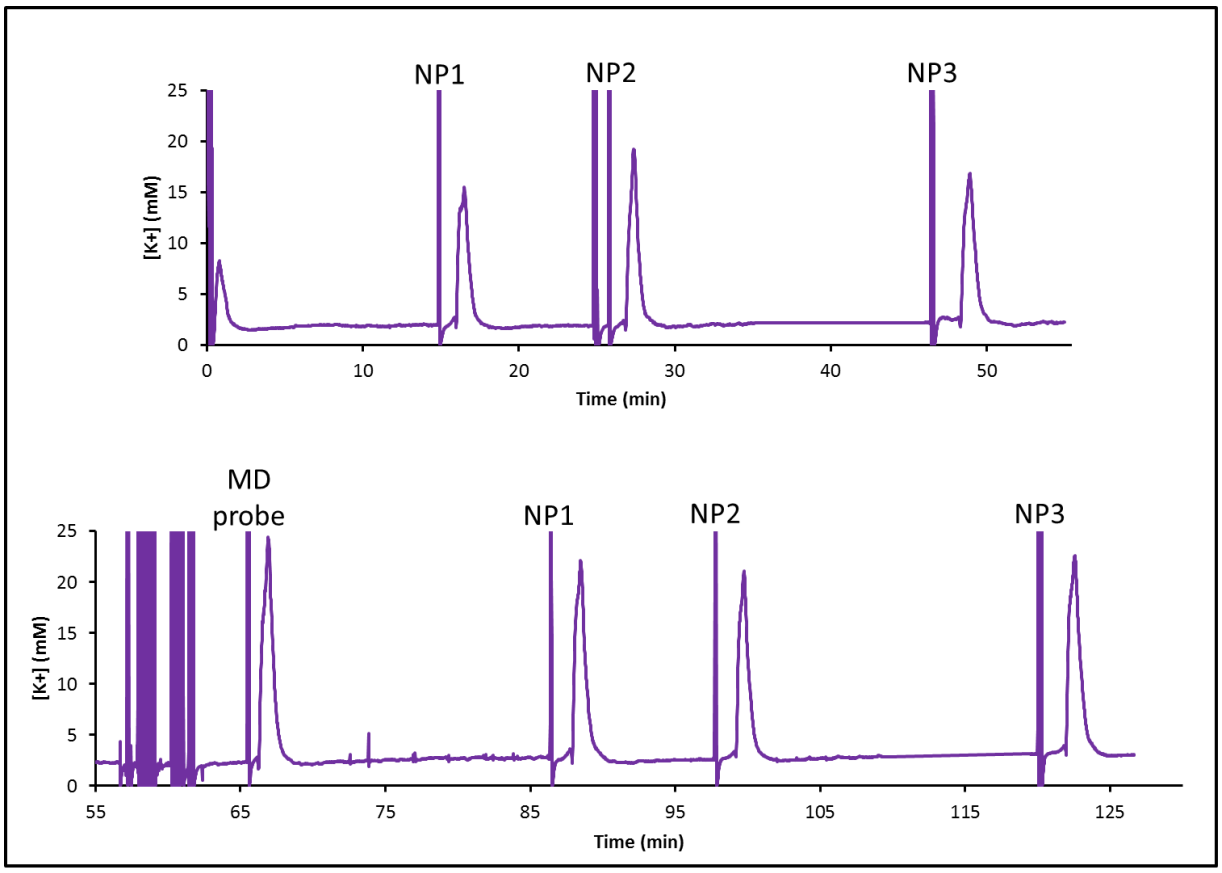

Figure 5.2. Representative experiment illustrating potassium concentration in the rat cortex vs. time. In the top portion of the graph, a potassium ISME was implanted at t=0 min. Needle pricks (NP) were performed followed by an observed increase in potassium concentration. In the bottom portion of the graph, a microdialysis (MD) probe was implanted at t=66 min followed by a large increase in potassium needle pricks trailing probe implantation were measure by ISME. Large spikes in the data are non-potassium related noise.

Potassium responses to needle pricks before microdialysis probe implantation were averaged ±SEM (Figure 5.3, n=7 rats). Basal potassium concentration before the needle prick was set to zero and the time of the prick was also set to zero. Needle pricks before probe implantation caused a 2.78 ± 1.37 mM change in potassium concentration in the cortex. The SD itself lasted for approximately two minutes.

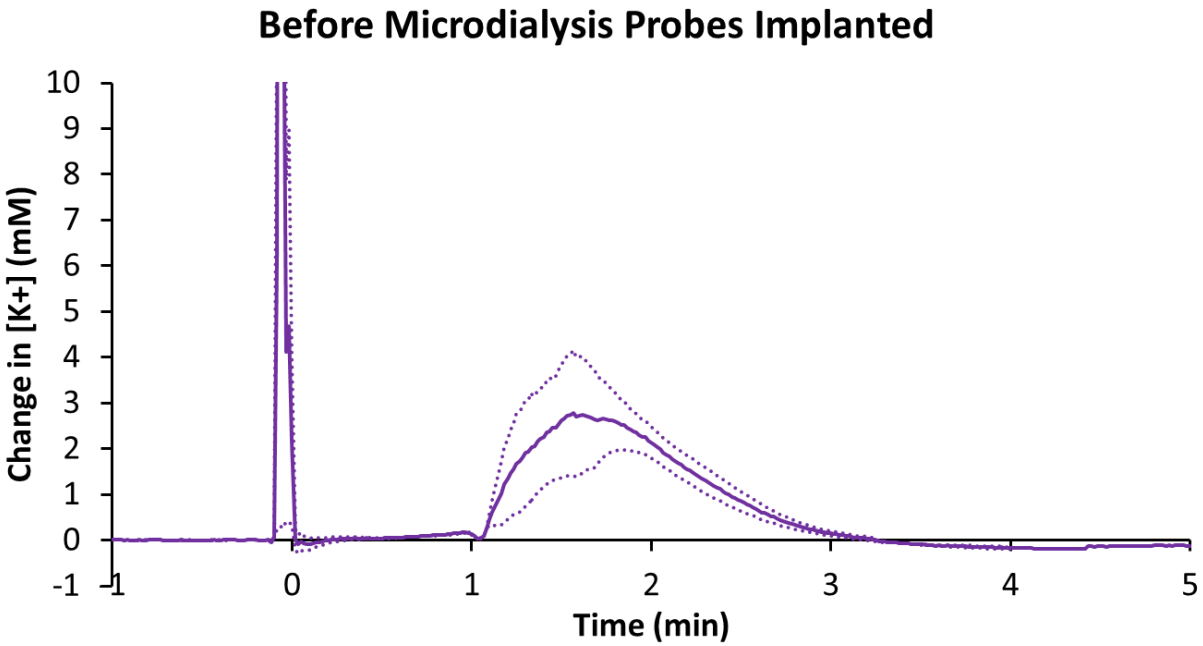

Figure 5.3. The change in potassium in response to needle pricks performed before microdialysis probes were implanted (n=7 rats). Data was adjusted so that needle pricks were at t=0 min. The spike just before t= 0 is noise caused by opening of the Faraday cage to perform the needle pricks; it is not a change in potassium. The solid purple line represents the average response, and dotted lines represent ±SEM for this figure and all remaining figures.

Microdialysis probes were implanted 1 mm away from ISME (Figure 5.4, n=7 rats). In five out of seven animals, probe implantation caused a SD, confirmed by a drastic increase in potassium concentration directly after probe implantation. The response to probe implantation was greater (4.06 ± 2.80 mM) than the SD's created by needle pricks. This may be due to the outer diameter of the probe being greater than that of the needle. In the animals in which a SD was not seen due to probe implantation, it was confirmed that the electrodes were still functioning. It is most likely that the SD event "missed" the ISME as SD waves do not follow a specific pattern.[143]

Initially, it was concerning that microdialysis probe implantation elicits an SD wave. Only one SD event was observed per probe implantation, implying that the probe induced injury was not severe enough to encourage multiple SD (as occurs in TBI).[34] Occasionally, implantation of the much smaller ISME would cause a small SD (Figure 5.1, t=0). The potassium levels return to baseline within a similar time frame as the potassium levels during a pre-probe needle pricks (2-3 minutes). It does not appear that probe implantation causes continuous SD's and thereby secondary injury to nearby tissue.

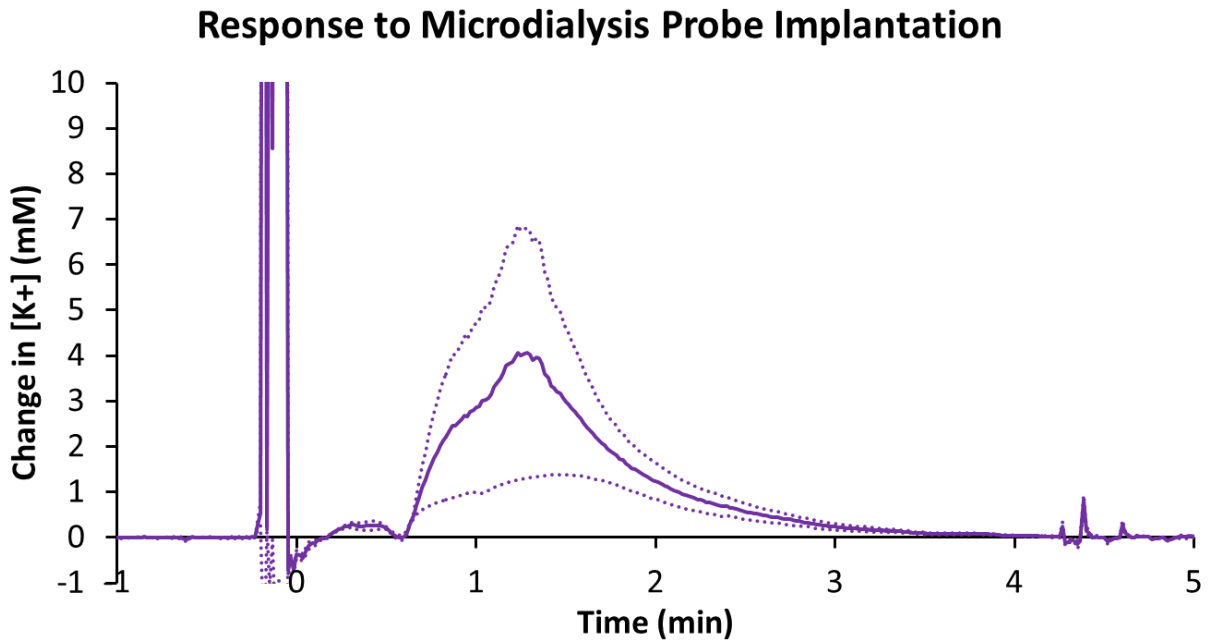

Figure 5.4. The change in potassium in response to microdialysis probe implantation (n=7 rats). Probes were implanted in all seven rats, however in 2 out of the 7 rats, a potassium change was undetected at the ISME. Data was adjusted so that microdialysis probes were implanted at t=0 min. The spike in the data just before t=0 min, is attributed to opening the Faraday cage to lower the probe: it is not a change in potassium.

After microdialysis probes were implanted and the potassium concentration returned to baseline, needle pricks recommenced. Changes in potassium were always observed following probe implantation in tissue 1 mm away (Figure 5.5). Average potassium changes to needle pricks post-probe (3.21 ± 2.30 mM) were similar compared to pre-probe responses. It appears as though the SD event is delayed post-probe implantation but we cannot confirm this, as the needle prick location was not consistently measured. Location of the needle prick alters the time in which it takes the SD wave to travel to the ISME. Overall, microdialysis probe implantation did not impact measurements SD events in tissue 1 mm away. Microdialysis probes do not affect the amplitude of potassium increase induced by a needle prick.

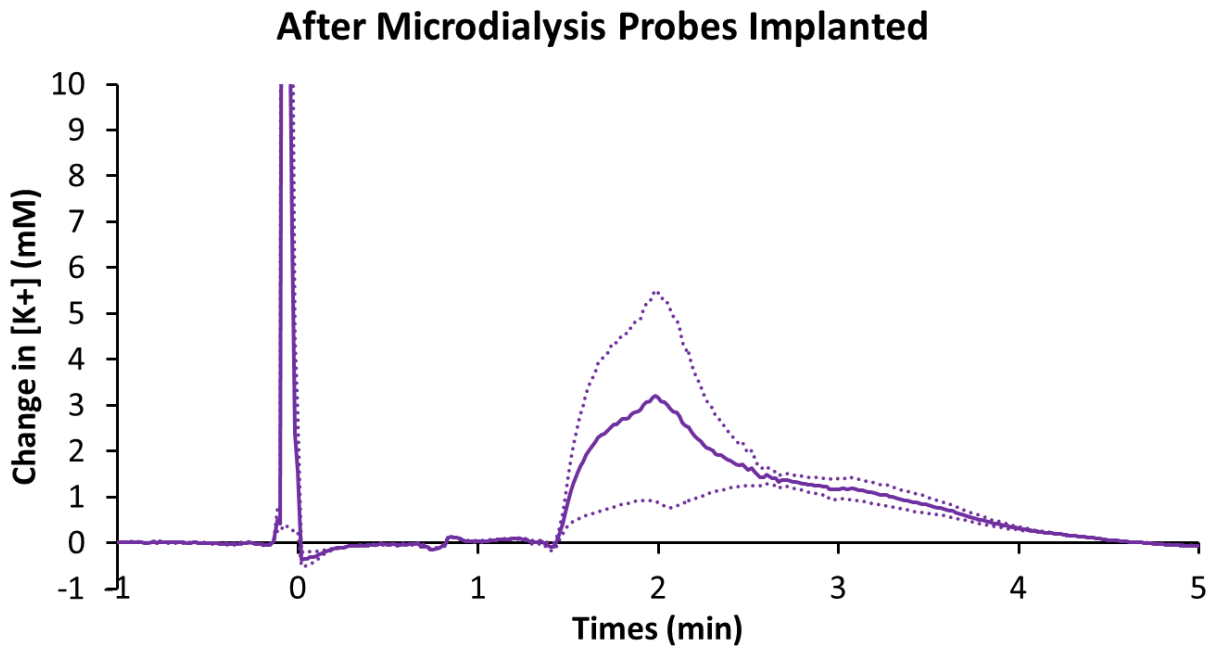

Figure 5.5. The change in potassium in response to needle pricks (NP) performed after microdialysis probes were implanted (n=7 rats). Data was adjusted so that needle pricks were at t=0 min. The spike just before t=0 is noise caused by the opening of the Faraday cage to perform the needle prick: it is not a change in potassium. Microdialysis probes did not affect the detection of potassium changes in the cortex.

5.4 CONCLUSIONS

Clinical microdialysis is currently used to monitor SD events in traumatic brain injured patients. As microdialysis probe implantation disrupts surrounding tissue, it is imperative to determine probe implantation's effect on monitoring SD events. Here, we demonstrated that microdialysis probe implantation does not affect potassium changes during an SD event measured 1 mm away. Microdialysis probe implantation causes a SD, however it does not impact the overall monitoring of succeeding SDs. This data represents a preliminary study to determine effects of probe implantation on potassium levels in surrounding tissue. As microdialysis samples from tissue directly next to the probe, further experiments involving electrode placement closer to the microdialysis probe are required to determine if potassium levels in adjacent tissue are affected.

6.0 SPATIAL MAPPING REVEALS FUNCTIONAL DOPAMINE SUB-REGIONS OF THE STRIATUM THAT CORRESPOND TO PATCH-MATRIX COMPARTMENTS

Partial contents of this chapter were previously published in: Taylor, I.M., Nesbitt, K.M., Walters, S.H., Varner, E.L., Shu, Z., Bartlow, K.M., Jaquins-Gerstl, A.S., Michael, A.C. *J. Neurochem*. **2015**, doi: 10.1111/jnc.13059.

I would like to acknowledge that the immunohistochemistry work in this chapter was performed by Andrea Jaquins-Gerstl.

6.1 INTRODUCTION

Dopamine (DA) is an immensely important neurotransmitter in the central nervous system. It contributes to motor control, reward-based learning, the regulation of mood and anxiety, and several other brain functions.[146-147] Pathology of the central DA systems is clearly implicated in Parkinson's disease, dystonia, schizophrenia, attention deficit hyperactivity disorder, and substance abuse.[148-151] Consequently, drugs that target DA systems have wide-ranging therapeutic applications and illicit uses. So, understanding brain DA activity per se and the mechanisms of action of DA-targeting drugs is immensely significant.[35, 152] Our previous findings, derived from voltammetric recordings in the rat brain, show that the dorsal striatum is organized as a patchwork of distinct DA kinetic domains.[53, 106, 153-154] We have named these

kinetic domains fast and slow because the initial rates of DA release are significantly faster in the former compared to the latter domains. These domains also respond differently to pharmacological manipulations with DA receptor antagonists and DA transporter inhibitors.[53, 106, 155] Our objective in this study is to explore their anatomy: we wish to know the distribution of the domains, and their anatomical relationship to the neurochemical marker of striatal structure, the μ-opiate receptor. The striatum is composed of a mosaic of spatial compartments known as the striosomes (patches) and the matrix. Extensive literature exists on the spatial organization of the patch and matrix compartments and their functions. However, little is known about these compartments as they relate to fast and slow kinetic DA domains observed by fast scan cyclic voltammetry. We achieve this objective by combining high spatial resolution voltammetric mapping with detailed immunohistochemical analysis these architectural compartments (patch and matrix) by means of fluorescence microscopy.

The discovery of these domains was an innovation in its own right, shedding new light on DA's spatial and kinetic heterogeneity. In this study, we used fast scan cyclic voltammetry (FSCV) to systematically characterize the domains as they pertain to two distinctive DA terminal fields the dorsal medial striatum (MS) and dorsal lateral striatum (LS) which has not been attempted before as far we know. The FSCV literature contains no examples of comprehensive striatal mapping such as we have done. Also, we correlate the domains with the known architecture of the striatum as embodied in the patch and matrix compartments (this subject is widely known and has been thoroughly reviewed.[156-157] Our work provides much more detail and much higher spatial resolution by using carbon fiber microelectrodes and FSCV. Detailed correlations between FSCV recordings and histochemical tissue markers, while not unheard of,[158-159] are quite rare and we are the first to correlate FSCV with patch and matrix

compartments via immunohistochemistry using the μ-opiate receptor. Our findings demonstrated a direct correlation between patch compartments with fast domain DA kinetics and matrix compartments to slow domain DA kinetics. We also investigated the kinetic domains in two very distinct sub-regions in the striatum. The lateral striatum as opposed to the medial striatum is mainly governed by fast kinetic DA domains. These finding are highly relevant as they may hold key promise in unraveling the fast and slow kinetic DA domains and their physiological significance.

6.2 EXPERIMENTAL SECTION

6.2.1 Carbon Fiber Microelectrodes

Borosilicate capillaries (0.58 mm I.D., 1.0 mm O.D., Sutter Instruments, Novato, CA), each containing a single carbon fiber (7μm diameter,T650, Cytec Carbon Fibers LLC., Piedmont, SC), are pulled to a fine tip using a vertical puller (Narishige, Los Angeles, CA, USA) and the tip is sealed with epoxy (Spurr Epoxy, Polysciences Inc., Warrington, PA, USA). Carbon fibers were cut to a length of 200 μm from the base of the capillary. The capillaries were filled with mercury and a nichrome wire (Goodfellow, Oakdale, PA) was inserted to complete electrical contact. Microelectrodes were pre-treated by soaking the tip in isopropyl alcohol (Sigma Aldrich, St. Louis, MO) for one hour.

6.2.2 Fast-Scan Cyclic Voltammetry

Voltammetry is performed with the EI 400 (Ensman Instruments, Bloomington, IN) and CV Tar Heels v4.3 software (Dr. Michael Heien, University of Arizona, Tucson AZ). The reference electrode is Ag/AgCl. The waveform starts at 0 V vs. Ag/AgCl, ramps linearly (400 V/s) to +1.0 V, then to -0.5 V, and returns to 0 V. The scan frequency is 10 Hz (scans at 100 ms intervals). DA is identified by the background-subtracted voltammograms and quantified from the magnitude of the oxidation current between 0.5 and 0.7 V. Calibration is performed in a flow cell with N_2-spurged artificial cerebrospinal fluid (aCSF: 142 mM NaCl, 1.2 mM $CaCl_2$, 2.7 mM KCl, 1.0 mM $MgCl_2$, 2.0 mM NaH_2PO_4, pH 7.40) containing freshly prepared DA (dopamine HCl, Sigma Aldrich, St. Louis, MO, USA) standards.

6.2.3 In vivo Procedures

All in vivo animal procedures were performed under approval of the Institutional Animal Care and Use of Committee of the University of Pittsburgh. Male Sprague-Dawley rats (250-350 g Charles Rivers, Raleigh, NC) are intubated and anesthetized with isoflurane (2.5% by volume) placed in a stereotaxic frame and wrapped in a 37˚C heating pad (Harvard Apparatus, Holliston, MA, USA). Holes are drilled through the skull for the reference, stimulating, and working electrodes. Two carbon fiber electrodes were implanted into the striatum (coordinates below). A stimulating electrode (bipolar stainless steel, MS303-1-untwisted, Plastics One, Roanoke, VA) was positioned over the medial forebrain bundle (MFB-4.3 mm posterior to bregma, 1.2 mm lateral from bregma, and 7.2-8.5 mm below the dura). The stimulating electrode was lowered until evoked DA was measured at both carbon fiber electrodes in the striatum. The electrical

stimulus is optically isolated and a biphasic, constant-current, square wave with the following parameters: 2 ms per pulse, 250 μA pulse height, and 60 Hz pulse frequency, 0.2, 1, or 3s duration (Neurolog 800, Digitimer, Herefordshire, England).All experiments were completed in the right hemisphere.

6.2.4 Classification of Fast and Slow Domains

In our previous studies,[53, 106, 153-154, 160] we identified fast and slow domains by means of a brief stimulus test (60 Hz, 250 μA, 200 ms). Recording sites that respond to the test stimulus are classified as fast: otherwise, they are classified as slow. Fast sites respond immediately to the stimulus and slow sites exhibit an initial lag. Most of the responses reported were evoked with the experimental stimulus selected for this work (60 Hz, 250 μA, 3 s).

6.2.5 Striatal Mapping

We implanted n=20 carbon fiber electrodes in the striatum of n=10 individual rats (two new electrodes per rat). One of these was implanted in the MS (1.6 mm anterior to bregma, 1.5 mm lateral from bregma, and 4.5 mm below the cortical surface) and the other in the LS (0.2 mm anterior to bregma, 3.8 mm lateral from bregma, and 4.5 mm below the cortical surface).[161] The two electrodes were stereotaxically lowered in 5x200 μm intervals (total track length = 1.0 mm). Each recording site was evaluated with the test stimulus (60 Hz, 250 μA, 200 ms) and the experimental stimulus (60 Hz, 250 μA, 3 s). After the recording session, the electrodes were lowered an additional 500 μm and used to mark the bottom of the track with an electrolytic

lesion (35-V AC 10 s). Post-mortem histological analysis confirmed that all the electrodes were properly positioned, consistent with their intended stereotaxic target.

6.2.6 Data Analysis

Statistical analysis of Figure 6.6 was performed by 3-way ANOVA with time (repeated measure), track, and depth as factors: time. Statistical analysis was performed with IBM SPSS software version 22.

6.2.7 Tissue Fixation and Processing

Tissue fixation, processing, immunochemistry and fluorescence microscopy followed our published procedures.[17-18] After in vivo recording, rats were perfused with PBS, paraformaldehyde, and a suspension of fluorescent beads (0.1 μm diameter, Molecular Probes: the beads label blood vessels and provide an assessment of vascular damage, which is minimal with these microelectrodes). The tissue was submerged in 2% paraformaldehyde for 2 hours and 30% sucrose overnight, frozen in liquid nitrogen-cooled 2-methylbutane, and stored at -80°C until sliced horizontally in a cryostat into 30-μm thick sections. The sections were placed into 24-well plates with cryoprotection solution and stored at 20°C until immunolabeling was performed.

6.2.8 Immunofluorescence Protocol and Fluorescence Microscopy

Tissue sections were labeled with antibodies (markers discussed below) and DAPI to visualize nuclei. Sections were examined by fluorescence microscopy (Olympus BX61, Olympus; Melville, NY) with a 1.25X or 10X objective and wavelength matched filter sets (Chroma Technology; Rockingham, VT). Images were analyzed and quantified with Metamorph/Fluor 7.1 (Universal Imaging Corporation; Molecular Devices), NIS Elements AR (Nikon Corporation; Tokyo, Japan) and OriginPro.

Using immunohistochemistry with tyramide signal amplification (TSA) protocol on free-floating sections we determined distributional patterns of the μ opioid receptor, MOR, (Koizumi et al 2013, Okita et al 2012). Rabbit polyclonal MOR antibodies (1:100,000; Millipore), was used as the primary antibody. Tissue sections were left in the primary antibody in a 20% goat serum blocking solution at room temperature for 48 hours. The bound primary antibody was detected with fluorescein (Perkin Elmer, Shelton, CT).

6.3 RESULTS AND DISCUSSION

6.3.1 Defining the Lateral and Medial Striatum

An extensive body of literature describes the anatomical studies which delineates the striatal sub-regions in terms of their afferent and efferent cortical projections.[156-157] The dorsal striatum in rodents is not clearly divided into caudate and putamen, however it does have a medial-lateral gradient of connectivity which is similar to the caudate and putamen connectivity of primates.[162-

[163] The medial portion of the dorsal striatum extends ventrally to the limits of the accumbens; it has been demonstrated to receive most of its input from associative areas of the cortex (i.e. caudate), whereas, the dorsal lateral striatal region receives input from the sensorimotor areas of the cortex like the putamen.[163] Furthermore, a gradient of behavior functions spans laterally across the striatum.[164-166] In our studies we have examined the distinct DA kinetics differences between the MS and the LS.

6.3.2 Domain Classification with Microelectrodes

To date, we have used microelectrodes to study DA's domains; the use of such small devices takes advantage of their higher spatial resolution. (Figure. 6.1). Figure 6.1 reports stimulus responses from six consecutively deeper recordings sites along a single microelectrode track (dorsal to ventral) in the LS track. Recording sites that do not respond to 200-ms stimuli are classified as slow (middle and right panel): these sites do respond to longer stimuli. Recording sites that do respond to 200 ms stimuli (left panel) are classified as fast. The far right panel indicates individual classification associated with the individual recording site described above. Three different stimulus lengths were recorded for each site 200 ms, 1 s and 3 s (60 Hz, 250 µA). The fast and slow responses are clearly distinct, so the classification is objective. Thus, Figure 6.2 confirms that it is feasible to both classify and map domains with microelectrodes in the same individual animal. In this particular example, Figure 6.2, most of the responses are predominately fast except for one (4.5mm below dura).

Using two carbon fiber electrodes simultaneously we were able to observe, for the first time, fast and slow DA responses during a single stimulation of the MFB (Figure 6.2). During a 200 ms stimulation of the MFB, evoked DA was measured at one electrode (left-red) and not

detected at the other electrode (left-blue). However, a longer stimulation (3s) produced evoked DA responses measurable at both electrodes. This confirms that the position of the stimulating electrode in the MFB doesn't cause DA responses to be fast or slow in the striatum. Diversity of DA responses is based on electrode location in the striatum.

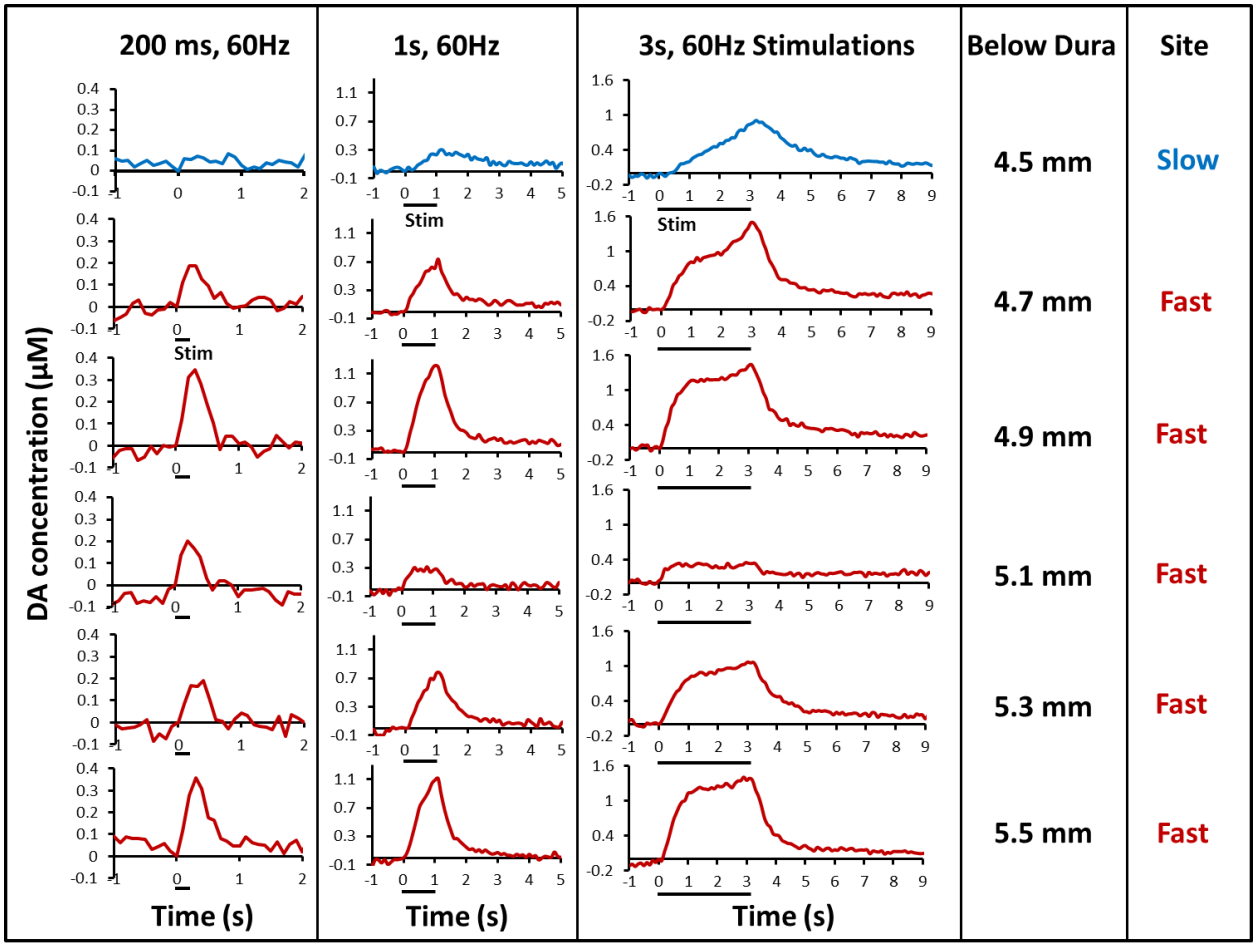

Figure 6.1. A representative set of individual responses recorded along a the LS track in a single animal. Three different test stimuli were recorded 200 ms, 1 s and 3 at 60 Hz, 250 µA. Each evoked response was then classified as either fast or slow (far right column).

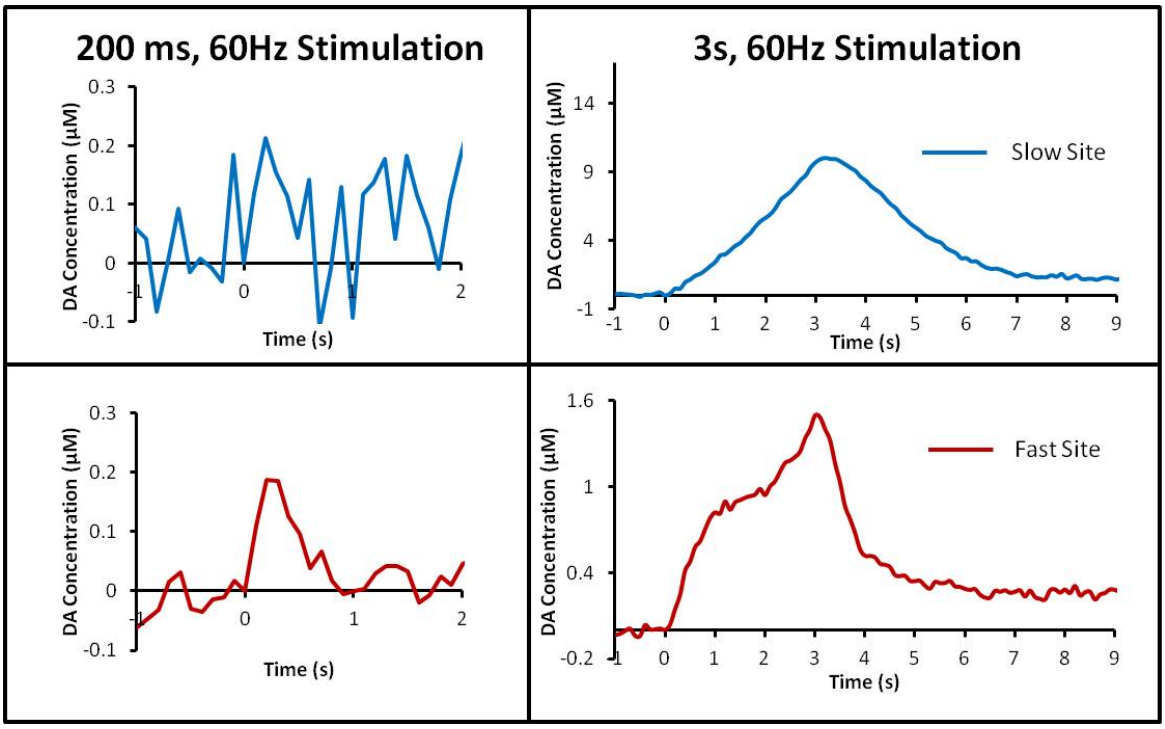

Figure 6.2. Individual representations of evoked DA responses during stimulation of the MFB measured by two electrodes implanted in different electrodes in the striatum.

6.3.3 Evoked DA Responses in the Medial and Lateral Striatum

It is well known that the kinetics of evoked DA release in the striatum is heterogeneous.[167-169] Although the practice of voltammetry often seeks "hot spots," sites that produce maximally concentrations of DA, this has created the impression that the striatum contains two types of DA responses "hot spots" and "cold spots," sites that produce less concentrations of DA.[159, 170-172] This idea undermines the ultrastructure of the striatum; studies show that the striatum contains DA terminals regularly spaced at 2-5 µm intervals.[173] Complex arrays of DA terminal are arranged in a lattice like structure, meaning that recording electrodes in the striatum are always physically close to DA terminals. Presently, the literature contains no explanation for what constitutes "hot" and "cold" spots or if there is functionality differences between the two.

We have investigated evoked DA responses and further classified them based on their kinetic responses to stimulation (fast and slow). A recent publication from our group shows that in the dorsal striatum, functionally distinct sub-regions express DA kinetic diversity in five different response types (1 slow and 4 fast) in the same location of the striatum of n= 168 individual animals.[154] Here, we have demonstrated that very distinctive kinetic differences are prominent even in the same electrode track of the same animal (Figure 6.3). Under the same stimulus conditions, 3s, 60 Hz stimulation, there is direct evidence of DA's heterogeneity in the striatum. The color coded arrows in the middle panel correspond to the individual FSCV recording and their classification (fast or slow). What is obvious is that the kinetic behaviors change frequently from slow-fast-slow (left hand electrode track) and vice versa, differences are within 0.2 mm (dorsal to ventral) separation.

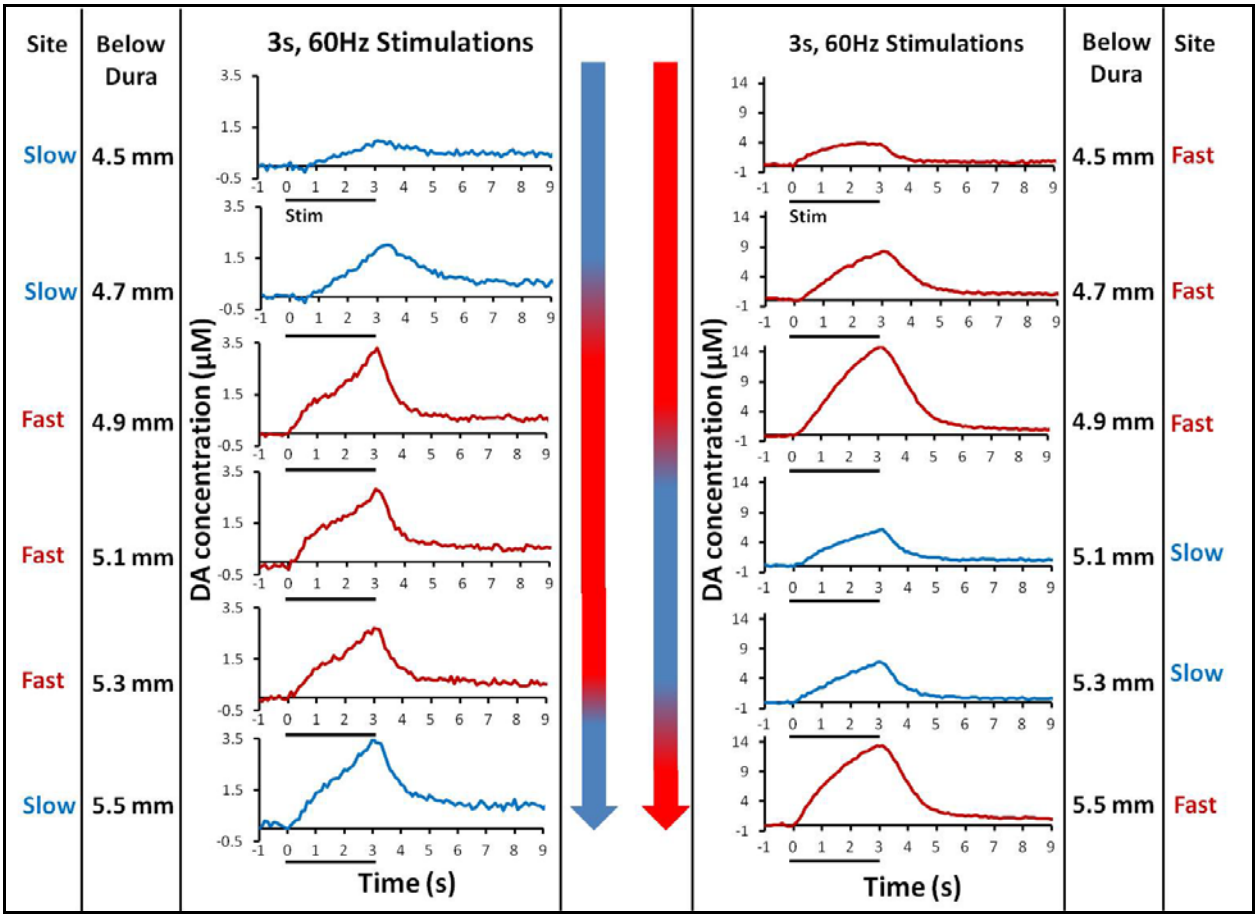

Figure 6.3. Individual evoked DA responses from two different electrode tracks of the same animal. Kinetically different DA responses change as the electrode is moved from dorsal to ventral in the striatum. Blue represents slow domains and red fast domains. The center arrows correspond to each electrode track; they are color coded to match the individual recording locations.

6.3.4 Fast Domains Prevail in the Lateral Striatum

Prior studies have identified fast and slow kinetic domains in the DS,[53, 106, 153-155, 160] and also in the core of the nucleus accumbens.[174-175] Further investigations into the striatum in this study now reveal that evoked DA responses recorded from the MS and the LS have very distinct kinetic profiles (Figure 6.4). Using n=20 individual electrodes to record evoked DA release at six sites along the MS and LS (n=10 rats). The right panels of Figure 6.4 give the location of each

recording site and count the number of times each site was classified objectively as fast (by means of a response to a 200 ms stimulation). The left panels of Figure 6.4 report averages of the responses at each site (SEMs reported in Figure 6.5). Responses recorded along the MS track and the LS, located in the medial and lateral sub-regions of the striatum, respectively, are distinct in both amplitude and profile. The responses along the MS track are predominantly slow while those along LS track are predominantly fast. The difference in response amplitudes between, but not within, the MS and LS tracks is statistically significant (Figure 6.6). These findings strongly support the conclusion that DA's kinetic diversity is sub-region dependent and that fast domains are more readily found in the LS than the MS.

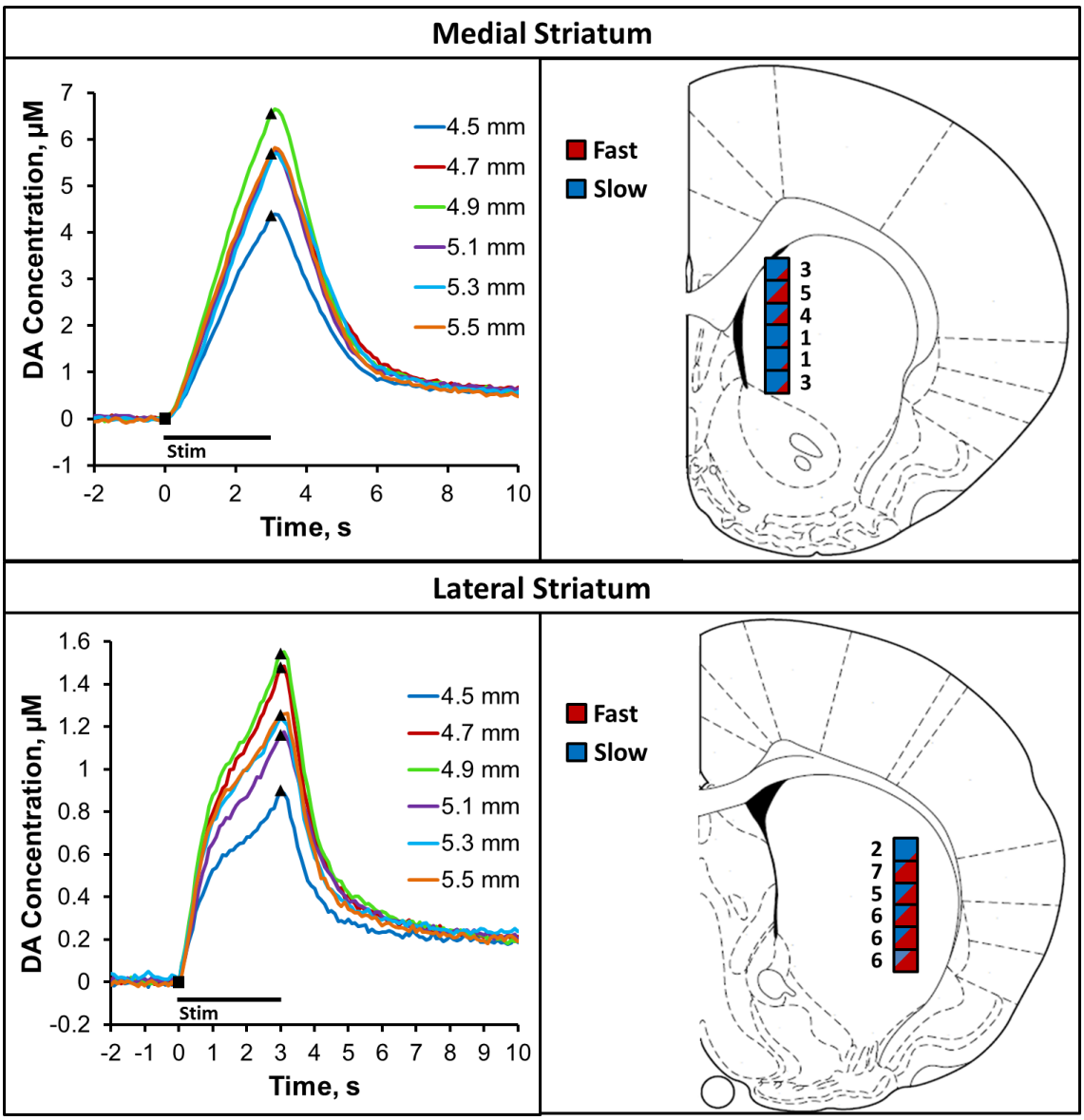

Figure 6.4. Striatal mapping along the MS track (top) and the LS track (bottom). Right Panels: the boxes show the anatomical location of each recording site and the number of fast responses observed at each location red represents fast and blue represents slow). Left Panels: average of the responses long the MS and the LS (n=10 electrodes per track, 1 track each per rat; SEMS reported in Figure 6.5).

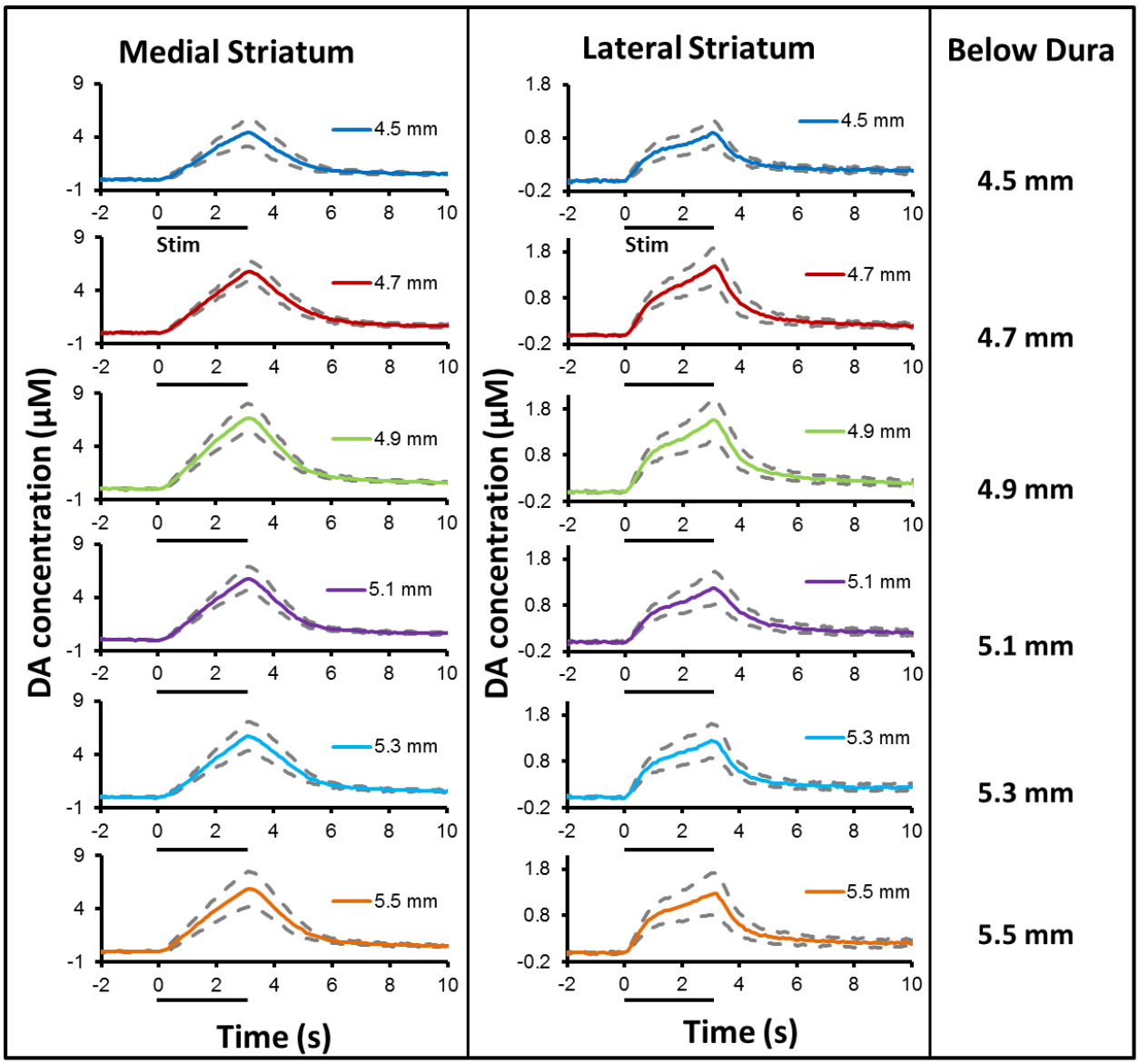

Figure 6.5. The averaged responses from Figure 6.4 (solid lines; n=10 electrodes per track, two tracks per animal) shown separately with their SEMs (dashed grey lines). See Figure 6.6 for statistical analysis.

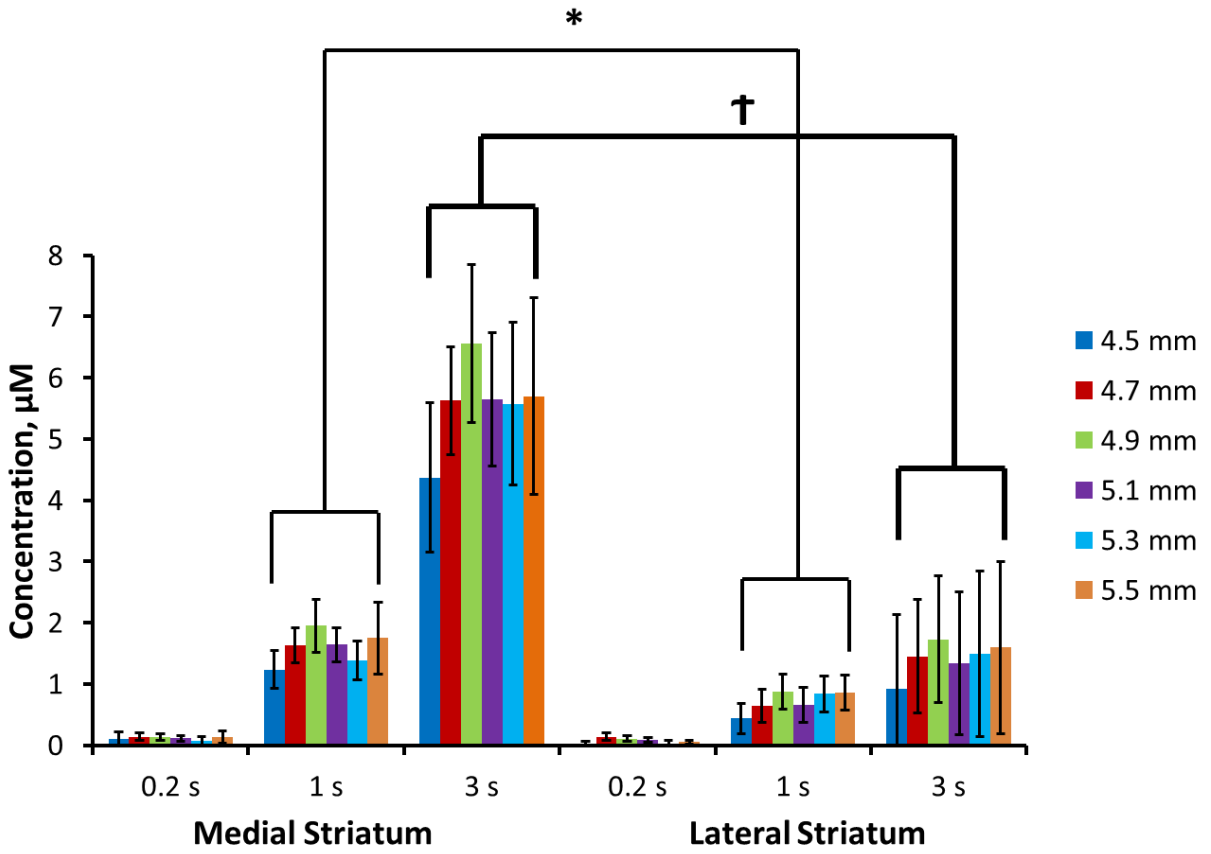

Figure 6.6. Evoked DA concentrations (mean ± SEM, n=10 electrodes per track, 2 tracks per rat) at t=0.2 , 1 , and 3 s after the onset of the stimulus. Statistical analysis was by 3-way ANOVA with time (repeated measure), track, and depth as factors: time $F(2, 216)=153.7$, $p< 0.00001$); track $F(1, 108)=51.0$, $p<0.00001$; time * track interaction $F(2,216)=64.4$, $p<0.00001$; depth was not a significant factor. Bonferroni post-hoc pairwise comparisons: the difference in amplitudes between Track A and Track B are significantly different at t=1 s (*$p< 0.00001$) and at t=3 s (†$p<0.00001$): differences in amplitudes within each track are not significant.

6.3.5 Correlation to Patches-Matrix Compartments

The anatomical organization of the striatum includes the patch: matrix compartmentalization and the direct and indirect pathways (for a detailed review, see (Crittenden & Graybiel 2011)).[156] The patches and matrix receive distinct DA inputs from the substantia nigra pars compacta (SNc),

while striatal neurons from the patches, but not the matrix, selectively project to the SNc. This provides a basis for anticipating anatomical organization of the DA terminal field as well. Investigators have previously speculated that a relationship might exist between the heterogeneity of evoked DA release and the patch-matrix striatal compartments.[169, 176] Moreover, the medial and lateral sub-regions of the DS are functionally distinct,[164-166] so it is also relevant to ask if such sub-regions are distinct with respect to DA kinetic diversity.

The μ opioid receptor and calbindin are widely used markers for the patch and matrix, respectively.[158, 177] In our study we labeled for only the μ opioid receptor (patch), within the striatum, if the tissue is not label with the μ opioid receptor then the surrounding area is designated as the matrix compartment. We correlated the electrochemical recordings with this marker in the two separate electrode tracks MS and LS shown in Figure 6.7.

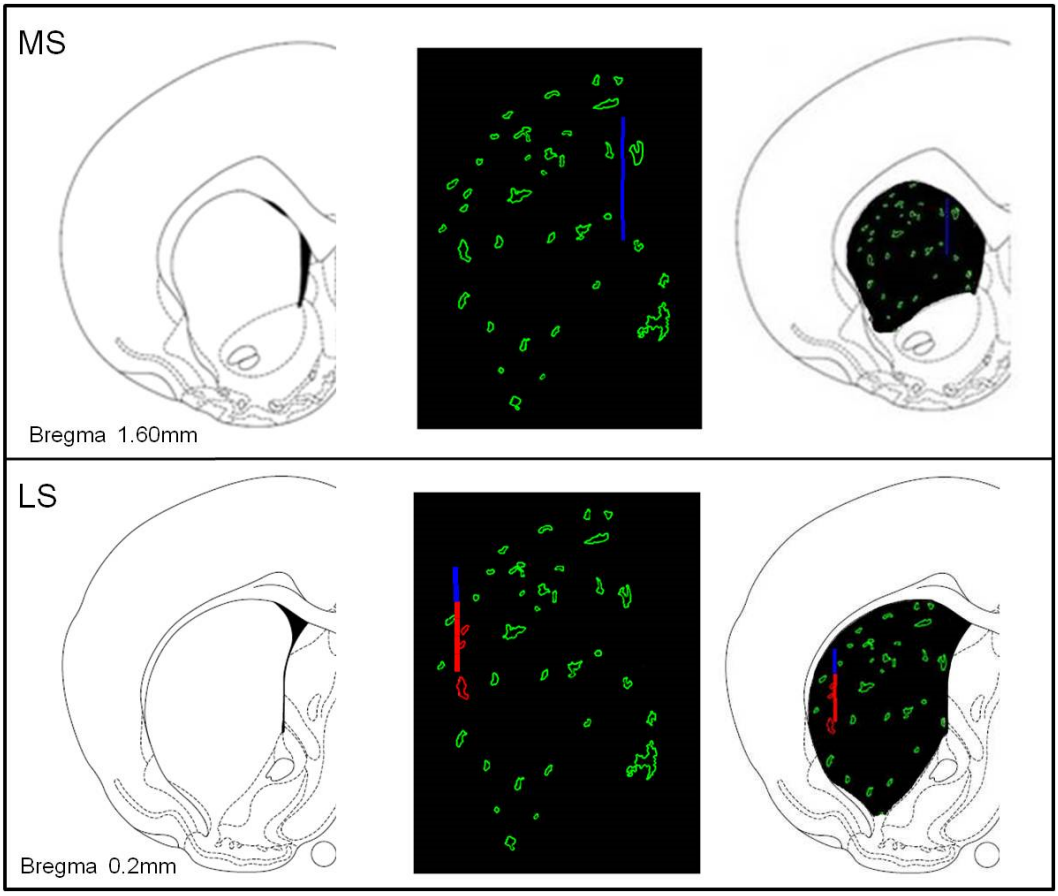

Figure 6.7. Scheme depicting the two electrode tracks and the patch-matrix compartments. Top represents the regions in the MS and bottom represents l regions in the MS. Blue and red patches correspond to slow and fast domains, respectively, that are in physical contact with the electrode. MS is 1.6 mm anterior to bregma, 1.5 mm lateral from bregma, and 4.5 mm below the cortical surface. LS is 0.2 mm anterior to bregma, 3.8 mm lateral from bregma, and 4.5 mm below the cortical surface, coordinates of Paxinos and Watson[161].

6.3.6 Determination of the μ-Opiate Receptors Rich, Patches-Matrix Compartments

We used polyclonal antibodies against C-terminal synthetic peptides for μ-opiate receptors, (MOR) in this study. Marked variations in the density and localization of the MOR were seen on horizontal sections of 30 μm sections of striatal tissue lesioned with a carbon fiber electrode, Figure 6.8. Electrolytic lesions made with the carbon fiber electrode were inconsistent; if lesions

were larger than three 30 µm sections, immunohistochemistry was not performed. If the lesion destroyed (burned) the tissue then immunohistochemistry was not performed. Only in experiments where lesions were contained within three 30 µm sections or less was staining performed for the MOR. Figure 6.8A is a differential interference contrast image of a horizontal tissue slices where a lesion made 500 µm below the last voltammetric recording; this is indicated in the darker area of the tissue in the LS (circled in red).

Using this antibody single-labeled immunohistochemistry showed heightened immunoreactivity for MOR in striatal slices. No specific immunoreactivity was found in other sections of tissue (Figure 6.8B and 6.8C). Obvious MOR labeling exhibited a striking mosaic distribution in the striatum, highly concentrated labeling in the patches and subcallosal streak was present.[178-179] A large matrix field (absence of labeling) is present in all striatal tissue slices. The subcallosal streak is in agreement with other studies using [^{3}H] naloxone binding which borders the striatum; this was observed in all sections.[180-181] In the rat [^{3}H] naloxone binding is generally used for autoradiographic visualization of striatal patches.[178-179] In figure 6.8B highly concentrated labeling in the patches and subcallosal streak are clearly evident, however, some of the myelinated axon bundles are visible but are less intensity compared to the patches. These myelinated axon bundles can be observed in Figure 6.8A as dark brown-black regions, for this reason, DIC images of each section were superimposed onto the fluorescence MOR labeled images to differentiate the patches from the myelinated axon bundles, see Supporting Information Figure S6.1.

Patches with the lowest fluorescence intensity were determined and used as a threshold to draw the outline of individual patches on horizontal sections using NIS Elements AR software (Figure 6.8D). An electrode drawing (drawn to scale) was superimposed on to these “outlined”

patches. If the electrode was in physical contact with a patch, from these drawings, the patch was outline in the corresponding FSCV recording (blue: slow domain, red: fast domain).

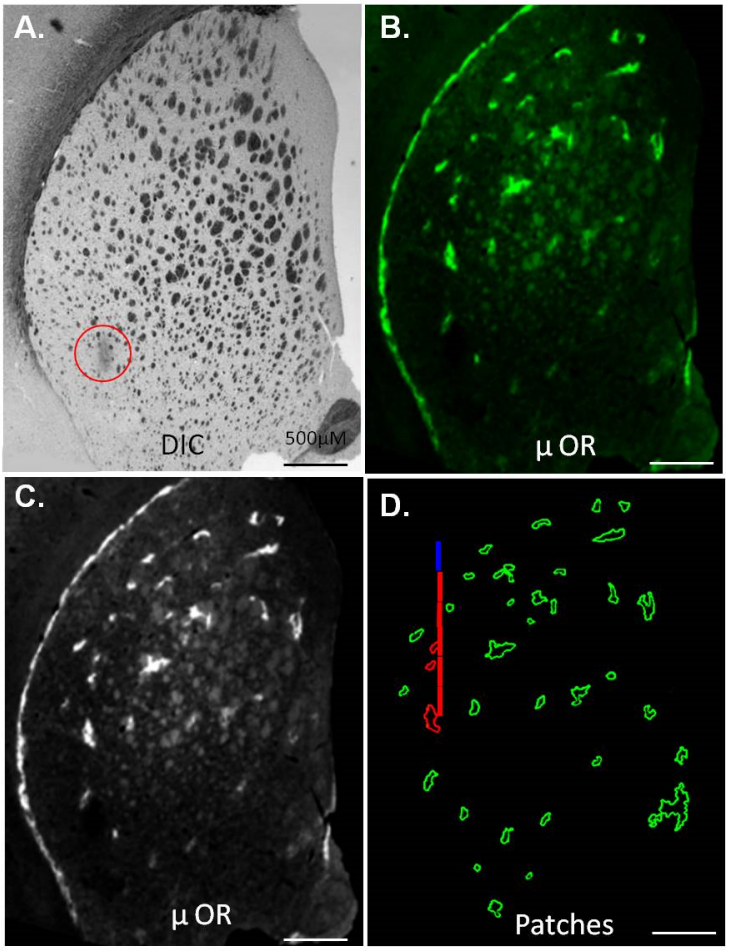

Figure 6.8. A representative collage of striatal patches identified by MOR immunohistochemistry staining. A) Differential interference contrast image of a horizontal tissue slices. The red circle indicates were the electrolytic lesion is on the tissue. B) This same section labeled for MOR (patches) in the bright green regions. The matrix is indicated by an absence of labeling (meaning no green regions). C) A black and white image of (B). D) Computer drawn patches based off a set threshold values of fluorescence intensities with an electrode drawing (drawn to scale) superimposed onto these patches. Color coded corresponding FSCV recording are presented on this schematic. Scale bars are 500 μm.

6.3.7 Mapping High-Resolution Voltammetric Recording of DA to Patch-Matrix Compartments

The FSCV literature contains no examples of comprehensive striatal mapping. We have correlated the domains with the known architecture of the striatum as embodied in the patch and matrix compartments. Past attempts have been described this in a series of papers from the Glowinski group in the 1990s.[181] Most of these studies used 3H-DA efflux from striosome-enriched regions of the striatum to associate DA kinetics with the striosomes. Detailed correlations between FSCV recordings and striosomes (patches) and matrix are demonstrated in Figure 6.9. Patches were outlined in green as previously described. The electrode track in Figure 6.9 is in the LS, as the electrode is lowered (dorsal to ventral) DA responses are collected. Each recording corresponds to the evoked DA profile to the right of the figure. All responses were classified as fast or slow domains. For clarity, we have color coded the electrode track and the evoked DA responses (red: fast domains and blue: slow domains.) If the actual electrode appears to physically touch a patch then the corresponding evoked DA response is outlined in a green box.

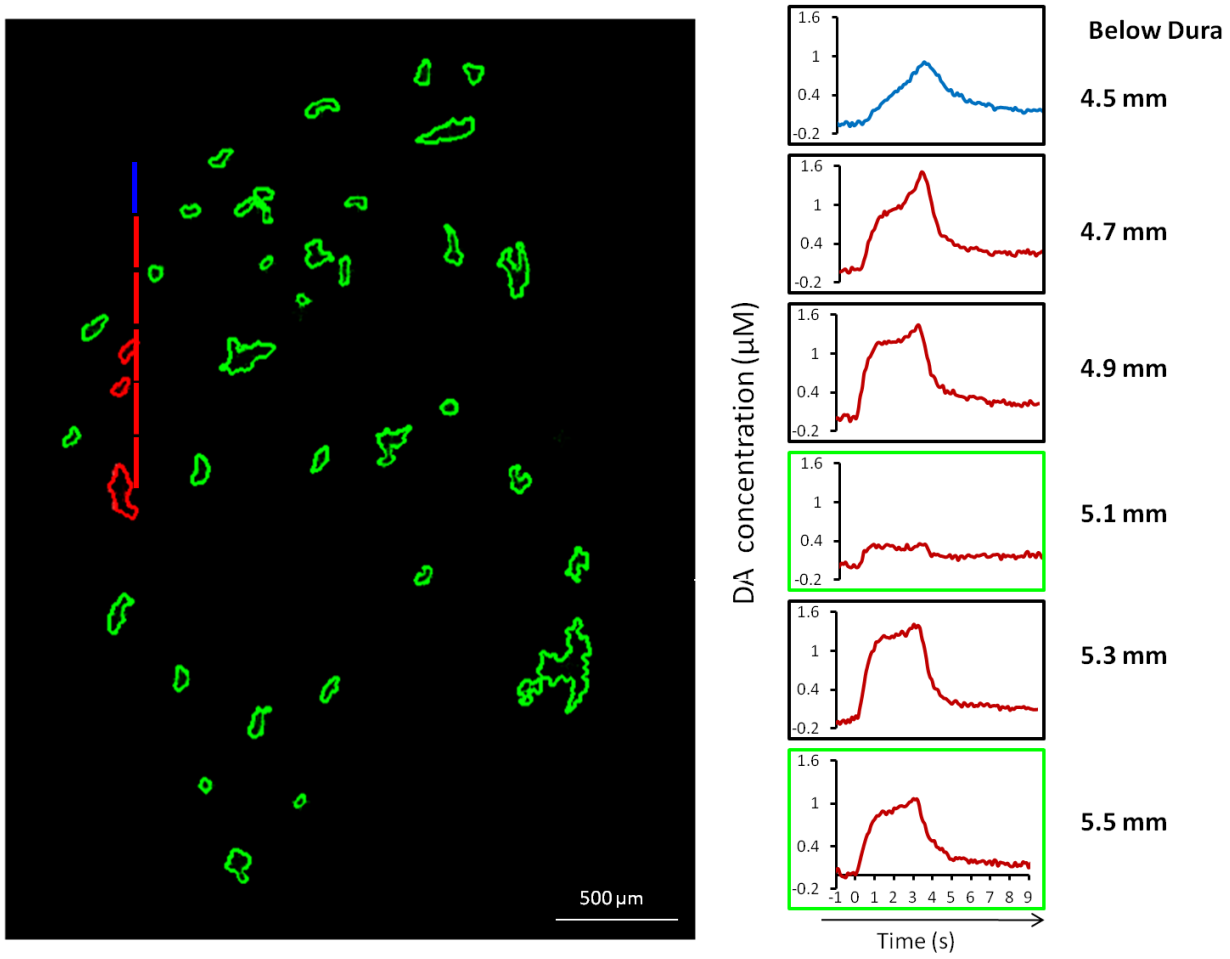

Figure 6.9. Represents mapping high-resolution voltammetric recording of DA in the striatum to MOR rich (patch) and poor (matrix) compartments. Drawing of the electrode track is superimposed onto tissue sections stained for MOR. FSCV recordings correspond to the electrode track (middle panel). If the electrode comes into contact with the patch then the voltammetry is outlined in a green box. Scale bar is 500 µm.

6.3.8 Comparisons of the Patch-Matrix Compartments in the Medial Striatum and the Lateral Striatum

A total of 7 different striatal tissue slices in the LS (n=2) and MS (n=5) were used to compare evoked DA responses (42 recordings) and MOR staining (Figure 6.10). The majority of the MS was made up of matrix. Of the 30 evoked DA responses recorded in the MS, the majority were in

the MOR poor (matrix) compartments, only a small number of patches (<17%) came into contact with the electrode track. In the MS only one of evoked responses was considered fast domains. Results for the LS were somewhat different than the MS; the evoked DA responses were 50% matrix and 50% patches. All of patches touching a recording site in the LS were also classified as fast domains. This came as somewhat of an unexpected finding but confirms our hypothesis that a relationship exists between the heterogeneity of evoked DA release and the patch-matrix striatal compartments. Because the domains are a feature of DA terminal fields in the striatum, we presume them to be physiologically significant although we have not yet identify how so exactly.

In summarizing these findings in donut plots (Figure 6.11A) the amount of patches present in fast domains was 87.5% while only 12.5% of these were matrix. The opposite is true for the slow domains as these were overwhelming dominated by matrix compartments (93.5%) and patches were only 6.5%. At a glance these two kinetically different DA domains are made up of two very distinct compartments. These are astonishing results that have not been reported before in the literature. Comparisons between the sub- region locations, MS and LS, versus patch and matrix compartments (Figure 6.11B) were also very interesting and informative. The patches present in the MS were 16.7% whereas the matrix was the predominated structure, 83.3% of this region. The LS region appeared to have each distribution of matrix and patch compartments (50% for both).

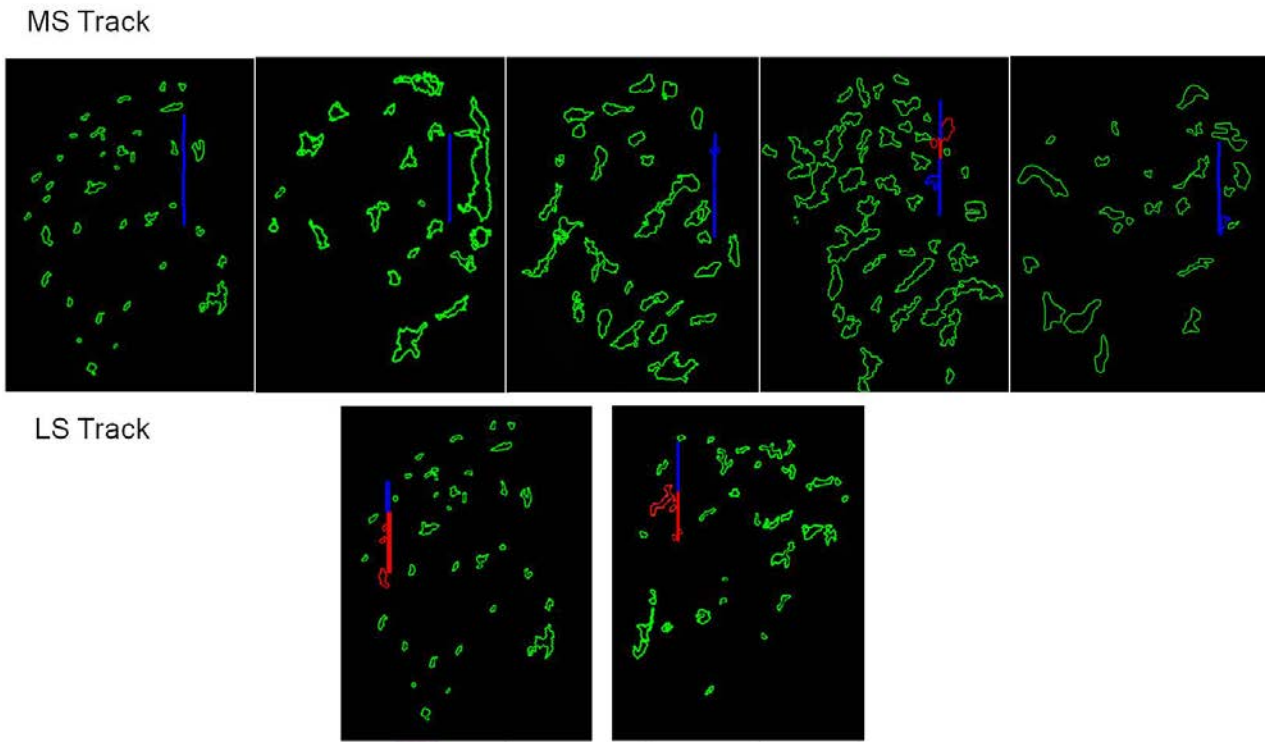

Figure 6.10. A comparison of patch and matrix compartments of the MS and LS and corresponding electrode locations for collection of evoked DA recordings of seven striatal tissue sections. Top panel represents the MS track electrode and the bottom panel represents the LS electrode track. Areas within the striatum that are not highlighted in green are the matrix compartments. The LS track has more fast domains and the medial track has more slow domains.

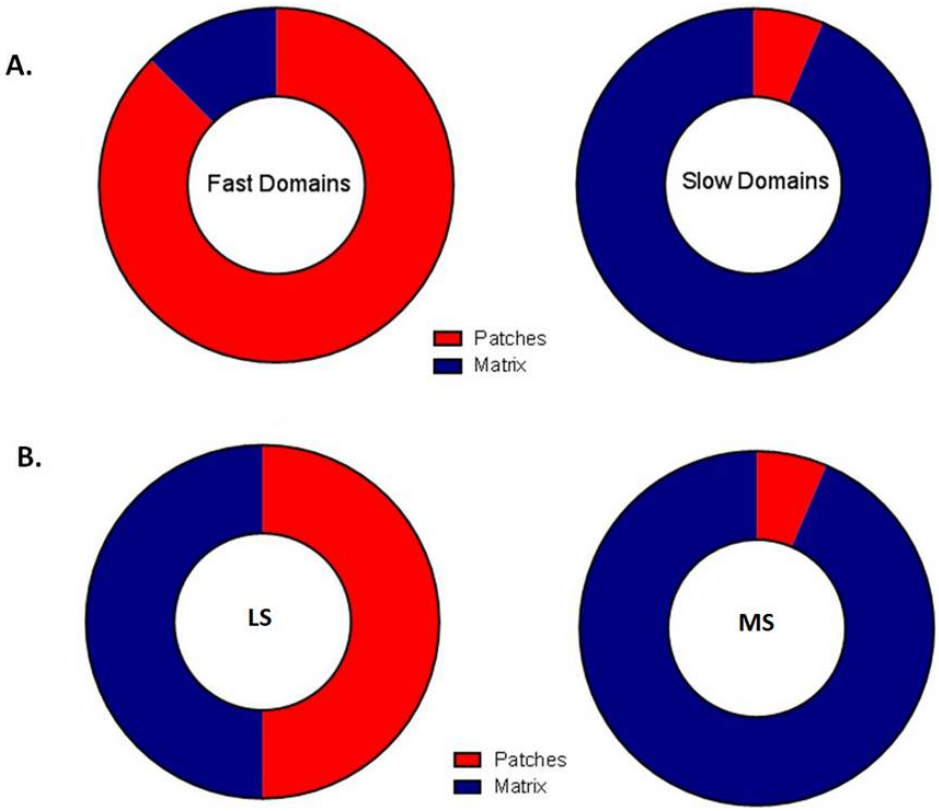

Figure 6.11. Donut plots of DA kinetic domains (fast and slow) and their anatomical architecture versus their sub-regions, LS and MS. Panel (A) represents the type of evoked DA response and their classification versus their location in patches (red) or matrix (blue). Panel (B) represents their sub-regions, LS and MS verse their location in patches (red) or matrix (blue).

6.3.9 Distance Dependence between Patch Compartments and Fast Domains

Our studies have examined the relationship between the patches-matrix and fast and slow evoked DA responses. We have only given consideration between these relationships if the electrode came into physical contact with patches. We now examine this relationship by looking at the distribution of the patches to fluorescence intensities and distance. Images were converted to surface intensity plots as demonstrated in Figure S6.2. The use of surface intensity plots shows

the distribution and pattern of fluorescence intensities in a 3-D topographical display, in this particular case blue represents the lowest intensity and pink the highest intensity.

We examined if physical contact between the patch and the electrode was a requirement which affected the corresponding DA kinetic profile or was there a distant dependence associate with the patches which distinguish the domains as fast or slow. In these measurements the subcallosal streak was excluded. Figure 6.12 demonstrates two distinctive kinetic profiles of DA in the LS. In this LS electrode track; all but one evoked DA response was classified as fast domains (red). The highest intensities, pink colors, are considered patches. Circles with distinctive diameters were drawn around the highest intensities to measure distances between the patches and the electrode track. Similar analysis was performed on MS (data not shown) however, in most of these surface intensity plots no patches were present, indicated by an absence of pink-red colors. These compartments are matrix (MOR poor) and are governed by slow domains, whereas in the patches (MOR rich) compartments the majority of DA domains are fast. Interestingly, fast domains are within 300 μm of the evoked DA recording site. In most situations, the closer the patches are to the electrode the high probability that the DA kinetics will be fast domains, this is evident in the LS panel. More studies need to be performed in the LS to provide the relationship between the distance of the electrode and the patches.

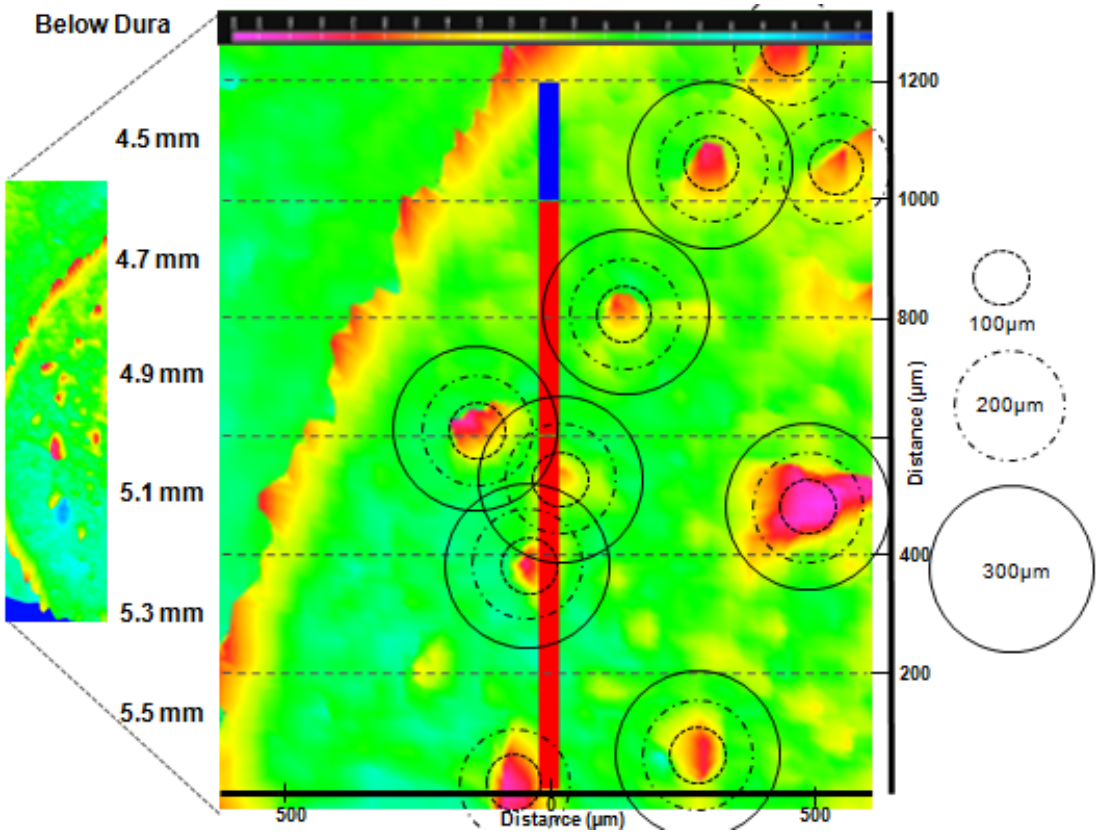

Figure 6.12. Illustrates surface intensity plots of LS-fast kinetic domains. The electrode track is in the center of the image. Most of the DA domains are fast (red) except for one. The length of the electrode is 200 µm; gray horizontal lines divide the individual evoked DA responses as the electrode traveled dorsal to ventral through brain tissue. Circles with distinctive diameters have been drawn around the highest intensities to measure distance. Intensity axis is at the top of each panel ranging from 0 (lowest) - 255 (highest).

6.4 CONCLUSIONS

In this study we have amassed a body of evidence showing that the DA terminal fields in the striatum of the rat brain are organized as fast and slow kinetic domains which corresponds to the biomarkers of striatal architecture, patch-matrix compartments. Comprehensive high resolution mapping in the MS and LS was performed using FSCV and correlated to patch-matrix

compartments. The majority of fast kinetic domains were located in the LS and the slow kinetic domains were more abundant in the MS. Interestingly, our findings conclude that the patch compartments correspond to fast domains and the slow domains to the matrix compartments. The closer the patches are in proximity to the recording site (~300μm) the more likely the kinetics is governed by fast domains; however a larger study will need to be performed. Because the domains are a feature of DA terminal fields in the striatum, and the mosaic organization of the patch-matrix reflects multiple levels of functional compartments we question "is there physiological significance?" Future studies include correlating other DA protein markers such as D2 autoreceptors, DAT and TH with DA kinetic domains. Another important consideration is characterizing how these striatal domains and compartments coordinated to cognitive and motor behavior.

6.5 SUPPLEMENTAL INFORMATION

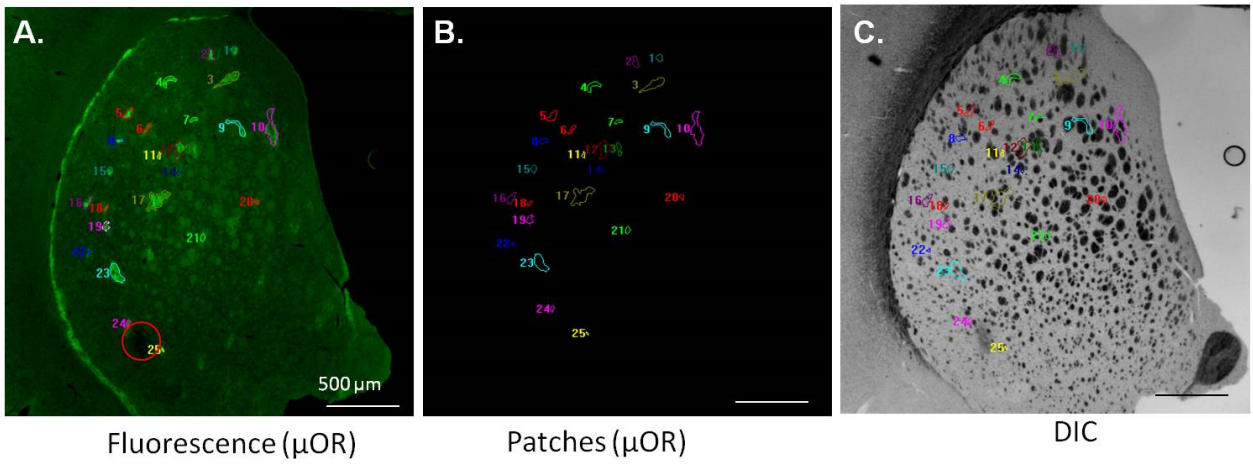

Figure S 6.1. A representative image of striatal patches identified by MOR immunohistochemistry staining. A) Using threshold settings patches were identified, numbered and outlined. B) Same image of (A) but only the outlined and numbered patches are shown. C) is the corresponding DIC image of (A) but image (B) has been superimposed on to it. Image (C) is used to confirm the patches are not non-specific binding of the µ-opiate receptor to myelinated axon bundles. Red circle in Image (A) corresponds to the location of the lesion. Scale bar is 500µm.

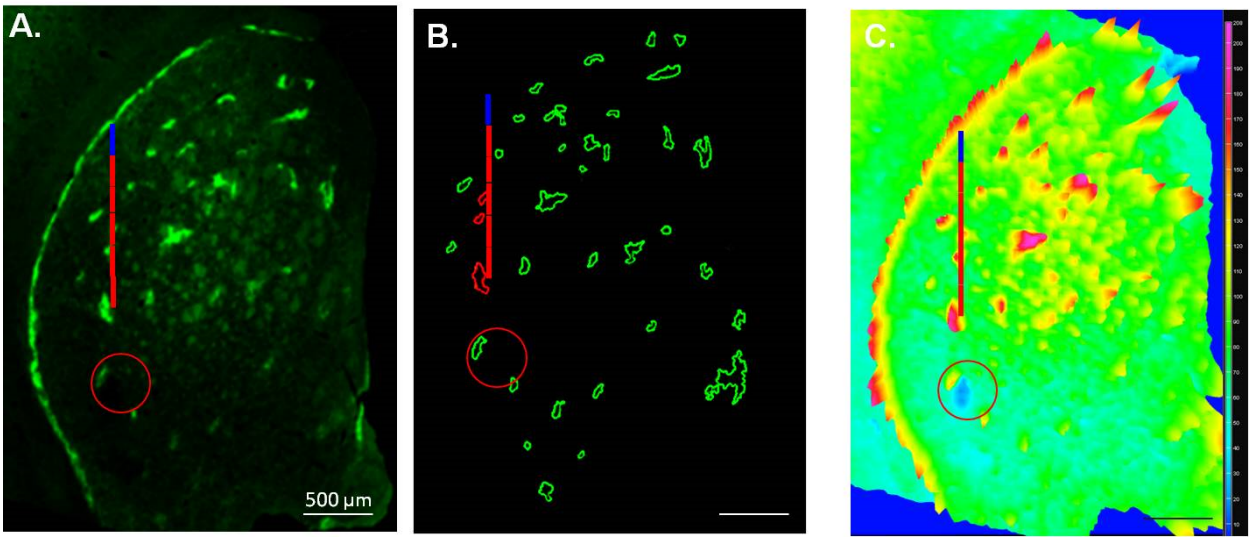

Figure S 6.2. Images of LS of the rat stained for MOR rich and poor compartments. A) Labeling of MOR rich compartments (patches). B) Corresponding patches are outlined in green. C) Images 10A is converted into a surface intensity plot. The intensity axis is located to the right of image (0 lowest intesity-255 highest intensity). The red circle indicates the location of the electrolytic lesion. The electrode track is shown in red and blue in each image. Scale bar is 500µm.

7.0 CONCLUSION

This dissertation details the potential of the in vivo techniques of microdialysis and voltammetry and their impact on understanding dopamine (DA) activity in the brain.

Microdialysis probe implantation disrupts DA activity in surrounding tissue; however DA terminals survive implantation, but cannot function on a normal level due to the probe induced penetration injury. Retrodialysis of the anti-inflammatory drug, dexamethasone (DEX), and the reactive oxygen species (ROS) scavenger, XJB-5-131, improved the health of the tissue around the probe which directly correlated to protection of striatal DA activity as assess by voltammetry near probes.[32] Initial investigations focused on four hour mitigation of the penetration injury directing us to the idea that acute mitigation of tissue damage could potentially chronically preserve tissue health.

Microdialysis in brain tissue is known to cause progressive neurochemical and histological disruptions in surrounding tissue.[18, 26, 42-43] As many microdialysis experiments are performed during a 4-24 hour time period, continued protection of DA activity is necessary. We proved that retrodialysis of DEX preserved DA activity for 24 hours through its anti-inflammatory actions on the surrounding tissue.[33] The actions of DEX are restricted to the tissue immediately adjacent to the probe, suggesting the DEX enhanced microdialysis is suitable for neurochemical monitoring, without having a global effect on the brain. The DA terminal marker

tyrosine hydroxylase, rebounded from 4 to 24 hours indicating the continued survival of DA terminals near the probe and justifying of our efforts to protect of these terminals.

A variety of other pharmaceutical agents proved to be effective at preserving DA activity in tissue surrounding microdialysis probes. Pharmacologically enhanced microdialysis is not limited to DEX, but can be achieved using non-steroidal anti-inflammatories, ibuprofen and PPads and novel ROS scavenger JRS527. General protection of the tissue health preserves DA activity.

Microdialysis is widely used to recovery not only DA, but many other small signaling molecules in the brain (neurotransmitters, amino acids, neuropeptides, ions). This method is an approved in vivo technique for monitoring traumatic brain injured patients therefore it is imperative that microdialysis performs at its full potential. We have performed a preliminary study investigating the effect of probe implantation on the ability to measure spreading depolarizations (marked by increases in extracellular potassium) in surrounding tissue. Probe implantation had no effect on measuring spreading depolarizations 1 mm away as assessed by potassium ion selective microelectrodes. Further work must be done to determine the effects, if any, on potassium measurements in tissue directly adjacent to the probe.

Microdialysis is often used to understand brain function and investigate neurological disorders. Understanding the penetration injury associated with probe implantation and providing protective strategies promotes long-term sampling by microdialysis and plays a lasting role in understanding the neurochemistry of the brain. The future of chronic microdialysis is unlimited. Microdialysis could be used to determine treatment for traumatic brain injury, to explore the development of a progressive neurological disease in a single animal, such as Parkinson's

disease and to continuously monitor different neurochemicals at all stages of substance abuse (addition, withdraw, relapse) in a single animal.

Finally, voltammetry coupled to carbon fiber microelectrodes was used to investigate DA neurotransmission in a more discrete manner. The small size of the electrodes provides excellent spatial and temporal resolution to map different kinetic DA domains in particular regions of the rat striatum. Sub-regions of the striatum were found to be distinct with respect to DA kinetic diversity.[154] Through voltammetry and histochemistry, DA terminal fields were determined to be anatomically organized depending on the initial rate of DA release in either patch or matrix compartments present in the striatum. As different sub-regions of the striatum are functionally distinct, the current findings show the importance of DA kinetics on DA function in the brain. These sub-regions are known to have distinct physiological functions so it makes sense that different types of DA signaling exist in different regions. Further insight into understanding the relationship between different DA kinetics and functionality can provide insight into drug addiction and neurological diseases such as Parkinson's disease.

BIBLIOGRAPHY

(1) Liu, Y.; Zhang, J.; Xu, X.; Zhao, M. K.; Andrews, A. M.; Weber, S. G. *Anal Chem* **2010,** *82*, 9611-9616.

(2) Church, W. H.; Justice, J. B. *Anal Chem* **1987,** *59*, 712-716.

(3) Tepper, J. M.; Creese, I.; Schwartz, D. H. *Brain Res* **1991,** *559*, 283-292.

(4) Shou, M.; Ferrario, C. R.; Schultz, K. N.; Robinson, T. E.; Kennedy, R. T. *Anal Chem* **2006,** *78*, 6717-6725.

(5) Badiani, A.; Oates, M. M.; Day, H. E.; Watson, S. J.; Akil, H.; Robinson, T. E. *J Neurosci* **1998,** *18*, 10579-10593.

(6) Santiago, M.; Westerink, B. H. *J Neurochem* **1991,** *57*, 738-747.

(7) Amanlou, M. S., S.D; Norouzian, D; Aghasadeghi, M.O.; Fathi-Moghaddam,H.; Piryaei, M.; Ardestani, S.H. *Iranian Journal of Basic Medical Sciences* **2010,** *14*, 107-115.

(8) Bosche, B.; Dohmen, C.; Graf, R.; Neveling, M.; Staub, F.; Kracht, L.; Sobesky, J.; Lehnhardt, F. G.; Heiss, W. D. *Stroke* **2003,** *34*, 2908-2913.

(9) Parkin, M.; Hopwood, S.; Jones, D. A.; Hashemi, P.; Landolt, H.; Fabricius, M.; Lauritzen, M.; Boutelle, M. G.; Strong, A. J. *J Cereb Blood Flow Metab* **2005,** *25*, 402-413.

(10) Sakowitz, O. W.; Stover, J. F.; Sarrafzadeh, A. S.; Unterberg, A. W.; Kiening, K. L. *J Trauma* **2007,** *62*, 292-298.

(11) Szarowski, D. H.; Andersen, M. D.; Retterer, S.; Spence, A. J.; Isaacson, M.; Craighead, H. G.; Turner, J. N.; Shain, W. *Brain Res* **2003,** *983*, 23-35.

(12) Turner, A. M.; Dowell, N.; Turner, S. W.; Kam, L.; Isaacson, M.; Turner, J. N.; Craighead, H. G.; Shain, W. *J Biomed Mater Res* **2000,** *51*, 430-441.

(13) Skousen, J. L.; Merriam, S. M.; Srivannavit, O.; Perlin, G.; Wise, K. D.; Tresco, P. A. *Prog Brain Res* **2011,** *194*, 167-180.

(14) Benveniste, H.; Diemer, N. H. *Acta Neuropathologica* **1987,** *74*, 234-238.

(15) Zhou, F.; Zhu, X.; Castellani, R. J.; Stimmelmayr, R.; Perry, G.; Smith, M. A.; Drew, K. L. *Am J Pathol* **2001,** *158*, 2145-2151.

(16) Clapp-Lilly, K. L.; Roberts, R. C.; Duffy, L. K.; Irons, K. P.; Hu, Y.; Drew, K. L. *J Neurosci Methods* **1999,** *90*, 129-142.

(17) Mitala, C. M.; Wang, Y.; Borland, L. M.; Jung, M.; Shand, S.; Watkins, S.; Weber, S. G.; Michael, A. C. *J Neurosci Methods* **2008,** *174*, 177-185.

(18) Jaquins-Gerstl, A.; Michael, A. C. *J Neurosci Methods* **2009,** *183*, 127-135.

(19) Whittle, I. R.; Glasby, M.; Lammie, A.; Bell, H.; Ungerstedt, U. *Neuroreport* **1998,** *9*, 2821-2825.

(20) Zhong, Y.; Bellamkonda, R. V. *J Control Release* **2005,** *106*, 309-318.

(21) Shain, W.; Spataro, L.; Dilgen, J.; Haverstick, K.; Retterer, S.; Isaacson, M.; Saltzman, M.; Turner, J. N. *IEEE Trans Neural Syst Rehabil Eng* **2003,** *11*, 186-188.

(22) Spataro, L.; Dilgen, J.; Retterer, S.; Spence, A. J.; Isaacson, M.; Turner, J. N.; Shain, W. *Exp Neurol* **2005,** *194*, 289-300.

(23) Zhong, Y.; Bellamkonda, R. V. *Brain Res* **2007,** *1148*, 15-27.

(24) Kurkowska-Jastrzebska, I.; Litwin, T.; Joniec, I.; Ciesielska, A.; Przybylkowski, A.; Czlonkowski, A.; Czlonkowska, A. *Int Immunopharmacol* **2004,** *4*, 1307-1318.

(25) Mou, X.; Lennartz, M. R.; Loegering, D. J.; Stenken, J. A. *J Diabetes Sci Technol* **2011,** *5*, 619-631.

(26) Jaquins-Gerstl, A.; Shu, Z.; Zhang, J.; Liu, Y.; Weber, S. G.; Michael, A. C. *Anal Chem* **2011,** *83*, 7662-7667.

(27) Wightman, R.; Amatorh, C.; Engstrom, R.; Hale, P.; Kristensen, E.; Kuhr, W.; May, L. *Neuroscience* **1988,** *25*, 513-523.

(28) Peters, J. L.; Miner, L. H.; Michael, A. C.; Sesack, S. R. *J Neurosci Methods* **2004,** *137*, 9-23.

(29) Borland, L. M.; Shi, G.; Yang, H.; Michael, A. C. *J Neurosci Methods* **2005,** *146*, 149-158.

(30) Borland, L. M.; Michael, A. C. *J Neurochem* **2004,** *91*, 220-229.

(31) Wang, Y.; Michael, A. C. *J Neurosci Methods* **2012,** *208*, 34-39.

(32) Nesbitt, K. M.; Jaquins-Gerstl, A.; Skoda, E. M.; Wipf, P.; Michael, A. C. *Anal Chem* **2013,** *85*, 8173-8179.

(33) Nesbitt, K. M.; Varner, E. L.; Jaquins-Gerstl, A.; Michael, A. C. *ACS Chemical Neuroscience* **2015,** *6*, 163-173.

(34) Feuerstein, D.; Manning, A.; Hashemi, P.; Bhatia, R.; Fabricius, M.; Tolias, C.; Pahl, C.; Ervine, M.; Strong, A. J.; Boutelle, M. G. *J Cereb Blood Flow Metab* **2010,** *30*, 1343-1355.

(35) Westerink, B. H.; Cremers, T. I. F. H., Eds *Handbook of Microdilaysis: Methods, Applications and Perspectivies*; Academic Press: London, 2007.

(36) Hopwood, S. E.; Parkin, M. C.; Bezzina, E. L.; Boutelle, M. G.; Strong, A. J. *J Cereb Blood Flow Metab* **2005,** *25*, 391-401.

(37) Watson, C. J.; Venton, B. J.; Kennedy, R. T. *Analytical Chemistry* **2006,** *78*, 1391-1399.

(38) Yang, H.; Thompson, A. B.; McIntosh, B. J.; Altieri, S. C.; Andrews, A. M. *ACS Chemical Neuroscience* **2013**.

(39) Lee, W. H.; Slaney, T. R.; Hower, R. W.; Kennedy, R. T. *Analytical Chemistry* **2013,** *85*, 3828-3831.

(40) Wang, M.; Slaney, T.; Mabrouk, O.; Kennedy, R. T. *Journal of Neuroscience Methods* **2010,** *190*, 39-48.

(41) Davalos, D.; Grutzendler, J.; Yang, G.; Kim, J. V.; Zuo, Y.; Jung, S.; Littman, D. R.; Dustin, M. L.; Gan, W. B. *Nat Neurosci* **2005,** *8*, 752-758.

(42) Holson, R. R.; Bowyer, J. F.; Clausing, P.; Gough, B. *Brain Res* **1996,** *739*, 301-307.

(43) Holson, R. R.; Gazzara, R. A.; Gough, B. *Brain Res* **1998,** *808*, 182-189.

(44) Grand, L.; Wittner, L.; Herwik, S.; Gothelid, E.; Ruther, P.; Oscarsson, S.; Neves, H.; Dombovari, B.; Csercsa, R.; Karmos, G.; Ulbert, I. *J Neurosci Methods* **2010,** *189*, 216-229.

(45) Fink, M. P.; Macias, C. A.; Xiao, J.; Tyurina, Y. Y.; Delude, R. L.; Greenberger, J. S.; Kagan, V. E.; Wipf, P. *Crit Care Med* **2007,** *35*, S461-467.

(46) Jiang, J.; Kurnikov, I.; Belikova, N. A.; Xiao, J.; Zhao, Q.; Amoscato, A. A.; Braslau, R.; Studer, A.; Fink, M. P.; Greenberger, J. S.; Wipf, P.; Kagan, V. E. *J Pharmacol Exp Ther* **2007,** *320*, 1050-1060.

(47) Wipf, P.; Xiao, J.; Jiang, J.; Belikova, N. A.; Tyurin, V. A.; Fink, M. P.; Kagan, V. E. *Journal of the American Chemical Society* **2005,** *127*, 12460-12461.

(48) Ji, J.; Kline, A. E.; Amoscato, A.; Samhan-Arias, A. K.; Sparvero, L. J.; Tyurin, V. A.; Tyurina, Y. Y.; Fink, B.; Manole, M. D.; Puccio, A. M.; Okonkwo, D. O.; Cheng, J. P.;

Alexander, H.; Clark, R. S.; Kochanek, P. M.; Wipf, P.; Kagan, V. E.; Bayir, H. *Nat Neurosci* **2012,** *15*, 1407-1413.

(49) Hunter, R. L.; Dragicevic, N.; Seifert, K.; Choi, D. Y.; Liu, M.; Kim, H.-C.; Cass, W. A.; Sullivan, P. G.; Bing, G. *Journal of Neurochemistry* **2007,** *100*, 1375-1386.

(50) Rabinovic, A. D.; Lewis, D. A.; Hastings, T. G. *Neuroscience* **2000,** *101*, 67-76.

(51) Card, J. P.; Sved, J. C.; Craig, B.; Raizada, M.; Vazquez, J.; Sved, A. F. *J Comp Neurol* **2006,** *499*, 840-859.

(52) Garris, P. A.; Wightman, R. M. *Synapse* **1995,** *20*, 269-279.

(53) Taylor, I. M.; Jaquins-Gerstl, A.; Sesack, S. R.; Michael, A. C. *J Neurochem* **2012**.

(54) Nicholson, C.; Rice, M. E., In *Volume transmission in the brain: novel mechanisms for neural transmission*, Fuxe, K. A., L.F., Ed. Raven Press: New York, 1991.

(55) Rinaman, L.; Card, J. P.; Enquist, L. W. *J Neurosci* **1993,** *13*, 685-702.

(56) Sauer, M.; Hofkens, J.; Enderlein, J. *Handbook of Fluorescence Spectroscopy and Imaging: From Ensemble to Single Molecules*; WILEY-VCH verlag & Co.: Germany, 2011.

(57) Han, N.; Rao, S. S.; Johnson, J.; Parikh, K. S.; Bradley, P. A.; Lannutti, J. J.; Winter, J. O. *Front Neuroeng* **2011,** *4*, 2.

(58) Hsiao, T. W.; Swarup, V. P.; Kuberan, B.; Tresco, P. A.; Hlady, V. *Acta Biomater* **2013**.

(59) Karumbaiah, L.; Norman, S. E.; Rajan, N. B.; Anand, S.; Saxena, T.; Betancur, M.; Patkar, R.; Bellamkonda, R. V. *Biomaterials* **2012,** *33*, 5983-5996.

(60) Lewitus, D. Y.; Smith, K. L.; Shain, W.; Bolikal, D.; Kohn, J. *Biomaterials* **2011,** *32*, 5543-5550.

(61) Xun, Z.; Rivera-Sanchez, S.; Ayala-Pena, S.; Lim, J.; Budworth, H.; Skoda, E. M.; Robbins, P. D.; Niedernhofer, L. J.; Wipf, P.; McMurray, C. T. *Cell Rep* **2012**.

(62) Carboni, E.; Spielewoy, C.; Vacca, C.; Nosten-Bertrand, M.; Giros, B.; Di Chiara, G. *J Neurosci* **2001,** *21*, Rc141: 141-144.

(63) Di Chiara, G.; Imperato, A. *Proceedings of the National Academy of Sciences* **1988,** *85*, 5274-5278.

(64) Di Chiara, G.; Tanda, G.; Carboni, E. *Behav Pharmacol* **1996,** *7*, 640-657.

(65) El Arfani, A.; Bentea, E.; Aourz, N.; Ampe, B.; De Deurwaerdere, P.; Van Eeckhaut, A.; Massie, A.; Sarre, S.; Smolders, I.; Michotte, Y. *Neuropharmacology* **2014,** *85*, 198-205.

(66) Sharp, T.; Maidment, N. T.; Brazell, M. P.; Zetterstrom, T.; Ungerstedt, U.; Bennett, G. W.; Marsden, C. A. *Neuroscience* **1984,** *12*, 1213-1221.

(67) Sharp, T.; Zetterström, T.; Ljungberg, T.; Ungerstedt, U. *Brain Research* **1987,** *401*, 322-330.

(68) Tossman, U.; Eriksson, S.; Delin, A.; Hagenfeldt, L.; Law, D.; Ungerstedt, U. *J Neurochem* **1983,** *41*, 1046-1051.

(69) Ungerstedt, U., Measurement of neurotransmitter release by intracranial dialysis. In *In Measurement of Neurotransmitter Release In Vivo*, Marsden, C. A., Ed. John Wiley & Sons: New York, 1984; pp 81-105.

(70) Westerink, B. H. *Behav Brain Res* **1995,** *70*, 103-124.

(71) Westerink, B. H.; De Vries, J. B. *J Neurochem* **1988,** *51*, 683-687.

(72) Wright, I. K.; Upton, N.; Marsden, C. A. *Psychopharmacology (Berl)* **1992,** *109*, 338-346.

(73) Abercrombie, E. D.; Zigmond, M. J. *J Neurosci* **1989,** *9*, 4062-4067.

(74) Arbuthnott, G. W.; Fairbrother, I. S.; Butcher, S. P. *J Neurosci Methods* **1990,** *34*, 73-81.

(75) Chefer, V. I.; Thompson, A. C.; Zapata, A.; Shippenberg, T. S., Overview of Brain Microdialysis. In *Current Protocols in Neuroscience*, John Wiley & Sons, Inc.: 2001.

(76) Davies, M. I.; Cooper, J. D.; Desmond, S. S.; Lunte, C. E.; Lunte, S. M. *Adv Drug Deliv Rev* **2000,** *45*, 169-188.

(77) Kehr, J., New methodological aspects of microdialysis. In *Handbook of Behavioral Neuroscience*, Ben, H. C. W.; Thomas, I. F. H. C., Eds. Elsevier: 2006; Vol. Volume 16, pp 111-129.

(78) Robinson, T. E.; Justice, J. B., Eds *Techniques in the Behavioral and Neural Sciences*; Elsevier: Amsterdam, 1991; Vol. *7: Microdialysis in the Neurosciences*.

(79) Zetterström, T.; Sharp, T.; Marsden, C. A.; Ungerstedt, U. *Journal of Neurochemistry* **1983,** *41*, 1769-1773.

(80) Bert, L.; Parrot, S.; Robert, F.; Desvignes, C.; Denoroy, L.; Suaud-Chagny, M. F.; Renaud, B. *Neuropharmacology* **2002,** *43*, 825-835.

(81) Emmett, M. R.; Andren, P. E.; Caprioli, R. M. *J Neurosci Methods* **1995,** *62*, 141-147.

(82) Santiago, M.; Westerink, B. H. *Naunyn Schmiedebergs Arch Pharmacol* **1990,** *342*, 407-414.

(83) Scott, D. E.; Grigsby, R. J.; Lunte, S. M. *Chemphyschem* **2013,** *14*, 2288-2294.

(84) Li, Q.; Zubieta, J. K.; Kennedy, R. T. *Anal Chem* **2009,** *81*, 2242-2250.

(85) Parrot, S.; Bert, L.; Mouly-Badina, L.; Sauvinet, V.; Colussi-Mas, J.; Lambas-Senas, L.; Robert, F.; Bouilloux, J. P.; Suaud-Chagny, M. F.; Denoroy, L.; Renaud, B. *Cell Mol Neurobiol* **2003,** *23*, 793-804.

(86) Zhang, J.; Jaquins-Gerstl, A.; Nesbitt, K. M.; Rutan, S. C.; Michael, A. C.; Weber, S. G. *Anal Chem* **2013,** *85*, 9889-9897.

(87) Tang, A.; Bungay, P. M.; Gonzales, R. A. *Journal of Neuroscience Methods* **2003,** *126*, 1-11.

(88) Zhou, F.; Braddock, J. F.; Hu, Y.; Zhu, X.; Castellani, R. J.; Smith, M. A.; Drew, K. L. *J Neurosci Methods* **2002,** *119*, 121-128.

(89) Hascup, E. R.; af Bjerken, S.; Hascup, K. N.; Pomerleau, F.; Huettl, P.; Stromberg, I.; Gerhardt, G. A. *Brain Res* **2009,** *1291*, 12-20.

(90) Bungay, P. M.; Newton-Vinson, P.; Isele, W.; Garris, P. A.; Justice, J. B. *J Neurochem* **2003,** *86*, 932-946.

(91) Major, O.; Shdanova, T.; Duffek, L.; Nagy, Z. *Acta Neurochir Suppl (Wien)* **1990,** *51*, 46-48.

(92) Planas, A. M.; Justicia, C.; Sole, S.; Friguls, B.; Cervera, A.; Adell, A.; Chamorro, A. *J Cereb Blood Flow Metab* **2002,** *22*, 918-925.

(93) Benveniste, H.; Drejer, J.; Schousboe, A.; Diemer, N. H. *J Neurochem* **1987,** *49*, 729-734.

(94) Kadota, E.; Nonaka, K.; Karasuno, M.; Nishi, K.; Nakamura, Y.; Namikawa, K.; Okazaki, Y.; Teramura, K.; Hashimoto, S. *Acta Neurochir Suppl (Wien)* **1994,** *60*, 162-164.

(95) Groothuis, J.; Ramsey, N. F.; Ramakers, G. M.; van der Plasse, G. *Brain Stimul* **2014,** *7*, 1-6.

(96) Imperato, A.; Di Chiara, G. *J Neurosci* **1985,** *5*, 297-306.

(97) Robinson, T. E.; Camp, D. M. *J Neurosci Methods* **1991,** *40*, 211-222.

(98) Westerink, B. H.; Tuinte, M. H. *J Neurochem* **1986,** *46*, 181-185.

(99) Church, W. H.; Justice, J. B., Jr.; Byrd, L. D. *Eur J Pharmacol* **1987,** *139*, 345-348.

(100) Pontieri, F. E.; Tanda, G.; Di Chiara, G. *Proceedings of the National Academy of Sciences* **1995,** *92*, 12304-12308.

(101) Rahman, S.; Zhang, J.; Engleman, E. A.; Corrigall, W. A. *Neuroscience* **2004,** *129*, 415-424.

(102) Lam, H. A.; Wu, N.; Cely, I.; Kelly, R. L.; Hean, S.; Richter, F.; Magen, I.; Cepeda, C.; Ackerson, L. C.; Walwyn, W.; Masliah, E.; Chesselet, M. F.; Levine, M. S.; Maidment, N. T. *J Neurosci Res* **2011,** *89*, 1091-1102.

(103) Amos, A. N.; Roberts, J. G.; Lingjiao, Q.; Sombers, L. A.; McCarty, G. S. *Sensors Journal, IEEE* **2014,** *14*, 2975-2980.

(104) Chang, S. Y.; Kimble, C. J.; Kim, I.; Paek, S. B.; Kressin, K. R.; Boesche, J. B.; Whitlock, S. V.; Eaker, D. R.; Kasasbeh, A.; Horne, A. E.; Blaha, C. D.; Bennet, K. E.; Lee, K. H. *J Neurosurg* **2013,** *119*, 1556-1565.

(105) Garris, P. A.; Christensen, J. R.; Rebec, G. V.; Wightman, R. M. *J Neurochem* **1997,** *68*, 152-161.

(106) Moquin, K. F.; Michael, A. C. *J Neurochem* **2009,** *110*, 1491-1501.

(107) Floresco, S. B.; West, A. R.; Ash, B.; Moore, H.; Grace, A. A. *Nat Neurosci* **2003,** *6*, 968-973.

(108) Lu, Y.; Peters, J. L.; Michael, A. C. *J Neurochem* **1998,** *70*, 584-593.

(109) Belle, A. M.; Owesson-White, C.; Herr, N. R.; Carelli, R. M.; Wightman, R. M. *ACS Chemical Neuroscience* **2013,** *4*, 761-771.

(110) Jones, S. R.; Garris, P. A.; Wightman, R. M. *J Pharmacol Exp Ther* **1995,** *274*, 396-403.

(111) Wu, Q.; Reith, M. E.; Kuhar, M. J.; Carroll, F. I.; Garris, P. A. *J Neurosci* **2001,** *21*, 6338-6347.

(112) Ciliax, B. J.; Heilman, C.; Demchyshyn, L. L.; Pristupa, Z. B.; Ince, E.; Hersch, S. M.; Niznik, H. B.; Levey, A. I. *J Neurosci* **1995,** *15*, 1714-1723.

(113) Freed, C.; Revay, R.; Vaughan, R. A.; Kriek, E.; Grant, S.; Uhl, G. R.; Kuhar, M. J. *J Comp Neurol* **1995,** *359*, 340-349.

(114) Sesack, S. R.; Hawrylak, V. A.; Matus, C.; Guido, M. A.; Levey, A. I. *J Neurosci* **1998,** *18*, 2697-2708.

(115) Winslow, B. D.; Christensen, M. B.; Yang, W. K.; Solzbacher, F.; Tresco, P. A. *Biomaterials* **2010,** *31*, 9163-9172.

(116) Bezard, E.; Dovero, S.; Imbert, C.; Boraud, T.; Gross, C. E. *Synapse* **2000,** *38*, 363-368.

(117) Finkelstein, D. I.; Stanic, D.; Parish, C. L.; Tomas, D.; Dickson, K.; Horne, M. K. *Neuroscience* **2000,** *97*, 99-112.

(118) Barlow, A. L.; Macleod, A.; Noppen, S.; Sanderson, J.; Guerin, C. J. *Microsc Microanal* **2010,** *16*, 710-724.

(119) Dunn, K. W.; Kamocka, M. M.; McDonald, J. H. *Am J Physiol Cell Physiol* **2011,** *300*, C723-742.

(120) Costes, S. V.; Daelemans, D.; Cho, E. H.; Dobbin, Z.; Pavlakis, G.; Lockett, S. *Biophys J* **2004,** *86*, 3993-4003.

(121) Adler, J.; Parmryd, I. *Cytometry A* **2010,** *77*, 733-742.

(122) Manders, E. M.; Stap, J.; Brakenhoff, G. J.; van Driel, R.; Aten, J. A. *J Cell Sci* **1992,** *103 (Pt 3)*, 857-862.

(123) Manders, E. M. M.; Verbeek, F. J.; Aten, J. A. *Journal of Microscopy* **1993,** *169*, 375-382.

(124) Schmerberg, C. M.; Li, L. *Analytical Chemistry* **2013,** *85*, 915-922.

(125) Lammers, C. H.; D'Souza, U. M.; Qin, Z. H.; Lee, S. H.; Yajima, S.; Mouradian, M. M. *Brain Res Mol Brain Res* **1999,** *69*, 281-285.

(126) Rostene, W.; Sarrieau, A.; Nicot, A.; Scarceriaux, V.; Betancur, C.; Gully, D.; Meaney, M.; Rowe, W.; De Kloet, R.; Pelaprat, D.; et al. *J Psychiatry Neurosci* **1995,** *20*, 349-356.

(127) Sadri-Vakili, G.; Johnson, D. W.; Janis, G. C.; Gibbs, T. T.; Pierce, R. C.; Farb, D. H. *J Neurochem* **2003,** *86*, 92-101.

(128) Kurumbail, R. G.; Stevens, A. M.; Gierse, J. K.; McDonald, J. J.; Stegeman, R. A.; Pak, J. Y.; Gildehaus, D.; Miyashiro, J. M.; Penning, T. D.; Seibert, K.; Isakson, P. C.; Stallings, W. C. *Nature* **1996,** *384*, 644-648.

(129) Schaaf, M. J.; Cidlowski, J. A. *J Steroid Biochem Mol Biol* **2002,** *83*, 37-48.

(130) Vane Dsc, F. R. S. J. R.; Botting PhD, R. M. *The American Journal of Medicine* **1998,** *104*, 2S-8S.

(131) Hunter, R. L.; Dragicevic, N.; Seifert, K.; Choi, D. Y.; Liu, M.; Kim, H. C.; Cass, W. A.; Sullivan, P. G.; Bing, G. *J Neurochem* **2007,** *100*, 1375-1386.

(132) Goff, J. P.; Epperly, M. W.; Dixon, T.; Wang, H.; Franicola, D.; Shields, D.; Wipf, P.; Li, S.; Gao, X.; Greenberger, J. S. *In Vivo* **2011,** *25*, 315-323.

(133) Rajagopalan, M. S.; Gupta, K.; Epperly, M. W.; Franicola, D.; Zhang, X.; Wang, H.; Zhao, H.; Tyurin, V. A.; Pierce, J. G.; Kagan, V. E.; Wipf, P.; Kanai, A. J.; Greenberger, J. S. *In Vivo* **2009,** *23*, 717-726.

(134) Faul, M.; Xu, L.; Wald, M. M.; Coronado, V. *Atlanta, GA: Centers for Disease Control and Prevention, National Center for Injury Prevention and Control* **2010**.

(135) Narayan, R. K.; Michel, M. E.; Ansell, B.; Baethmann, A.; Biegon, A.; Bracken, M. B.; Bullock, M. R.; Choi, S. C.; Clifton, G. L.; Contant, C. F. *Journal of neurotrauma* **2002,** *19*, 503-557.

(136) Aronowski, J.; Zhao, X. *Stroke* **2011,** *42*, 1781-1786.

(137) Haddad, S. H.; Arabi, Y. M. *Scand J Trauma Resusc Emerg Med* **2012,** *20*, 12-27.

(138) Hartings, J. A.; Watanabe, T.; Bullock, M. R.; Okonkwo, D. O.; Fabricius, M.; Woitzik, J.; Dreier, J. P.; Puccio, A.; Shutter, L. A.; Pahl, C.; Strong, A. J. *Spreading depolarizations have prolonged direct current shifts and are associated with poor outcome in brain trauma*; 2011; Vol. 134, p 1529-1540.

(139) Lauritzen, M.; Dreier, J. P.; Fabricius, M.; Hartings, J. A.; Graf, R.; Strong, A. J. *J Cereb Blood Flow Metab* **2011,** *31*, 17-35.

(140) Strong, A. J.; Hartings, J. A.; Dreier, J. P. *Current Opinion in Critical Care* **2007,** *13*, 126-133.

(141) Somjen, G. G. *Physiological reviews* **2001,** *81*, 1065-1096.

(142) Martins-Ferreira, H.; Nedergaard, M.; Nicholson, C. *Brain research reviews* **2000,** *32*, 215-234.

(143) Rogers, M. L.; Feuerstein, D.; Leong, C. L.; Takagaki, M.; Niu, X.; Graf, R.; Boutelle, M. G. *ACS Chemical Neuroscience* **2013,** *4*, 799-807.

(144) Stiefel, M. F.; Marmarou, A. *J Neurosurg* **2002,** *97*, 97-103.

(145) Walker, J. L. *Analytical Chemistry* **1971,** *43*, 89A-93a.

(146) Rice, M. E.; Patel, J. C.; Cragg, S. J. *Neuroscience* **2011,** *198*, 112-137.

(147) Schultz, W. *Annu. Rev. Neurosci.* **2007,** *30*, 259-288.

(148) Bao, L.; Patel, J. C.; Walker, R. H.; Shashidharan, P.; Rice, M. E. *Journal of neurochemistry* **2010,** *114*, 1781-1791.

(149) de la Fuente-Fernández, R.; Schulzer, M.; Kuramoto, L.; Cragg, J.; Ramachandiran, N.; Au, W. L.; Mak, E.; McKenzie, J.; McCormick, S.; Sossi, V. *Annals of neurology* **2011,** *69*, 803-810.

(150) Koob, G. F.; Bloom, F. E. *Science* **1988,** *242*, 715-723.

(151) Russell, V. A.; Sagvolden, T.; Johansen, E. B. *Behavioral and Brain functions* **2005,** *1*, 9.

(152) Virdee, K.; Cumming, P.; Caprioli, D.; Jupp, B.; Rominger, A.; Aigbirhio, F. I.; Fryer, T. D.; Riss, P. J.; Dalley, J. W. *Neuroscience & Biobehavioral Reviews* **2012,** *36*, 1188-1216.

(153) Moquin, K. F.; Michael, A. C. *Journal of neurochemistry* **2011,** *117*, 133-142.

(154) Taylor, I. M.; Nesbitt, K. M.; Walters, S. H.; Varner, E. L.; Shu, Z.; Bartlow, K. M.; Jaquins-Gerstl, A. S.; Michael, A. C. *J Neurochem* **2015**.

(155) Wang, Y.; Moquin, K. F.; Michael, A. C. *Journal of neurochemistry* **2010,** *114*, 150-159.

(156) Crittenden, J. R.; Graybiel, A. M. *Frontiers in neuroanatomy* **2011,** *5*.

(157) Gerfen, C.; Herkenham, M.; Thibault, J. *The Journal of Neuroscience* **1987,** *7*, 3915-3934.

(158) Cline, E. J.; Adams, C. E.; Larson, G. A.; Gerhardt, G. A.; Zanhizer, N. R. *Experimental neurology* **1995,** *134*, 135-149.

(159) Venton, B. J.; Zhang, H.; Garris, P. A.; Phillips, P. E.; Sulzer, D.; Wightman, R. M. *J Neurochem* **2003,** *87*, 1284-1295.

(160) Taylor, I. M.; Ilitchev, A. I.; Michael, A. C. *ACS Chemical Neuroscience* **2013,** *4*, 870-878.

(161) Paxinos, G.; Watson, C. J., *The Rat Brain in Stereotaxic Coordinates*. Fourth Edition ed.; Academic Press,: New York, 1998.

(162) McFarland, N. R.; Haber, S. N. *J Neurosci* **2000,** *20*, 3798-3813.

(163) Voorn, P.; Vanderschuren, L. J.; Groenewegen, H. J.; Robbins, T. W.; Pennartz, C. M. *Trends in neurosciences* **2004,** *27*, 468-474.

(164) Yin, H. H.; Knowlton, B. J.; Balleine, B. W. *European Journal of Neuroscience* **2005,** *22*, 505-512.

(165) Yin, H. H.; Knowlton, B. J.; Balleine, B. W. *Behavioural Brain Research* **2006,** *166*, 189-196.

(166) Yin, H. H.; Ostlund, S. B.; Knowlton, B. J.; Balleine, B. W. *European Journal of Neuroscience* **2005,** *22*, 513-523.

(167) Garris, P. A.; Ciolkowski, E. L.; Pastore, P.; Wightman, R. *The journal of neuroscience* **1994,** *14*, 6084-6093.

(168) Zachek, M. K.; Takmakov, P.; Park, J.; Wightman, R. M.; McCarty, G. S. *Biosensors and Bioelectronics* **2010,** *25*, 1179-1185.

(169) May, L. J.; Wightman, R. M. *Brain research* **1989,** *487*, 311-320.

(170) Iravani, M. M.; Kruk, Z. *Journal of neurochemistry* **1996,** *66*, 1076-1085.

(171) Limberger, N.; Trout, S. J.; Kruk, Z. L.; Starke, K. *Naunyn-Schmiedeberg's archives of pharmacology* **1991,** *344*, 623-629.

(172) Robinson, D. L.; Wightman, R. M., Rapid Dopamine Release in Freely Moving Rats. In *Electrochemical Methods for Neuroscience*, Michael, A. C.; Borland, L. M., Eds. CRC Press: Boca Raton (FL), 2007.

(173) Moss, J.; Bolam, J. P. *The Journal of Neuroscience* **2008,** *28*, 11221-11230.

(174) Shu, Z.; Taylor, I. M.; Michael, A. C. *European Journal of Neuroscience* **2013,** *38*, 3221-3229.

(175) Shu, Z.; Taylor, I. M.; Walters, S. H.; Michael, A. C. *European Journal of Neuroscience* **2014,** *40*, 2320-2328.

(176) Rodriguez, M.; Morales, I.; Gomez, I.; Gonzalez, S.; Gonzalez-Hernandez, T.; Gonzalez-Mora, J. L. *Journal of Pharmacology and Experimental Therapeutics* **2006,** *319*, 31-43.

(177) Hanley, J. J.; Bolam, J. P. *Neuroscience* **1997,** *81*, 353-370.

(178) Herkenham, M.; Lynn, A. B.; Johnson, M. R.; Melvin, L. S.; de Costa, B. R.; Rice, K. C. *J Neurosci* **1991,** *11*, 563-583.

(179) Herkenham, M.; Pert, C. B. *Proc Natl Acad Sci U S A* **1980,** *77*, 5532-5536.

(180) Koizumi, H.; Morigaki, R.; Okita, S.; Nagahiro, S.; Kaji, R.; Nakagawa, M.; Goto, S. *Frontiers in cellular neuroscience* **2013,** *7*.

(181) Krebs, M.-O.; Gauchy, C.; Desban, M.; Glowinski, J.; Kemel, M. *The Journal of neuroscience* **1994,** *14*, 2435-2443.